Optimization of Nanocomposite Membrane for Membrane Distillation

Viyash Murugesan

A thesis submitted to the
in partial fulfillment of the requirements for

Master of Applied Science in Chemical Engineering

Department of Chemical and Biological Engineering
Faculty of Engineering

uOttawa

University of Ottawa

Abstract

In this study, effects of nanoparticles, including 7 nm TiO_2, 200 nm TiO_2, and hydrophilic and hydrophobic SiO_2 with mean diameter in the range of 15–20 nm and their concentration on the membrane properties and vacuum membrane distillation (VMD) performance were evaluated. The effect of membrane thickness and support materials were also investigated. The membranes were characterised extensively in terms of morphology (SEM), water contact angle, water liquid entrance pressure (LEPw), surface roughness, and pore size. While the best nanocomposite membranes with 200 nm TiO_2 Nanoparticles(NPs) were obtained at 2% particle concentration, the optimal particle concentration was 5% when 7 nm TiO_2 was integrated. Using nanocomposite membrane containing 2 wt% TiO_2 – 200 nm nanoparticles, VMD flux of 2.1 kg/m^2h and LEPw of 34 PSI was obtained with 99% salt rejection. Furthermore, it was observed that decreasing the membrane thickness would increase the portion of finger-like layer in membrane and reduce the spongy-like layer when hydrophilic nanoparticles were used. Using continuous flow VMD, a flux of 3.1 kg/m^2h was obtained with neat PVDF membranes, which was 600% higher than the flux obtained by the static flow VMD with the same membrane at the same temperature and vacuum pressure. The fluxes of both static and flow-cell VMD increased with temperature. Furthermore, it was evident that the continuous flow VMD at 2 LPM yielded 300% or higher flux than static VMD at any given temperature, indicating strong effects of turbulence provided in the flow-cell VMD.

Abstrait

Dans cette étude, les effets des nanoparticules, y compris le TiO_2 de 7 nm, le TiO_2 de 200 nm et le SiO_2 hydrophile et hydrophobe avec un diamètre moyen dans la gamme de 15-20 nm et leur concentration sur les propriétés de la membrane et la distillation de la membrane sous vide (VMD) ont été évalués. Les effets de l'épaisseur de la membrane et des matériaux de support ont également été étudiés. Les membranes ont été caractérisées en termes de morphologie (SEM), d'angle de contact avec l'eau, de pression d'entrée d'eau liquide (LEPw), de rugosité de surface et de taille des pores. Bien que les meilleures membranes de nanocomposite avec des molécules de TiO_2 200 nm aient été obtenues à 2% de concentration de particules, la concentration optimale de particules était de 5% lorsque le TiO_2 de 7 nm était intégré. En utilisant une membrane nanocomposite contenant 2% en poids de nanoparticules TiO_2 - 200 nm, un flux VMD de 2,1 kg/m^2h et LEPw de 34 PSI a été obtenu avec 99% de rejet de sel. En outre, il a été observé que la diminution de l'épaisseur de la membrane augmenterait la partie de la couche de type doigt dans la membrane et réduirait la couche de type spongieuse lorsque des nanoparticules hydrophiles étaient utilisées. À l'aide de VMD à flux continu, un flux de 3,1 kg/m^2h a été obtenu avec des membranes de PVDF soignées, soit 600% de plus que le flux obtenu par VMD à flux statique avec la même membrane à la même température et à la même pression de vide. Les flux de VMD statiques et de cellules d'écoulement ont augmenté avec la température. En outre, il était évident que le VMD à flux continu à 2 LPM a donné un flux de 300% ou plus que le VMD statique à n'importe quelle température donnée, ce qui indique des effets forts de la turbulence fournis dans le VMD à flux cellulaire.

Acknowledgment

I would like to express my sincere thanks to my supervisor and co-supervisor Dr. Christopher Lan, Dr. Takeshi Matsuura, and Dr. Dipak Rana who have been tremendous mentors to me, guiding and providing me with all the necessary support. I would like to thank themfor encouraging my research and giving me the opportunity to grow as a research engineer. All your effort and dedication is priceless.

My gratitude also goes to the administrative and technical staff Sylvie Saindon, Francine Pétrin**,** Louis Tremblay, Franco Ziroldo and Gerard Nina in the Department of Chemical and Biological Engineering, Faculty of Engineering at the University of Ottawa.

I also would like to acknowledge the support of the staff in Carleton University SEM lab and Dr. Jianqun Wang for their tremendous support with SEM analysis.

Arkema Inc. (Philadelphia, PA, USA) are also appreciated for their donation of the poly(vinylidene) fluoride, the base polymer for this study.

Special gratitude to all the members of our industrial membrane research group especially Mohammadali Baghbanzadeh, Johnson Efome, Fan Yang, Zhelun Li, Yifan Yang and also my other friends Nirmal Balaji Kannan, Tamil Magan and everyone for their inspirational support, through the course of this work.

Finally, I am grateful and would like to dedicate all the credits to my lovely mother Meena, father Murugesan and Almighty GODfor their wisdom, good guidance in life and love which made this project complete.

Table of Contents

List of Figures

List of Tables

Nomenclature

a	Amortization factor
A	Area
c	Concentration
C	Conductivity
C_m	Membrane coefficient
c_p	Specific heat capacity
d	Diameter/Mean pore size
D	Diffusion coefficient
dt	Temperature rise
e	Electricity cost
f	Plant availability
g	Gravity of Earth
Gr	Grashof number
h	Heat transfer coefficient/Heat exchanger cost per area
i	Annual interest rate
J	Flux
k	Thermal conductivity
K	Mass transfer coefficient
k_B	Boltzmann constant
Kn	Knudsen number
l	Purchased piping cost per length/Gap thickness
L	Length
m	Mass flowrate/Weight
M	Molecular weight
m*	Membrane cost per area
n	Plant life time
Nu	Nusselt number
P	Pressure
P*	Vapour pressure
P_s	Brake power

Pr	Prandtl number
q	Volume flowrate
Q	Heat
r	Pore radius/Replacement rate
R	Universal gas constant/Rejection
r_{max}	Maximum pore size
RR	Recovery ratio
t	Time
T	Temperature
U	Global heat transfer coefficient
w	Weight
W	Plant capacity
γ	Surface tension
δ	Membrane thickness
ΔH_v	Heat of vaporization
ε	Porosity
η	Efficiency
θ	Contact angle
λ	Mean free path of the molecule
μ	Viscosity
Π	Thermal efficiency
ρ	Density
τ	Tortuosity/Penetration time
□	Concentration polarization coefficient

Subscript

c	Coolant
f	Feed
g	Gas inlet
LMTD	Logarithmic mean of temperature difference
m	Membrane interface

min	Minimum
out	outlet
p	Permeate
pol	Polymer

1. Introduction

Seventy one percent of the surface of earth is covered by, yet the demand for pure water is rapidly increasing each and every day. Out of this large percent of water, 96.5% of the water exists in the ocean floor which couldn't be used without a proper treatment for both domestic and industrial purposes.

1.1 Desalination

People started to use the ocean water with small treatment long before the technologies were known to mankind [1]. During earlier days, people used solar treatment to purify the sea water. The first ever solar distillation was discovered by Wheelers and Evans in 1870. After two years, , first large scale solar distillation was built in Las Salinas, Chile [2]. After that, till 1930 there were only few developments in the desalination technique but the severe drought in California this year encouraged the scientists to think for new methods. After World War II, the increase in human population forced this American president J.F.Kennedy to authorise US $75 billion for research in desalination during 1960-69 [3]. The first commercial electrodialysis plant was erected in 1962, at Webster, South Dakota, USA by Ionics, Watertown [4]. In the meantime, in South Africa, Electrodialysis method was invented early in 1950 in the National Research Lab., and the South African Council of Scientific Research (C.S.I.R.) installed 50 electrodialysis units in Pretoria of 250 gph (24 m^3d^{-1}) capacity [5]. Even though research and developments have been going on throughout the century, no permanent solution has been found so far to solve this water crisis. Currently, it is estimated that 1.8 billion people would be in absolute water scarcity and two-third of the world population would suffer from water stress by 2025 [6]. Due to this fact, scientists have started to focus on more efficient techniques that are based on

membrane separation. Membrane separation techniques attained more focus over this last few decades due to their efficiency, high yield and low investments compared to other methods. Membrane separation includes,

- Pressure-driven processes, such as reverse osmosis (RO), nanofiltration (NF), ultrafiltration (UF), microfiltration (MF), or gas separation (GS); or partial-pressure-driven processes, such as pervaporation (PV).
- Concentration-gradient-driven processes, such as dialysis.
- Temperature-driven processes, such as membrane distillation (MD).
- Electrical-potential-driven processes, such as electrodialysis (ED).

Among these, although all the methods were used for desalination, reverse osmosis was the predominant method used in industries. Besides its high efficiency, RO showed some disadvantages like high operating pressure, intense pre-treatment and higher rate of fouling [7]. 40% of its overall cost was consumed by electrical energy [8].

1.2 Membrane Distillation for desalination

To overcome these difficulties MD methods were preferred as they have no transmembrane pressure, mild pre-treatment, high recovery ratio with low operating pressure and low electric energy consumption. Even with these advantages MD is not suitable for industrial scale because of its high thermal consumption and high membrane cost which controls the overall cost of the operation. Thus, research has been conducted to minimize these costs and make them commercially available. Many improvements have been made in MD to make it possible which where explained in the following chapter 2.

1.3 The Challenge

As mentioned above, the limitations of MD made the scientists look for a way to overcome it. Due to immense work on this, MD has been studied both microscopically and macroscopically which makes the work lighter for the scientists who are beginning to work on this issue. Scientist have developed multi-effect MD configuration which requires very low heat energy and works have been carried in the prospect of developing a low-cost membrane with high efficiency by controlling the pore size, porosity, roughness and contact angle of the membranes. By doing so the MD configuration's operation cost has been brought down. Initially, the cost to produce pure water through MD was estimated $\$1.0/m^3$ comparing with RO which could be done at $\$0.40/m^3$. But Baghbanzadeh et al.[9] estimated that by using Zero Thermal Input Membrane Distillation (ZTIMD) the cost of the desalination can be reduced further to about $\$0.28/m^3$ at a specific consumption rate of 0.45 kW h/m^3. By this, the overall cost could be cut down into half which leaves the focus to the second issue, membrane cost. Many research activities has been done to diminish the cost but still there is a large gap to fill before achieving the best membrane with low cost and high efficiency.

1.4 Thesis Objective

The objective of the thesis is two-fold:

1) Improve the structure and performance of distillation membranes by optimizing the conditions for membrane fabrication

2) Advance our understanding to vacuum membrane distillation (VMD) processes by studying the mass and heat transfer in different vacuum membrane distillation configurations, including still cylinder and flow cell VMD configurations. Studies on the

improvement of membrane fabrication focused on the effects of different nanoparticles, membrane thickness, and support materials on the structure and VMD performance of nanocomposite membranes.

Reference

[1] J. D. Birkett, "A brief illustrated history of desalination. From the bible to 1940," *Desalination*, vol. 50, no. C, pp. 17–52, 1984.

[2] E. Delyannis, "Historic background of desalination and renewable energies," *Sol. Energy*, vol. 75, no. 5, pp. 357–366, 2003.

[3] U. . Congress, *An Act, Public Law 448-82d congress, Chapter 568-2d session, H.R. 6578 Saline water conversion report for 1959, 1960,90-91,Saline water conversion report for 1970-1971*. .

[4] S. M., "Large scale brackish water consersion-electrodialysis demonstration plant at webster, South Dakota, USA," 1962.

[5] J.R.Wilson, "Demineralization by Electrodialysis," *Butterworth's Sci. Publ. London*, p. 380 pp, 1960.

[6] V. G. Gude, "Desalination and sustainability - An appraisal and current perspective," *Water Res.*, vol. 89, pp. 87–106, 2016.

[7] P. Wang and T. S. Chung, "Recent advances in membrane distillation processes: Membrane development, configuration design and application exploring," *J. Memb. Sci.*, vol. 474, pp. 39–56, 2015.

[8] L. Ophek, L. Birnhack, O. Nir, E. Binshtein, and O. Lahav, "Reducing the specific energy consumption of 1st-pass SWRO by application of high-flux membranes fed with high-pH, decarbonated seawater," *Water Res.*, vol. 85, pp. 185–192, 2015.

[9] M. Baghbanzadeh, D. Rana, C. Q. Lan, and T. Matsuura, "Zero thermal input membrane distillation, a zero-waste and sustainable solution for freshwater shortage," *Appl. Energy*, vol. 187, pp. 910–928, 2017.

2. Literature Review

The demand for fresh water is increasing drastically in the modern decades. Engineers and scientists are discovering many novel methods and technologies to fulfill those demands. In the last century, they have given a promising method which could lead us to fulfill our needs efficiently, membrane separation. Membrane separation is the process of separating material, through pores or small gaps of the membrane. Itis classified by the size of pores and the driving force by which the material is separated. Reverse osmosis, ultra-filtration, micro-filtration and membrane distillation, these separation methods are the significant classifications under membrane separation. Membrane separation uses very little heat energy or does not use heat energy at all so it is more convenient and energy efficient than the conventional thermal separation methods which include distillation, crystallization, sublimation, etc. The fundamental principles of few membrane separation techniques will be explained briefly later. Though the membrane separation techniques yield good results there are some problems to be solved. The major concern is the characteristics of the membrane which must be used in the process. Many researches have been conducted to overcome these drawbacks. This thesis proposes some of the ways to improve membrane characteristics.

2.1 Principles of Membrane separation

Though there are many desalination processes, researchers concentrate on the membrane based separation processes nowadays due to their low energy consumption. Thus, today, membranes are used on a large scale to produce potable water from the sea[1]; to concentrate, purify, or fractionate macromolecular solutions[2]; to clean industrial effluents and recover valuable constituents[3]; in the food and drug industries and to remove urea and other toxins from the blood stream in an artificial kidney[4]. Membrane can to a certain extent be “tailor-

made", so that their separation properties can be adjusted to a specific separation task[5]. There are many kinds of membrane separation processes which are described as follows.

2.1.1 Reverse Osmosis

The phenomenon of osmosis occurs when pure water flows from a dilute saline solution through a membrane into a higher concentrated saline solution. The phenomenon of osmosis is illustrated in **Figure 2. 1** Osmosis and **Reverse Osmosis**[21]. A semi-permeable membrane is placed between two compartments. "Semi-permeable" means that the membrane is permeable to

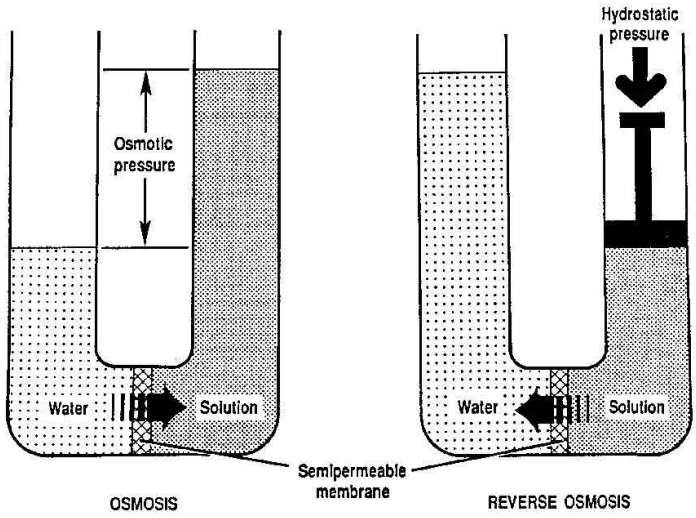

Figure 2. 1 Osmosis and Reverse Osmosis[21]

some species, and not permeable to others. Assume that this membrane is permeable to water, but not to salt. Then, place a salt solution in one compartment and pure water in the other compartment. The membrane will allow water to permeate through it to either side. But salt cannot pass through the membrane.

As a fundamental rule of nature, this system will try to reach equilibrium. That is, it will try to reach the same concentration on both sides of the membrane. The only possible way to reach equilibrium is for water to pass from the pure water compartment to the salt containing

compartment, to dilute the salt solution. **Figure 2. 1** also shows that osmosis can cause a rise in the height of the salt solution. This height will increase until the pressure of the column of water (salt solution) is so high that the force of this water column stops the water flow. The equilibrium point of this water column height in terms of water pressure against the membrane is called osmotic pressure. If a force is applied to this column of water, the direction of water flow through the membrane can be reversed. This is the basis of the term reverse osmosis. Note that this reversed flow produces pure water from the salt solution, since the membrane is not permeable to salt.

2.1.2 Pressure Driven Membrane Separation Processes

There are other pressure driven membrane processes than reverse osmosis. They are classified depending on the size of the solute (and the pore) as shown in Figure 2.2 [6]

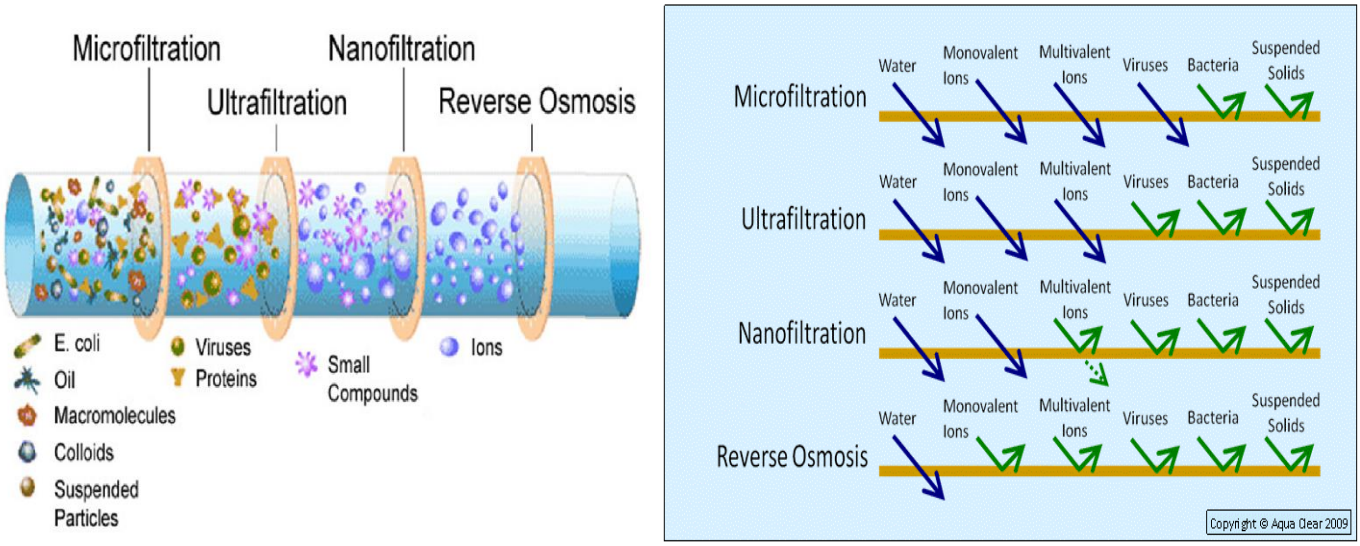

Figure 2. 2 Difference between various pressure driven membrane separation

2.1.3 Membrane Distillation

Membrane distillation is the emerging separation technology which might overcome some limitations of reverse osmosis. It is a thermally driven separation technique which uses the difference in vapour pressure induced by the temperature difference across the membrane. The membranes selected for this process should be hydrophobic to avoid the intrusion of liquid water into the pore. The principle of membrane distillation can be described as

1. Evaporation of feed solution in the liquid/vapour interface on the surface of the hydrophobic membrane
2. Diffusion of vapour through the pores of the membrane due to the difference in vapour pressure across the membrane
3. Condensation of vapour in the permeate side or externally.

The hydrophobic membrane allows the passage of vapours but completely block the passage of liquid water through the pore. Surface tension of the water prevents it from entering the membrane. There are many classifications in the membrane distillation. Because the process can take place at normal pressure and low temperature, membrane distillation could be used to solve various wastewater problems, to separate and recover chemicals, and to concentrate aqueous solutions of substances sensitive to high temperatures. The possibility of using solar, wave or geothermal energy, or existing low temperature gradients typically available in industrial processing plants is particularly attractive. There are many classifications in the membrane distillation. These classifications are based on the difference in condensation methods used to condense the permeate.

2.2 Different Configurations of Membrane Distillation

2.2.1 Direct Contact Membrane Distillation (DCMD)

In Direct Contact Membrane Distillation, the hot feed side is in direct contact with the membrane whereas the other side of the membrane is in contact with the cold permeate and due to their difference in vapour pressure, the vapour will pass through the membrane and will be condensed in the other side. This is the simplest configuration in the membrane distillation. This configuration has applications in desalination and concentration of aqueous solutions[7][8]. Even with its simple configuration it faces great difficulty to become commercialized. It also suffers from few disadvantages like heat loss due to conduction through the membrane which in turn decreases its thermal efficiency[9]. DCMD suffers a higher heat loss through conduction in comparison with other MD configurations[10]. **Figure 2. 3** shows a schematic of DCMD concept.

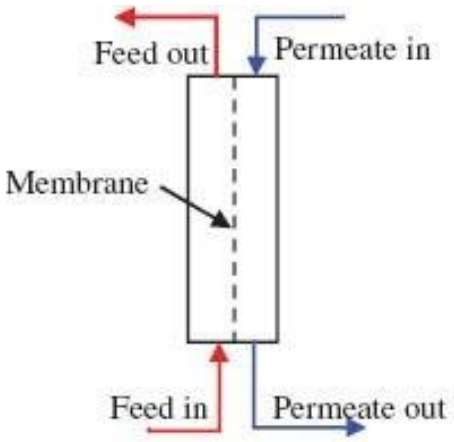

Figure 2. 3 Direct Contact Membrane Distillation [25]

2.2.2 Air Gap Membrane Distillation (AGMD)

In Air Gap Membrane Distillation, an air gap is introduced between the membrane and condensing surface. This MD configuration has similar setup in the feed/hot side as DCMD. The vapour from the hot side will pass through the air gap to condense at the plate cooled by the cooling water. Due to the presence of air gap, there is a mass transfer resistance but AGMD has less heat loss than DCMD. Usually, air gap will be thicker than the membrane which prevents heat loss and due to this more heat energy is used to evaporate water. Mass transfer and heat transfer in this configuration largely depends on the air gap. Due to low temperature difference across the membrane, this configuration requires larger surface area and yields lower flux[11][12]. Figure 2.4 shows a schematic picture of AGMD concept.

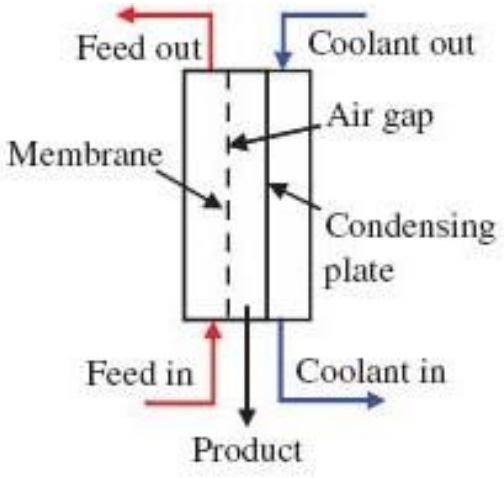

Figure 2. 4 Air Gap Membrane Distillation [25]

2.2.3 Memstill

Memstill is a novel configuration based on the energy efficient AGMD concept. In this design cold seawater, while passing through a condenser tube as a cooling media, is heated, before it enters into the vaporization tube, where the water evaporates. The vapour diffuses through the membrane pore and the air gap before reaching the condenser surface where it is

condensed. Memstill has the lowest thermal energy required among the other configurations (56-100 kWh/m^3) which would result in the highest gain output ratio (GOR) that has been ever reported[13]. Feed temperature should be within 80-90˚C and electrical energy required is about 0.75 kWh/m^3[14]

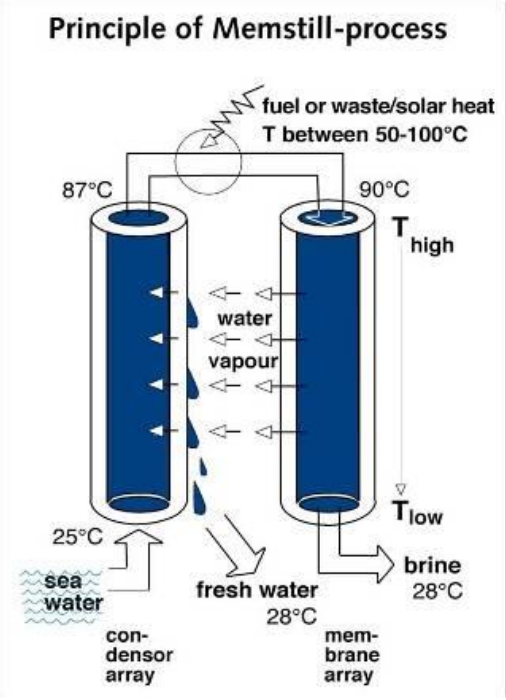

Figure 2. 5 Memstill Configuration [12]

2.2.4 Permeate/Liquid Gap Membrane Distillation (PGMD/LGMD)

PGMD has been configured in such a way to overcome the disadvantage of both AGMD and DCMD. In this configuration, air gap is replaced by a liquid which has been exposed to ambient atmosphere and pressure with a closed bottom. A thin foil is introduced between the permeate gap and coolant which increases the thermal resistance and increases effective

temperature difference across the membrane thus yielding higher permeate flux contrary to AGMD[15]. Also, this configuration makes sure that the permeate flux does not mix with the cooling stream which gives this system an advantage in comparison with DCMD. Due to this, it is possible to use different fluids for cooling purpose. In addition to this, at low feed temperatures, PGMD has lower specific thermal energy consumption compared to AGMD. **Figure 2.6** shows a schematic picture of PGMD concept.

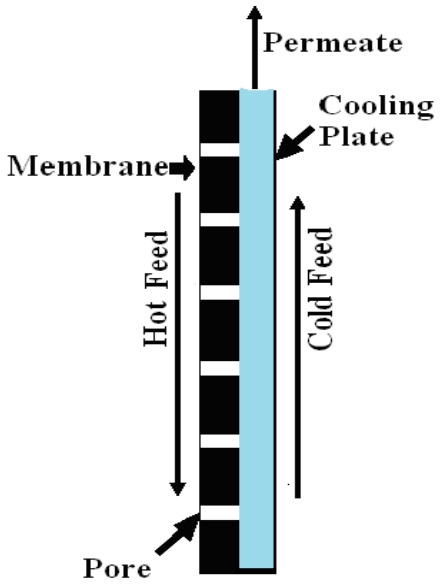

Figure 2. 6 Permeate Gap Membrane Distillation (PGMD) [12]

2.2.5 Sweep Gas Membrane Distillation (SGMD)

Sweep Gas Membrane Distillation is similar to AGMD but instead of a stagnant air gap, it has non-stagnant inter gas (stripping gas) which carries the vapour to an external condenser. Due to this configuration, the mass resistance in AGMD is eliminated, facilitating higher mass transfer coefficient and acquires lower heat loss than DCMD. This configuration is used to remove volatiles from an aqueous solution[16][17]. Due to the use of external condenser and

blower there is a high probability for increased capital cost which can be overcome by combining both AGMD and SGMD. In the AGMD configuration. If the air gap is replaced by sweep gas, then the permeate will be partially cooled by condensing stream in AGMD and remaining gas can be cooled by the external condenser. This configuration is called thermostatic sweep gas membrane distillation (TSGMD)[17]. Figure 2.7 shows a schematic picture of SGMD concept.

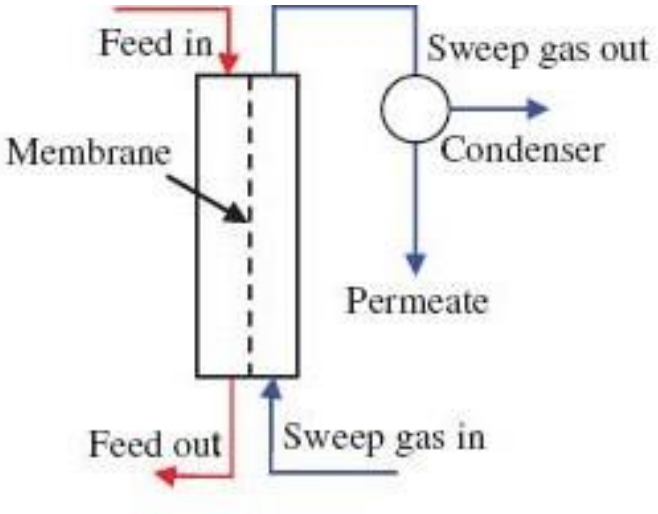

Figure 2. 7 Sweep Gap Membrane Distillation (SGMD) [25]

2.2.6 Vacuum Membrane Distillation (VMD)

Vacuum Membrane Distillation includes a vacuum pump at the permeate side to maintain

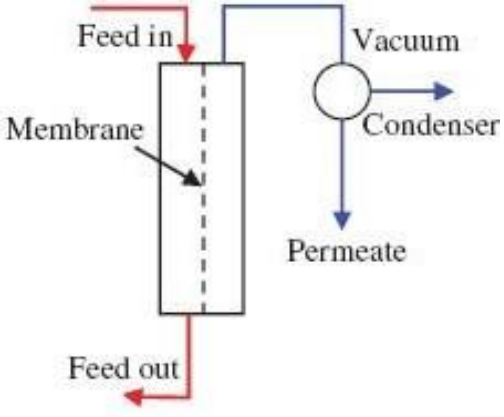

Figure 2. 8 Vacuum Membrane Distillation(VMD) [25]

vacuum which creates a vapour pressure difference between the feed and the permeate sides that acts as a driving force. To increase the mass transfer the pressure should always be maintained below the equilibrium vapour pressure of the feed. VMD is beneficial for removing volatiles from an aqueous solution[18][16]. In VMD, the water from feed side is vaporized at the surface of the membrane and it is diffused through the membrane due to vapour pressure difference across the membrane (Knudsen mechanism). To maintain this driving force, the permeate vapour should be removed continuously to be cooled externally. Since vapour pressure at permeate side is maintained near zero, VMD can give higher driving force at the same feed temperature compared to other MD configurations. VMD is an approach to reduce heat losses and to reach the higher vapour flow rates. It should be mentioned that the possibility of liquid penetration in this configuration is higher than the other configurations and a membrane with the smaller pore size should be employed[19]. **Figure 2.8** shows a schematic picture of VMD concept.

2.2.7 Vacuum Gap Membrane Distillation (VGMD)

VGMD (Figure 2.9) has a configuration very similar to PGMD that combines the configuration of VMD and AGMD, thus, the liquid gap is replaced with application of slight vacuum. The

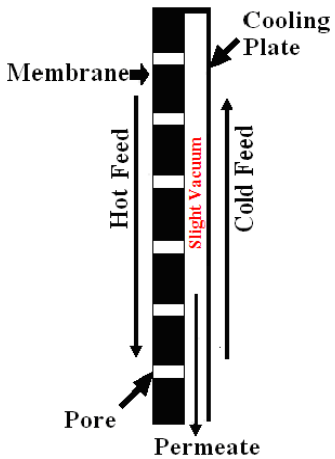

Figure 2. 9 Vacuum Gap Membrane Distillation (VGMD) [12]

vacuum can be given by external vacuum pump or air ejector[15]. Due to slight vacuum utilization, rather than high vacuum pressure as VMD, the electric energy could be greatly saved. Also, it is unnecessary to remove vacuum continuously in contrast to VMD. Hollow fibre membrane degassing of feed can be done to eliminate the loss of vacuum due to the presence of non-condensable liquids. At a very slight vacuum of 0.9 bar, VGMD has a performance between PGMD and AGMD in terms of permeate flux and specific thermal energy consumption. It is predicted to enhance its function by decreasing the pressure.

2.2.8 Multi-Stage and Multi-Effect Membrane Distillation (MEMD)

MEMD (Figure 2.10) is a modified configuration of AGMD under the concept of multistage and multi-effect. This configuration is built to increase the internal heat recovery. The permeate side is placed above the cold feed which serves as condensing agent and at the mean time gains some heat from the permeate. Thus, very little heat is necessary for the pre-heated feed which increases the heat energy efficiency.

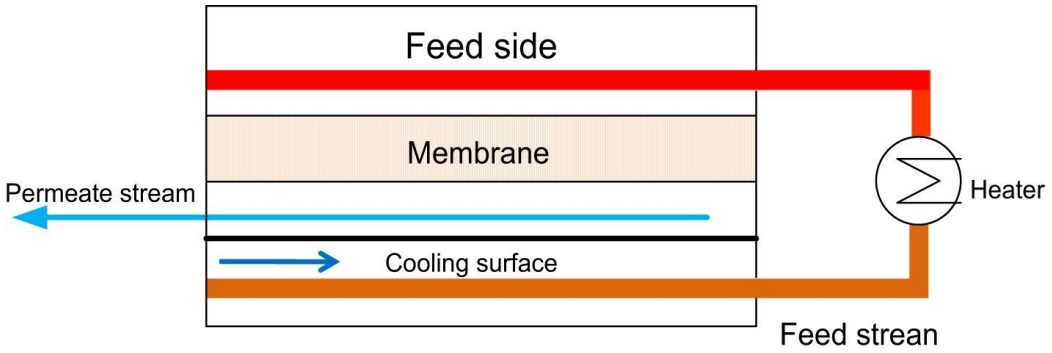

Figure 2. 10 Illustration of an AGMD configuration with internal heat recovery [29]

2.2.9 Multi-Effect Vacuum Membrane Distillation (MEVMD)

MEVMD (Figure 2.11) is a novel configuration of VGMD that is very similar to MEMD. This configuration has been successfully tested in a pilot scale[20]. A Memsys module consists of a steam raiser, multiple stages and a condenser. Vacuum is applied between each air gap which collects the vapour condensed by the next stage's feed which initializes a multiple effect phenomenon. Membranes which act as vapour channels are made from polytetrafluoroethylene (PVDF). Vacuum pressure varies within 0.1 to 0.3 bar in different stages[20]. The temperature of the feed solution must be between 60 C and 100˚C, whereas the cooling temperature is lower than 40˚C. Thermal and electrical energy consumption of Memsys module are within 175-350 kWh/$m^3$and 0.75-1.75 kWh/m^3, respectively.

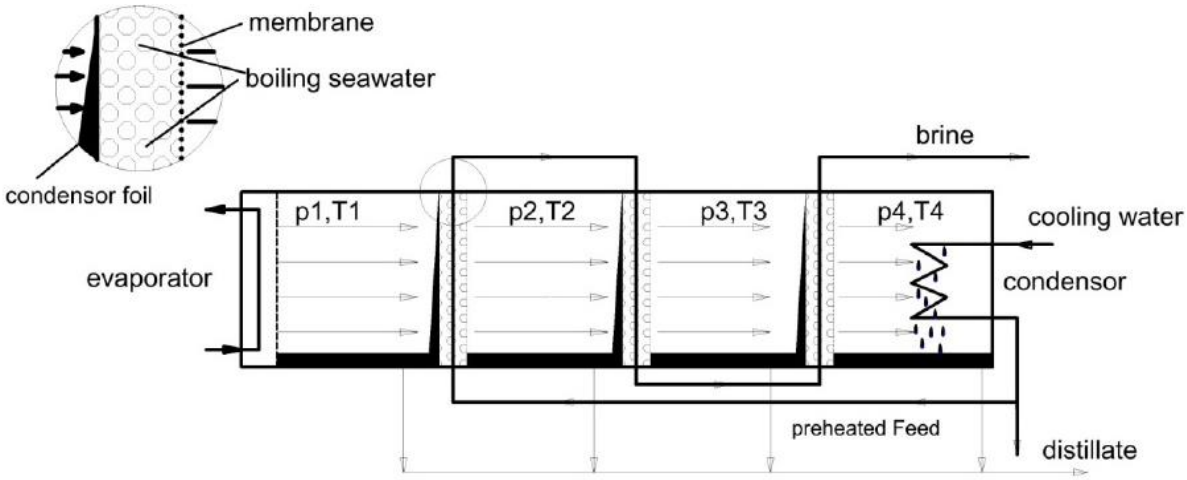

Figure 2. 11 Multi-Effect Vacuum Membrane Distillation (MEVMD) [21]

2.3 Membrane Characteristics in MD

MD process uses hydrophobic microporous membranes which have high thermal and chemical resistance at very high temperatures against acidic and basic solutions. In the following, some important characteristics of the membranes in a MD process are mentioned.

2.3.1 Liquid Entry Pressure (Wetting Pressure) of water

The maximum pressure that can be applied to feed fluid without permeation of the liquid is called Liquid Entry Pressure (LEP). Pore wetting (i.e. penetration of feed liquid into the membrane pores) occurs once the pressure becomes above the LEP of that membrane. The main factors which affect the LEP are solute concentration of feed solution, maximum pore size and hydrophobicity of the membrane. LEP depends on the nature of the organic solute, its concentration and feed temperature[22]. For example, when the liquid is aqueous ethanol solution, increasing the feed ethanol concentration linearly decreases the LEP.

Equation 1 is often used to show the relationship between LEP and hydrophobicity and pore size of the membrane, LEP[23].

$$\Delta P = P_f - P_p = \frac{-2B\gamma_l \cos\theta}{r_{\max}} \quad (1)$$

P_f and P_p are the hydraulic pressure on the feed and permeate sides, B is a geometric pore coefficient (equal to 1 for cylindrical pores), γ_l is liquid surface tension, θ and r_{max} are contact angle (between the solution and membrane surface) and maximum pore size, respectively. When the liquid is water and the solute is sodium chloride, the surface tension depends on the salt concentration and can be calculated by the following equation[24]:

$$\gamma_l = \gamma_{l,water} + 1.467 c_f \quad (2)$$

$\gamma_{,waterl}$ is the surface tension of pure water and equals to 72 mN/m at 25˚C. Regarding equation 1, a membrane with a high contact angle (equivalent to high hydrophobicity) and small pore size is highly desired to reach a higher LEP for the feed solution.

2.3.2 Membrane Thickness

Membrane thickness is a primary factor which gives mass transfer resistance to the flux across the membrane. Thus, in many cases, permeate flux is inversely proportional to the membrane thickness. Though the increase in thickness reduces the flux, it increases the resistance to heat loss by conduction, thus Laganà et al. proposed that optimum membrane thickness is in the range of 30-60 μm [25]. It is important to note that the membrane thickness affects all the MD configuration except AGMD, since its mass transfer is controlled by the thickness of the air gap. Even though membrane thickness can be measured by many instruments like micrometer and fractional caliper, due to their lack of accuracy, cross-sectional SEM images are often used to measure the thickness of the membrane more accurately.

2.3.3 Membrane Porosity and Tortuosity

Tortuosity expresses the discrepancy between the real pore structure and the straight cylindrical pore. Presence of tortuosity increases the residence time of vapour in the membrane which also increases the mass transfer resistance, and thus decreases the permeate flux. Macki and Meares suggested the following relation between porosity and tortuosity[26][21]

$$\tau = \frac{(2-\varepsilon)^2}{\varepsilon} \qquad (3)$$

Where τ is tortuosity and ε is porosity.

Ratio of volume occupied by the pores (void volume fraction) to the total volume of membrane is known as porosity (ε). Permeate increases whereas mechanical strength and heat loss by conduction decrease with an increase in porosity. Generally, membranes porosity varies

in between 30% and 85% [27]. Smolder–Franken equation is used for calculating the porosity. [28][29]

$$\varepsilon = 1 - \frac{\rho_m}{\rho_{pol}} \tag{4}$$

Where ρ_m is the density of membrane and ρ_{pol} is the density of the polymers

2.3.4 Mean pore size and pore size distribution

Pores are the void space in the membrane which enhances the permeate flux by allowing the vapour to pass through them. But since the pore size is often not uniform, mean pore size is obtained from pore size distribution to find an approximate value for the permeate flux. Permeate flux increases but LEP decreases with an increase in the pore size, thus an optimum size should be chosen. Usually for the membranes used in MD, the pore size will be in between 100 to 1000 nm[27][30]. There are many methods to measure the pore size of the membrane. The common methods used are SEM image analyses, AFM and gas permeation test[31].

2.3.5 Thermal conductivity

Generally, membrane distillation requires membranes with high thermal resistivity to decrease the sensible heat transfer and to increase the interfacial temperature difference, which results in higher flux[13]. Thermal conductivity of a membrane (k_m) can be calculated using the equation 5[32],

$$k_m = \left(\frac{\varepsilon}{k_g} + \frac{1-\varepsilon}{k_s} \right)^{-1} \tag{5}$$

Where k_s and k_g are polymer and gas thermal conductivities. Due to negligible difference in their thermal conductivity, the water and vapour are assumed to be homogenous and gas thermal conductivity at the temperature around 40 ˚C is calculated according to equation 6 [12],

$$k_g = 1.5 \times 10^{-3} \sqrt{T} \qquad (6)$$

T denotes the absolute temperature. Thermal conductivity of the polymer k_s depends on the temperature, degree of crystallinity and the shape of the crystal[19]. Thermal conductivities of most hydrophobic polymers are similar. Equation 7 has been suggested to calculate the thermal conductivity of PTFE.

$$k_s = 4.86 \times 10^{-4} T + 0.253 \qquad (7)$$

2.4. Membrane fabrication

Membranes used in MD should have some specific properties like high hydrophobicity, thermal and chemical resistance, mechanical strength and low surface tension[33]. It is very difficult to find a single polymer which excels in all these properties. For this reason, researchers are still debating on the method of fabricating membranes with optimal properties. Polytetrafluoroethylene (PTFE) has the highest hydrophobicity, stability and oxidation resistance but due to its high thermal conductivity it has uncontrollable heat loss. Polymers like fluorinated ethylene propylene (FEP) can be used to produce highly hydrophobic membranes and polyacrylonitrile (PAN) can be used to produce highly hydrophilic membranes but they have complexity in dissolution of polymer. PVDF and polypropylene (PP) are widely used in MD due to their high hydrophobicity and simplicity in dissolution of polymers. Though our research mainly focus on phase inversion method for membrane fabrication, various other methods are also discussed in the following sections.

2.4.1 Phase Inversion Method

Phase inversion is defined as change of homogeneous polymer solution from liquid to solid. This phase change can be attained through various processes like thermally induced phase separation (TIPS), vapour induced phase separation (VIPS), immersion precipitation (IP) and controlled evaporation of solvent from a three-phase system.

2.4.1.1 Thermally Induced Phase Separation (TIPS)

Thermally induced phase separation is one of the common methods used to fabricate membranes. In this method, a solvent of high boiling point is used to dissolve the polymer at high temperature and the solution is then cast on top of the suitable support and allowed to cool down. The phase separation is induced while the cast film is cooling and the polymer will solidify into a semi-crystalline form. When the solvent is removed, micro pores are created in the membrane. TIPS involve removal of thermal energy to induce phase change. The polymer crystallization determines the membrane morphology, pore size, mechanical strength and permeate flux. Solvent used in this process plays the key role in crystallizing the polymer in addition to the cooling and quenching process. Dibutyl phthalate is used as the solvent for PVDF membrane in TIPS[34]. It has been confirmed that increasing the cooling rate will decrease the crystallization process[35].

2.4.1.2 Vapour Induced Phase Separation (VIPS)

In this method, the dope solution consisting of polymer and solvent is used to cast into a film. The cast film is then immersed in a non-solvent (usually water) which is miscible with solvent. The phase change will take place while the exchange of solvent with non-solvent occurs. The rapid mass transfer will induce the formation of a dense top layer surface of the membrane. In the vapour-induced phase-separation (VIPS) process, the cast film is first exposed to humid

air prior to immersion in the coagulation bath. Typically for these systems, water is a non-solvent such that the water transfer caused by the humid air exposure step leads to phase separation. The extent and rate of water transfer can be controlled by adjusting the velocity, relative humidity and temperature of the air as well as the exposure time. By a sensible combination of these variables, membranes with large pores at the top surface can be obtained[36][37]–[40].

2.4.1.3 Immersion Precipitation

Immersion precipitation is another common and simple method used in fabrication of membrane. This method is very similar to VIPS but in this process the cast solution is not exposed to humid air. Instead, it is immersed in the bath immediately. The phase inversion and the coagulation takes place inside the bath due to the exchange of solvent to non-solvent. Many researchers have worked on this system to enhance the membrane performance by changing various parameters in this method. To produce super hydrophobic membranes Kuo et al.[41] changed the non-solvent from water to alcohol and Yang et al.[42] prepared membranes in the coagulant bath at ambient temperature only to improve the membrane performance other techniques like changing the temperature of the coagulation medium, immersing the cast solution into the bath at different timing (Penetration time)[43] and using different solvents[44] were tried.

2.4.2 Sintering

This is another widely used fabrication process of membrane. Mostly this method is used to prepare membrane with PTFE polymer. PDVF can also be used in this method. Glasrock Product Inc. and Solvay et al. [45], [46] have obtained the patent on preparation of porous PVDF membrane using sintering technique. In this method, the polymer powder of particular size is heated to the temperature where it gets sintered without being liquefied. This sintered polymer

will form the porous membrane. Methyl isobutyl ketone(MIBK) was used to disperse PVDF powder and the dispersion was broken down into small pieces which were sintered to form porous PVDF membrane[46]. Porosity of the membranes prepared by this method is in range of 10% - 40% and their pore size is in the range of 200nm to 20µm[13].

2.4.3 Stretching

In this method, the polymeric powders are heated until they almost reach their melting point. They are then extruded to form polymeric layers and stretched rapidly to form porous

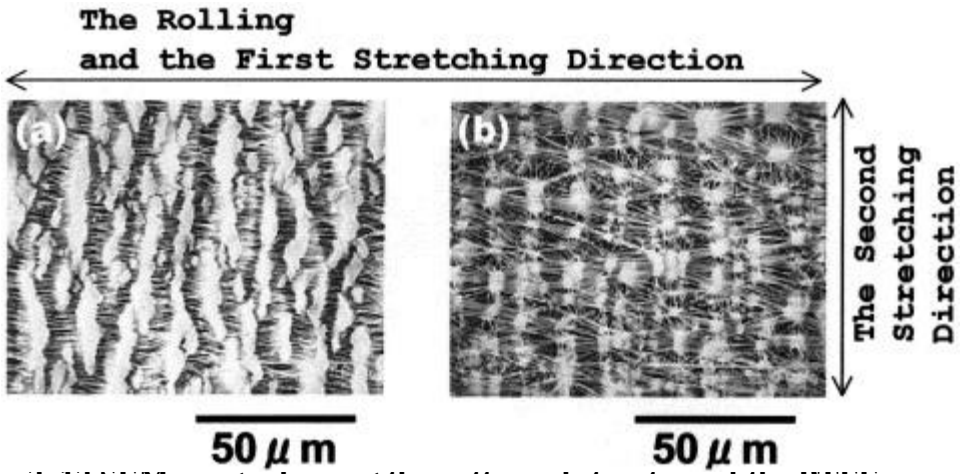

Figure 2. 12 SEM image showing the patterned structure of the PTFE porous membranes produced by the stretching operation: (a) uniaxially stretched membrane, and (b) biaxially [47]

membranes[47], [48]. In this process, stretching can be done in two steps; first, cold stretching to nucleate the micro pores in the precursor followed by hot stretching to increase the final pore structure of the membrane. The physical properties of the material like crystallinity, melting point and tensile strength and applied processing parameters control the final pore structure[47]. Membranes formed by this method has porosity around 90%[13].

2.4.4 Track etching

In this method, nonporous polymeric film is irradiated with heavy ions to form linearly damaged track across the polymeric film. The main advantage of this system is obtaining precise

control on pore size distribution. Pore size and pore density are independent and can be controlled to get few nanometers to tens of micrometer and $1–10^{10}$ cm^{-2}, respectively. Duration of radiation determines the membranes porosity and etching time and temperature controls the pore size [49]. In PVDF membrane track etching, the polymer film is exposed to the radiation particles applied perpendicular to the material surface. Thereafter etching in an acid or alkaline bath follows [50].

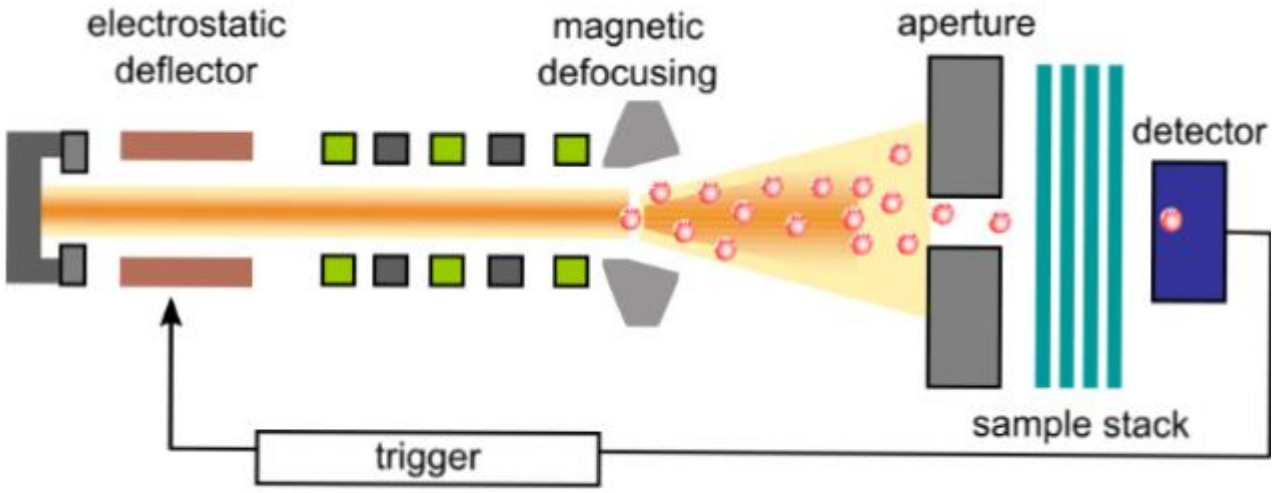

Figure 2. 13 Schematic showing single ion-irradiation setup used to fabricate track etched membrane [50]

2.4.5 Electrospinning

Electrospinning is a comparatively new technique to fabricate porous membranes for various applications including filtration and desalination. A high potential is applied between the polymer solution droplet, and the grounded collector. When the electrostatic potential becomes sufficiently high to overcome the surface tension of the droplet, a charged liquid jet is formed. The unique features of these fibrous membranes are controllable aspect ratios (aspect ratio = L/d; L—length of the fiber and d—diameter of the fiber) and morphology of the nano-/micro-fibers

which is achieved by varying the solution viscosity, environmental conditions, applied electric potential and the flow rate of the solution[51]. Porosity, pore size distribution, hydrophobicity

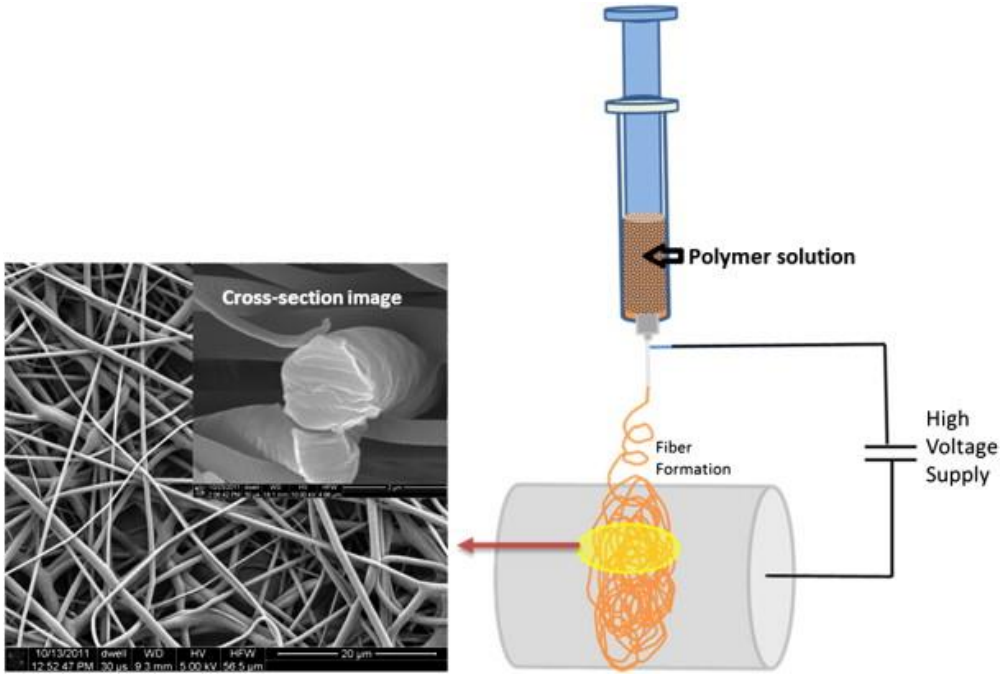

Figure 2. 14 Schematic showing electrospinning of polymer solution [28]

and surface morphology of the electrospun mats are controlled by the fiber diameter and its morphology [52]. Due to the precise control on the fiber size, shape and morphology electrospun fibrous membranes have been used for filtration and MD processes [52]–[54]. Zong et al. investigated the effect of polymer solution viscosity, applied potential, solution feed rate and ionic salt addition (to improve the conductivity of solution) on the fiber diameter and nanostructured morphology [55].

2.5 Heat and Mass transfer in MD

In membrane distillation, the vapour from the feed moves through the air and condenses at the cooled surface. The mass transfer is affected by diffusion and free convection due to the

concentration difference of vapour. Heat conduction and mass transfer of membrane distillation also affect the heat transfer. In MD, a coupled heat and mass transfer occurs and an enthalpy flux exists across the hydrophobic membrane from the feed to the permeate. Both heat and mass transfer are explained briefly in the following.

2.5.1 Heat transfer in MD

Heat transfer from feed bulk to the permeate side includes two steps. First of all, heat is transferred from the hot side to the cold side through the membrane as sensible heat and latent heat. Sensible heat is conducted across the membrane, while the latent heat is carried out by the vapour molecules from the hot side to the cold side through the membrane pores. As the result of sensible and latent heat transfers, a temperature difference between boundary layer and bulk flow in the hot side is provided that would result in the second step. In the last step, heat is transferred from the bulk feed to the hot side boundary layer by the convection mechanism. It is worth to mention that heat transfers in both steps are equal. The above mentioned is quantitatively stated below.

Heat transfer via convection in the feed boundary layer:

$$Q_f = h_f (T_f - T_{f,m}) \tag{8}$$

Where h_f represents heat transfer coefficient at the feed boundary layer. T_f is the temperature of the bulk feed and $T_{f,m}$ is the temperature at the membrane surface on the feed side.

Heat transfer across the membrane via conduction and vapour molecules movement:

$$Q_m = \frac{k_m}{\delta}(T_{f,m} - T_{p,m}) + J\Delta H_v \tag{9}$$

Where k_m, δ, J and ΔH_v are membrane thermal conductivity, membrane thickness, permeate flux and heat of vaporization, respectively. $T_{p,m}$ is the temperature at the membrane surface on the permeate side,

$$Q_f = Q_m \qquad \rightarrow \qquad \frac{k_m}{\delta}(T_{f,m} - T_{p,m}) + J\Delta H_v = h_f(T_f - T_{f,m}) \tag{10}$$

It should be noted that the above equations are employed for heat transfer analysis at the hot side and across the membrane for all the MD configurations except VMD that heat conduction through the membrane is not applicable in that arrangement.

Surface temperatures of both sides of membrane ($T_{f,m}$ and $T_{p,m}$) cannot be obtained experimentally, and a mathematical iterative model according to equation 11 has been proposed by Termpiyakul et al [56]to estimate them.

$$\begin{cases} T_{f,m} = T_f - \dfrac{J\Delta H_v + k_m(T_{f,m} - T_{p,m})/\delta}{h_f} \\ T_{p,m} = T_p - \dfrac{J\Delta H_v + k_m(T_{f,m} - T_{p,m})/\delta}{h_p} \end{cases} \tag{11}$$

Heat transfer at the permeate side of the DCMD, SGMD and VMD could be given by the following equation:

$$Q_p = h_p(T_{p,m} - T_p) \tag{12}$$

Where h_p and T_p are the heat transfer coefficient and the bulk temperature on the permeate side.

As for AGMD configuration the heat transfer includes two parts. The first is related to heat transfer across the stagnant air gap that occurs by conduction and vapour molecules transport, and the second is for heat convection through the permeate boundary layer.

$$Q_{AG} = \frac{k_{AG}}{l_{AG}}(T_{p,m} - T_{film}) + J\Delta H_v = Q_p = h_p(T_{film} - T_p) \tag{13}$$

Where T_{film} – temperature at film, heat transfer coefficient (h_p) in the condensate film on a vertical plate is obtained from the equation 13 [57].

$$h_p = \frac{2}{3}\sqrt{2}\left(\frac{k_{film}^3 \rho^2 g \Delta H_v}{\mu L(T_{film} - T_p)}\right)^{\frac{1}{4}} \tag{14}$$

If the air gap distance is over 5 mm, free convection would take place between two vertical plates across the air gap region and heat transfer coefficient could be obtained from the following equation:

$$Nu = c(\mathrm{Pr}\,Gr)^n\left(\frac{l}{L}\right)^{\frac{1}{9}} \quad , \quad \begin{cases} 10^5 < Gr < 10^7 \rightarrow \begin{cases} c = 0.07 \\ n = 1/3 \end{cases} \\ 10^4 < Gr < 10^5 \rightarrow \begin{cases} c = 0.2 \\ n = 1/4 \end{cases} \end{cases} \tag{15}$$

2.5.1.1 Thermal efficiency and heat loss

In a MD module, thermal efficiency (Π) is defined as the ratio of the heat transfer by latent heat of vaporization to the total (latent and sensible) heat transfer[19]. Usually, thermal efficiency is enhanced by increasing the feed temperature, feed flow rate and membrane thickness. On the other hand, it would decrease with an increase in solute concentration in

feed[58]. Equations 16 and 17 are used to determine thermal efficiency of the DCMD and AGMD[59], respectively.

$$\Pi = \frac{J\Delta H_v}{\frac{k_m}{\delta}(T_{f,m} - T_{p,m}) + J\Delta H_v} \tag{16}$$

$$\Pi = 1 - \frac{\alpha T_a^{-2.1}}{\lambda}\left(\frac{(T_f - T_p)c_p}{\alpha T_a^{-2.1} + \beta} + \frac{k_a}{l}\right) \tag{17}$$

α and β are obtained experimentally for an air gap distance less than 5 mm, and T_a is average MD temperature between 30-80˚C. c and k_a are specific heat and air gap thermal conductivity, respectively.

According to Martinez-Diez et al. [60], heat loss reduces by increasing the feed temperature and flow rate. Three sources of heat loss in a MD module are: presence of air inside the membrane pores, heat loss across the membrane via conduction and heat loss due to temperature polarization. To minimize heat loss in a MD module, degassing of feed solution, increasing the membrane thickness, providing an air gap between the membrane and the condensation surface and working within a turbulent regime have been suggested[19]. Using heat recovery in a MD configuration results in better performance for the process, however it needs a heat exchanger and membrane with larger area that increases capital costs.

2.5.2 Mass transfer in MD

Mass transfer in MD includes three steps. First of all, liquid feed solution vaporizes in liquid-gas interface. Second vapour molecules go through the membrane pores toward the cold interface as a result of vapour pressure difference, and finally, according to the MD

configurations, vapour molecules would be condensed in a liquid stream, stagnant or moving gas or reduced pressure space. Thus, there are two main factors that control mass transfer. The first is vapour pressure difference and the second is the membrane permeability. Mass transfer in MD is limited by mass transfer through the membrane if fluid dynamics on hot and cold sides of the membrane shows a good condition.

A global transport equation (18) for mass transfer through the membrane is considered that correlates mass flux to vapour pressure gradient across the membrane by introducing a membrane coefficient (C_m) that is related to the dominant mechanism for mass transport through the membrane.

$$J = C_m(P_f - P_p)$$

(18)

Where P_f and P_p are the vapour pressure at the membrane feed and permeate surfaces, respectively, and could be found from the Antoine equation.

There are several points that should be considered in mass transfer through the membrane:

1. Since the porosity of a membrane is always less than 100%, the effective area for mass transfer is lower than that of the total area of the membrane.
2. Since the membrane pores do not go straight through the membrane, vapour molecules travel a greater path than the membrane thickness.
3. Resistance to diffusion increases by the inside walls of the pores due to a decrease in momentum of the vapour molecules.

Regarding the presence or absence of air molecules inside the membrane pores, there are three basic mechanisms which are responsible for mass transfer through the membranes: Knudsen diffusion (K), Poiseuille or viscous flow (P) and Molecular diffusion (M). A combination of these mechanisms could happen, which is known as transition mechanism. Knudsen region means the molecule-pore wall collisions are dominant over molecule-molecule collision. Molecular diffusion means the vapour molecules collide with each other, while a Knudsen/Molecular diffusion mechanism means the transition where Knudsen and molecular diffusion occur simultaneously. In Poiseuille flow (viscous flow), the gas molecules act as a continuous fluid driven by a pressure gradient[19]. To determine which mechanism is dominant in mass transfer across the membrane, Knudsen number is defined by the following equation:

$$Kn = \frac{\lambda}{d}$$

(19)

λ is the mean free path of the molecules (the average distance traveled by a molecule between consecutive collisions) and d is the mean pore size of the membrane. λ is obtained from the kinetic theory and using the following equation:

$$\lambda = \frac{k_B T}{\sqrt{2}\pi P d_e^2} \qquad (20)$$

k_B, T and P are Boltzmann constant, absolute temperature, and average pressure within the membrane pores, respectively.

Kn is used to determine the dominant mechanism for mass transfer through the membrane. A large Kn means that the mean free path of vapour molecules is large in comparison with the

membrane mean pore size, while a small amount of *Kn* proves that membrane have the large pore size.

In AGMD configuration, mass transfer through the stagnant air is controlled by molecular diffusion and vapour molecules are transferred from the cold surface of membrane to the condensation film by using the above-mentioned mechanism. Mass transfer layer in the stagnant air gap is equal to gap thickness. Flux in air gap layer is calculated by equation 21.

$$N_{Air\ \ Gap} = \frac{D}{RT}\frac{P}{l_{Air\ \ Gap}P_{lm}}\Delta P_{Air\ \ Gap} = C_{Air\ \ Gap}\Delta P_{Air\ \ Gap} \tag{21}$$

The total vapour flux in an AGMD would be estimated by the following equation:

$$N_{Vap-AGMP} = \left(\frac{1}{C_m} + \frac{1}{C_{Air\ \ Gap}}\right)^{-1} \Delta P_{Total} \tag{22}$$

Considering the equation 8, C_m, membrane coefficient, is a function of temperature, pressure, membrane structure and diffusing species, while the driving force (P_f - P_p) is a function of liquid solution temperature and compositions at hot and cold membrane sides. As well, it can be concluded that in a MD process, flux is enhanced by increasing the pore size and membrane porosity, and by reducing the membrane tortuosity and thickness. However, when the thickness of membrane decreases, sensible heat loss from the hot side to cold side would increase. Therefore, an optimum thickness for the membrane should be found.

2.6 Other Transport phenomena in MD

2.6.1 Temperature and concentration polarization

The feed solution in MD evaporates at the membrane hot surface and creates a heat transfer boundary layer in the hot side. As well, by condensing the vapour molecules on the other side, the permeate heat transfer boundary layer would be generated on the cold side. The presence of boundary layers caused a temperature difference between the liquid-vapour interface and bulk fluids to be produced that is known as temperature polarization. It is introduced by the following relation:

$$\psi = \frac{T_{m,f} - T_{m,p}}{T_f - T_p} \tag{23}$$

On the other hand, temperature polarization is defined according to the equation 24 for a VMD module[7]:

$$\psi = \frac{T_f - T_{m,f}}{T_f - T_p} \tag{24}$$

Actually, temperature polarization shows the effect of heat transfer boundary layers on total heat transfer resistance of the system[19]. It means by reducing the boundary layer resistances, temperature difference between the liquid-vapour interface and bulk fluids comes close together and ψ approaches 1. In addition, if the heat transfer is controlled by the boundary layer resistances, system approaches a high degree of temperature polarization and ψ becomes zero. According to [19](Alkhudhiri et al., 2012), for DCMD arrangements, ψ is within 0.4-0.7. It is worth to know that temperature polarization is more important at high concentration, high

temperature and low feed velocity, when the boundary layer resistances become greater. Usually, by introducing turbulences using spacer materials, temperature polarization could be reduced.

Concentration polarization is stated according to equation 25 as the increase of solute concentration on the membrane surface to the solute concentration of the bulk, and is shown by Φ.

$$\Phi = \frac{C_m}{C_f} \tag{25}$$

Solute concentration on the membrane surface is obtained from the following equation[19]:

$$C_m = C_f \exp(\frac{j}{\rho K}) \tag{26}$$

ρ and K are liquid density and mass transfer coefficient, respectively.

Since the accumulated solute on the membrane surface produces a diffusive flow back to the feed[19], in modeling purposes, concentration polarization and fouling should be taken into account, and vapour flux cannot be estimated only by Knudsen, molecular and Poiseuille flow mechanisms, due to the differences between the properties of boundary layer at the membrane surface and the bulk solution.

2.6.2 Fouling

Fouling means the creation of an additional layer on the membrane surface formed with the particles present in the liquid solution. It can be biological fouling (by bacteria) or scaling as the result of high solute concentration. Fouling and scaling cause the membrane pores to be blocked, and it would reduce effective area of the membrane, and finally decrease permeate flux.

Furthermore, it acts as an additional resistance against heat transfer. As well, it may cause a pressure drop and higher temperature polarization effects.

The following equation is used to describe heat transport in the additional layer that is created by fouling. Heat is transferred through the layer via conduction.

$$Q_{fouling} = \frac{k_{fouling}}{\delta_{fouling}} (T_{f,fouling} - T_{f,m}) \tag{27}$$

Fouling highly depends on membrane and feed solution properties, module geometry and operating conditions[61]. It can be inhibited by using pre-treatment methods or membrane cleaning. In addition, working at low temperature with high feed flow rate results in a decrease in tendency to the fouling.

2.7 Nanocomposite for enhanced membrane distillation

After recognising MD as the best configuration to yield better results with low energy consumption and higher salt rejection, works were focused to increase the configuration's efficiency higher than before. The two-major problem that were faced by MD configuration from commercializing were higher thermal energy consumption and membrane cost. Casting a highly efficient and low-cost membrane has always been an challenge for all the membrane processes. Thus, many works were done to increase the efficiency of the membrane and to find a perfect membrane for MD configurations. One of the main and effective method that have been found so far was to add nanoparticle additives in the dope solution which increases the membrane morphology and characteristics. Even though the effects of nanoparticles on MD have not been established very thoroughly as they have been on other conventional methods like RO, UF, NF

etc. some researches have been done which assure that the addition of nanoparticles yield better and positive results.

Some of the major researchers like Dumée et al. and Koo et al. [62]–[66] have done significant work in this area and has provided that, the addition of nanoparticles increases the permeate flux, salt rejection, pore size and able to obtain high porosity (~90%). The application of nanoparticles mixed matrix membranes in MD will be reviewed in the following section.

2.7.1 Effects of Nanoparticles on the MD membranes

2.7.1.1 Porosity and Mean pore size

In recent works, Baghbanzadeh et al.[67][68] demonstrated that addition of nanoparticles increases the pore size than the neat PVDF but the effect will be different depending on the nanoparticles. In his work, he showed that the addition of CuO nanoparticles increased till 2wt% after which the pore size started decreasing but whereas in case of hydrophilic SiO_2 the pore size increased till 9wt%. The optimum concentration at which the membrane get the largest pore size depends on the type of nanoparticles used in it. In another work, Efome et al.[69] has also proved that the addition of nanoparticles which in his case hydrophobic SiO_2 increased the pore size of the membrane and reached its optimum at 7wt%. But in case of porosity it shows that addition of hydrophilic nanoparticles (CuO, SiO_2) increases with the increase in nanoparticle concentration but shows the opposite in addition of hydrophobic nanoparticles (SiO_2). In another work, Kim et al.[70] used a sol-gel reaction of tetramethylorthosilicate (TMOS) followed by thermal treatment of the membrane to incorporate silica nanoparticles in electro-spun nano-fibrous PVDF membranes. It was showed that membrane porosity decreased with concentration of TMOS but after thermal treatment, due to the increase of fiber diameter through membrane shrinkage that

increased the porosity with increase in concentration [71]. Also, Hou et al.[72] showed that mean pore size decreases as a result of the addition of the $CaCO_3$ nanoparticles but the porosity of the membrane increased till the optimum concentration beyond which it decreased due to the agglomeration of nanoparticles. In his another, work Hou et al.[73] confirmed that addition of CaCO3 narrowed the pore size distribution with increase in concentration. In another work, it was reported that the mean pore size and porosity of the flat sheet membrane with TiO_2 coating and fluorosilanization remained almost unchanged in comparison with the neat PVDF membrane [74].

2.7.1.2 Roughness

There were several works in which surface roughness of an MD membrane increased with the addition of nanomaterials into the host polymer [70][72][74]. However, based upon the results in the work of Baghbanzadeh et al. and Efome et al.[67][69] membrane surface became smoother upon the introduction of the CuO nano-additives to the PVDF membrane, however, as the filler concentration was elevated, surface roughness increased.

2.7.1.3 Water contact angle

Efome et al.[69] showed that the addition of hydrophobic SiO_2 nanoparticle increases the surface contact angle with increase in nanoparticle concentration. He obtained higher surface contact angle above 90^o at the optimum concentration. Baghbanzadeh et al.[67] showed that hydrophilic CuO nanoparticles could increase the surface contact angle of the PVDF membrane at the medium concentrations. Hou et al. also reported that inorganic hydrophobic modified CaCO3 nanoparticle increases the hydrophobicity of a PVDF membrane[73]. Hydrophobic nature of carbon nanotubes [75] or thermal treatment of the membranes after the addition of

hydrophilic TiO_2 nanoparticles resulted in more hydrophobic membranes. At concentration less than that of the maximum, the contact angle paralleled the roughness behavior but above that concentration the contact angle decreased because of the presence of the hydrophilic nanoparticles over the membrane surface.

To develop a super hydrophobic surface, reducing the surface free energy via the functionalization with low surface energy materials, or creating a hierarchical nanostructure surface morphology through multilevel surface roughness could be applied. To produce a super hydrophobic DCMD membrane, a microfiltration PVDF membrane was modified via roughening its surface by coating with TiO_2 nanoparticles through a low temperature hydrothermal process, and then reducing surface energy through surface fluorosilanization[74]. Introducing TiO_2 nanoparticles into the virgin membrane reduced the water contact angle, but after fluorosilanization, a super hydrophobic membrane with the water contact angle of more than 160˚ and self-cleaning properties was obtained.

2.7.1.4 Morphology

Pure PVDF membrane has two different structures in it which includes the finger like layer on the top and a sponge like layer on the bottom. Baghbanzadeh et al. showed that addition of hydrophilic nanoparticle like CuO and SiO_2 increases the size of finger like layer by diminishing the size of sponge like layer[67][68]. But in a similar study, Efome et al. demonstrated that addition of hydrophobic SiO_2 thickens the sponge like layer[69]. Hou et al.[73] reported that at low concentration, hydrophobic modified $CaCO_3$ particles acted as the nucleating agents increased the rate of phase inversion, and brought about a flat sheet membrane with higher porosity, larger mean pore size, and larger micro-pores within the sponge-like layer.

But at high concentrations, excess amounts of the nanoparticles agglomerated, acted as the anti-nucleating agents, which resulted in a membrane with dense structure and smaller mean pore size, that could reduce the membrane permeability. Hou et al.[72] demonstrated that using hydrophobic modified CaCO3 nanoparticles optimized the sandwich-like morphology of the neat PVDF membrane, while mean pore size decreased as a result of the nanoparticle incorporation.

2.7.2 Performance improvement by addition of Nanoparticle in MD membranes

2.7.2.1 Liquid Entry Pressure of water (LEPw)

Hou et al.[73] showed that incorporation of nanoparticles increases the LEPw of the membrane but he revealed that there was a threshold concentration above which the LEPw began to decrease. Similar trend was reported by Baghbanzadeh et al in his work with hydrophilic CuO membranes for a vacuum membrane distillation(VMD). Efome et al. has also reported that the maximum LEPw was obtained at 7wt% of hydrophobic SiO_2 above which the LEPw started decreasing. Although there were decrease in LEPw, the nanoparticle incorporated membranes always exhibit LEPw higher than the minimum pressure needed to operate in MD configuration.

2.7.2.2 Permeability

Gethard et al.[75] showed that incorporation of carbon nanotube in neat PP membrane increases the flux in sweep gas membrane distillation (SGMD). Carbon nanotubes changes the vapour-membrane interactions and act as the sorbent sites for vapour transport. Also, CNIM composite membrane exhibited higher mass transfer coefficient than the unmodified PP membrane, which was due to an increment in the diffusion coefficient. In another study, Bhadra et al.[76] reported that incorporation of carboxylated carbon nanotube in PP membrane increases the permeability and water flux compared to unmodified PP membranes. Carboxylation

improved interactions between the nanotubes and polar water vapour molecules, resulting in enhanced desalination efficiency. Hou et al.[73][72] reported the same trend he observed in the porosity and pore size for the flux and thermal efficiency. He observed a threshold concentration of PVDF/$CaCO_3$ hollow fibers and flat sheet membranes. The membrane with optimum concentration showed higher flux and thermal efficiency due to the formation of thinner skin layer. He also reported that the durability of the membrane was enhanced by the addition of $CaCO_3$ nanoparticles, which attributes to the narrow pore size distribution. In a similar work, Baghbanzadeh et al.[67][68] showed that the incorporation of nanoparticles like CuO, $CaCO_3$, Hydrophilic SiO_2 significantly increases the permeate flux than the neat PVDF membranes. In his work, he compared the effect of CuO and $CaCO_3$ nanoparticles and proved that the former yields higher permeate flux than the latter. Efome et al.[69] also showed the hydrophobic SiO_2 yields higher flux than the neat PVDF. Despite the type of nanoparticles used, the permeate flux always higher than the neat membranes.

2.7.2.3 Rejection and Fouling

Gethard et al.[75] reported that immobilization of carbon nanotubes on the pores of a PP membrane results in an increment in its rejection performance. Since CNTs act as both molecular transporters and sorbents, they can enhance the permeability of the target component over the others, thus increasing its selectivity. Hou et al.[73] also demonstrated that CaCO3 nanoparticles enhance the rejection performance of a PVDF membrane. According to Baghbanzadeh et al.[67][68], the increase in the water permeability was without any compromise in the salt rejection and both the neat and PVDF-nanocomposite membrane showed a perfect rejection of NaCl (99.99%). The same was reported by Efome et al.[69] with hydrophobic SiO_2 incorporated membranes.

Razmjou et al.[74] reported, permeate (water) of the super hydrophobic membrane of PVDF/TiO_2 had higher quality compared to that of the neat PVDF membrane

because of the partial pore wetting in the neat membrane. Moreover, the treated membrane possessed higher flux recovery after chemical cleaning of the membrane, which confirmed its better antifouling performance.

According to the discussion here, the incorporation nanoparticles always yields better performance. Despite the kind of nanoparticles, both hydrophobic and hydrophilic nanoparticles enhance the flux and pore size of the membrane. Specifically, hydrophilic nanoparticles give significantly higher permeate flux, pore size, porosity and enhance the structure. This bolsters the need to study the effects of nanomaterials type and characterisation on the membrane properties and performance in this field.

REFERENCES

[1] H. K. Lonsdale, "The growth of membrane technology," *J. Membr.Sci*, vol. 10, no. 2–3, pp. 81–181, 1982.

[2] M. C. Porter, *Membrane Filtration : Handbook of Separation Techniques for Chemical Engineers*. P. A. Schweitzer, McGraw Hill, New York, NY, 1979.

[3] R. E. Lacey and S. Loeb, *Industrial Processing with Membranes,*. New York: Wiley-Interscience, 1972.

[4] S. Shaldon, H. Silva, and S. M. Rosen, "Technique of refrigerated coil preservation haemodialysis with femoral venous catheterization," *Br. Med. J.*, vol. 2, no. 5406, pp. 411–413, 1964.

[5] A. S. Michaels, "'New separationn technique for the CPI,'" in *Chem. Eng. Prog*, 12th ed., 1968, pp. 31–42.

[6] “Ultrafiltration, Nanofiltration, and Reverse Osmosis, Wiki Mini for Chem, Doi: http://wikiminiforchem.blogspot.ca/2014/10/ultrafiltration-nanofiltration-and.html; Reverse Osmosis versus Nanafiltration and Other Filtration Technologies, Aqua Clear Water Tr.” .

[7] K. W. Lawson and D. R. Lloyd, “Membrane distillation .1. Module design and performance evaluation using vacuum membrane distillation,” *J. Membr.Sci.*, vol. 120, no. 1, pp. 111–121, 1996.

[8] L. Martínez-Díez and M. I. Vázquez-Gonzàlez, “Temperature polarization in mass transport through hydrophobic porous membranes,” *AIChE J.*, vol. 42, no. 7, pp. 1844–1852, 1996.

[9] M. N. Chernyshov, G. W. Meindersma, and A. B. de Haan, “Comparison of spacers for temperature polarization reduction in air gap membrane distillation,” *Desalination*, vol. 183, no. 1–3, pp. 363–374, 2005.

[10] G. W. Meindersma, C. M. Guijt, and A. B. de Haan, “Desalination and water recycling by air gap membrane distillation,” *Desalination*, vol. 187, no. 1–3, pp. 291–301, 2006.

[11] A. M. Alklaibi and N. Lior, “Membrane-distillation desalination: Status and potential,” *Desalination*, vol. 171, no. 2, pp. 111–131, 2005.

[12] A. S. Jönsson, R. Wimmerstedt, and A. C. Harrysson, “Membrane distillation - A theoretical study of evaporation through microporous membranes,” *Desalination*, vol. 56, pp. 237–249, 1985.

[13] L. M. Camacho *et al.*, “Advances in membrane distillation for water desalination and purification applications,” *Water (Switzerland)*, vol. 5, no. 1, pp. 94–196, 2013.

[14] K. Tarnacki, M. Meneses, T. Melin, J. van Medevoort, and A. Jansen, “Environmental assessment of desalination processes: Reverse osmosis and Memstill??,” *Desalination*, vol. 296, pp. 69–80, 2012.

[15] A. Cipollina, M. G. Di Sparti, A. Tamburini, and G. Micale, “Development of a

membrane distillation module for solar energy seawater desalination," *Chem. Eng. Res. Des.*, vol. 90, no. 12, pp. 2101–2121, 2012.

[16] M. Khayet, P. Godino, and J. I. Mengual, "Nature of flow on sweeping gas membrane distillation," *J. Memb. Sci.*, vol. 170, no. 2, pp. 243–255, 2000.

[17] M. C. García-Payo, C. A. Rivier, I. W. Marison, and U. Von Stockar, "Separation of binary mixtures by thermostatic sweeping gas membrane distillation II. Experimental results with aqueous formic acid solutions," *J. Memb. Sci.*, vol. 198, no. 2, pp. 197–210, 2002.

[18] G. C. Sarti, C. Gostoli, and S. Bandini, "Extraction of organic components from aqueous streams by vacuum membrane distillation," *J. Memb. Sci.*, vol. 80, no. 1, pp. 21–33, 1993.

[19] A. Alkhudhiri, N. Darwish, and N. Hilal, "Membrane distillation: A comprehensive review," *Desalination*, vol. 287, pp. 2–18, 2012.

[20] K. Zhao *et al.*, "Experimental study of the memsys vacuum-multi-effect-membrane-distillation (V-MEMD) module," *Desalination*, vol. 323, pp. 150–160, 2013.

[21] Aquatechnology, "Reverse Osmosis Water Treatment: Aqua 'Water system technology for the 21st century.'" .

[22] M. C. García-Payo, M. A. Izquierdo-Gil, and C. Fernández-Pineda, "Wetting study of hydrophobic membranes via liquid entry pressure measurements with aqueous alcohol solutions," *J. Colloid Interface Sci.*, vol. 230, no. 2, pp. 420–431, 2000.

[23] A. C. M. Franken, J. A. M. Nolten, M. H. V Mulder, D. Bargeman, and C. A. Smolders, "Wetting criteria for the applicability of membrane distillation," *J. Membr.Sci.*, vol. 33, no. 3, pp. 315–328, 1987.

[24] J. Zhang, N. Dow, M. Duke, E. Ostarcevic, J. De Li, and S. Gray, "Identification of material and physical features of membrane distillation membranes for high performance desalination," *J. Memb. Sci.*, vol. 349, no. 1–2, pp. 295–303, 2010.

[25] F. Laganà, G. Barbieri, and E. Drioli, “Direct contact membrane distillation: Modelling and concentration experiments,” *J. Membr.Sci.*, vol. 166, no. 1, pp. 1–11, 2000.

[26] S. Srisurichan, R. Jiraratananon, and A. G. Fane, “Mass transfer mechanisms and transport resistances in direct contact membrane distillation process,” *J. Memb. Sci.*, vol. 277, no. 1–2, pp. 186–194, 2006.

[27] M. S. El-Bourawi, Z. Ding, R. Ma, and M. Khayet, “A framework for better understanding membrane distillation separation process,” *J. Membr.Sci.*, vol. 285, no. 1–2, pp. 4–29, 2006.

[28] K. S. and A. D. M. Franken, “Terminology for membrane distillation,” *Desalination*, vol. 72, no. 1–3, pp. 249–262, 1989.

[29] M. Tomaszewska, “Preparation and properties of flat-sheet membranes from poly(vinylidene fluoride) for membrane distillation,” *Desalination*, vol. 104, no. 1–2, pp. 1–11, 1996.

[30] K. W. Lawson and D. R. Lloyd, “Membrane distillation,” *J. Membr.Sci.*, vol. 124, no. 1, pp. 1–25, 1997.

[31] M. Khayet and T. Matsuura, “Pervaporation and vacuum membrane distillation processes: Modeling and experiments,” *AIChE J.*, vol. 50, no. 8, pp. 1697–1712, 2004.

[32] J. Phattaranawik, R. Jiraratananon, and A. G. Fane, “Heat transport and membrane distillation coefficients in direct contact membrane distillation,” *J. Memb. Sci.*, vol. 212, no. 1, pp. 177–193, 2003.

[33] P. Wang and T. S. Chung, “Recent advances in membrane distillation processes: Membrane development, configuration design and application exploring,” *J. Memb. Sci.*, vol. 474, pp. 39–56, 2015.

[34] D. R. Lloyd, K. E. Kinzer, and H. S. Tseng, “Microporous membrane formation via thermally induced phase separation. I. Solid-liquid phase separation,” *J. Memb. Sci.*, vol. 52, no. 3, pp. 239–261, 1990.

[35] M. Gu, J. Zhang, X. Wang, H. Tao, and L. Ge, “Formation of poly(vinylidene fluoride) (PVDF) membranes via thermally induced phase separation,” *Desalination,* vol. 192, no. 1–3, pp. 160–167, 2006.

[36] K. N. J. Sasaki, “Asymmetric micro-porous membrane containing a layer of minimum size pores below the surface thereof,” 1990.

[37] S. O. J. Sasaki, A. Adachi, K. Naruo, Y. Shinagawa, “Fine porous membrane and process for producing the same,” 1989.

[38] I. F. Wang, “Highly asymmetric polyethersulfone filtration membranes,” 5869174, 1999.

[39] I. F. Wang, J. F. Ditter, “Microfiltration membranes having high pore density and mixed isotropic and anisotropic structure,” 5906742A, 1999.

[40] I. F Wang, R. A. Morris, “Highly assymetric [sic], hydrophilic, microfiltration membranes having large pore diameters,” 6045899A, 2000.

[41] C. Y. Kuo, H. N. Lin, H. A. Tsai, D. M. Wang, and J. Y. Lai, “Fabrication of a high hydrophobic PVDF membrane via nonsolvent induced phase separation,” *Desalination,* vol. 233, no. 1–3, pp. 40–47, 2008.

[42] Y. Yang, D. Rana, T. Matsuura, S. Zheng, and C. Q. Lan, “Criteria for the selection of a support material to fabricate coated membranes for a life support device,” *RSC Adv.,* vol. 4, no. 73, pp. 38711–38717, 2014.

[43] M. Baghbanzadeh, N. Hirceaga, D. Rana, T. Matsuura, and C. Q. Lan, “Effects of polymer ratio and film-penetration time on the properties and performance of nanocomposite PVDF membranes in membrane distillation,” *Ind. Eng. Chem. Res.,* vol. 55, no. 37, pp. 9971–9982, 2016.

[44] L. Garcia-Fernandez, M. C. Garcia-Payo, and M. Khayet, “Effects of mixed solvents on the structural morphology and membrane distillation performance of PVDF-HFP hollow fiber membranes,” *J. Memb. Sci.,* vol. 468, pp. 324–338, 2014.

[45] J. L. P. Georlette, “Composition comprising a vinylidene fluoride polymer and a blowing agent,” 4425443, 1984.

[46] C. A. D. and J. E. McDaniel, “Method of producing spherical thermoplastic particles,” 3896196, 1975.

[47] A. Saffar, “Development of polypropylene microporous hydrophilic membranes through cast extrusion and stretching,” *Ph.D. Thesis, Ec. Polytech. Montr. Montr. Canada*, pp. 1–200, 2014.

[48] C. Guo, L. Zhou, and J. Lv, “Effects of expandable graphite and modified ammonium polyphosphate on the flame-retardant and mechanical properties of wood flour-polypropylene composites,” *Polym. Polym. Compos.*, vol. 21, no. 7, pp. 449–456, 2013.

[49] R. L. Fleischer, P. B. Price, and R. M. Walker, *Nuclear Tracks in Solids: Principles and Applications*. Berkley, CA: University of California Press, 1975.

[50] M. Mulder, *Basic Principles of Membrane Technology*. Springer, Dordrecht, Netherlands, 1996.

[51] N. Bhardwaj and S. C. Kundu, “Electrospinning: A fascinating fiber fabrication technique,” *Biotechnol. Adv.*, vol. 28, no. 3, pp. 325–347, 2010.

[52] B. S. Lalia, E. Guillen-Burrieza, H. A. Arafat, and R. Hashaikeh, “Fabrication and characterization of polyvinylidenefluoride-co-hexafluoropropylene (PVDF-HFP) electrospun membranes for direct contact membrane distillation,” *J. Memb. Sci.*, vol. 428, pp. 104–115, 2013.

[53] R. Gopal, S. Kaur, Z. Ma, C. Chan, S. Ramakrishna, and T. Matsuura, “Electrospun nanofibrous filtration membrane,” *J. Memb. Sci.*, vol. 281, no. 1–2, pp. 581–586, 2006.

[54] C. Feng *et al.*, “Production of drinking water from saline water by air-gap membrane distillation using polyvinylidene fluoride nanofiber membrane,” *J. Membr.Sci.*, vol. 311, no. 1–2, pp. 1–6, 2008.

[55] X. Zong, K. Kim, D. Fang, S. Ran, B. S. Hsiao, and B. Chu, “Structure and process relationship of electrospun bioabsorbable nanofiber membranes,” *Polymer (Guildf).*, vol. 43, no. 16, pp. 4403–4412, 2002.

[56] P. Termpiyakul, R. Jiraratananon, and S. Srisurichan, “Heat and mass transfer characteristics of a direct contact membrane distillation process for desalination,” *Desalination*, vol. 177, no. 1–3, pp. 133–141, 2005.

[57] S. Kimura, S.-I. Nakao, and S.-I. Shimatani, “Transport phenomena in membrane distillation,” *J. Membr.Sci.*, vol. 33, no. 3, pp. 285–298, 1987.

[58] S. Al-Obaidani, E. Curcio, F. Macedonio, G. Di Profio, H. Al-Hinai, and E. Drioli, “Potential of membrane distillation in seawater desalination: Thermal efficiency, sensitivity study and cost estimation,” *J. Memb. Sci.*, vol. 323, no. 1, pp. 85–98, 2008.

[59] M. Khayet, M. P. Godino, and J. I. Mengual, “Theoretical and experimental studies on desalination using the sweeping gas membrane distillation method,” *Desalination*, vol. 157, no. 1–3, pp. 297–305, 2003.

[60] L. Martínez-Díez, F. J. Florido-Díaz, and M. I. Vázquez-González, “Study of evaporation efficiency in membrane distillation,” *Desalination*, vol. 126, no. 1–3, pp. 193–198, 1999.

[61] S. Shirazi, C. J. Lin, and D. Chen, “Inorganic fouling of pressure-driven membrane processes - A critical review,” *Desalination*, vol. 250, no. 1, pp. 236–248, 2010.

[62] J. W. Koo, J. H. Han, S. H. Lee, J. S. Sohn, and J. S. Choi, “Development of nano-carbon bucky-paper membranes for membrane distillation,” *Mater. Sci. Forum*, vol. 724, pp. 408–411, 2012.

[63] L. Dumée *et al.*, “The impact of hydrophobic coating on the performance of carbon nanotube bucky-paper membranes in membrane distillation,” *Desalination*, vol. 283, pp. 64–67, 2011.

[64] L. Dumée *et al.*, “Enhanced durability and hydrophobicity of carbon nanotube bucky paper membranes in membrane distillation,” *J. Memb. Sci.*, vol. 376, no. 1–2, pp. 241–

246, 2011.

[65] L. Dumée, K. Sears, J. Schü tz, N. Finn, M. Duke, and S. Gray, “Carbon nanotube based composite membranes for water desalination by membrane distillation,” *Desalin. Water Treat.*, vol. 17, no. 1–3, pp. 72–79, 2010.

[66] L. F. Dumée *et al.*, “Characterization and evaluation of carbon nanotube Bucky-Paper membranes for direct contact membrane distillation,” *J. Memb. Sci.*, vol. 351, no. 1–2, pp. 36–43, 2010.

[67] M. Baghbanzadeh, D. Rana, T. Matsuura, and C. Q. Lan, “Effects of hydrophilic CuO nanoparticles on properties and performance of PVDF VMD membranes,” *Desalination*, vol. 369, pp. 75–84, 2015.

[68] M. Baghbanzadeh, D. Rana, C. Q. Lan, and T. Matsuura, “Effects of hydrophilic silica nanoparticles and backing material in improving the structure and performance of VMD PVDF membranes,” *Sep. Purif. Technol.*, vol. 157, pp. 60–71, 2015.

[69] J. E. Efome, M. Baghbanzadeh, D. Rana, T. Matsuura, and C. Q. Lan, “Effects of superhydrophobic SiO2 nanoparticles on the performance of PVDF flat sheet membranes for vacuum membrane distillation,” *Desalination*, vol. 373, pp. 47–57, 2015.

[70] Y. J. Kim, C. H. Ahn, and M. O. Choi, “Effect of thermal treatment on the characteristics of electrospun PVDF-silica composite nanofibrous membrane,” *Eur. Polym. J.*, vol. 46, no. 10. pp. 1957–1965, 2010.

[71] S. S. Choi, Y. S. Lee, C. W. Joo, S. G. Lee, J. K. Park, and K. S. Han, “Electrospun PVDF nanofiber web as polymer electrolyte or separator,” *Electrochim. Acta*, vol. 50, no. 2–3, pp. 339–343, 2004.

[72] D. Hou, J. Wang, X. Sun, Z. Ji, and Z. Luan, “Preparation and properties of PVDF composite hollow fiber membranes for desalination through direct contact membrane distillation,” *J. Memb. Sci.*, vol. 405–406, pp. 185–200, 2012.

[73] D. Hou, G. Dai, H. Fan, J. Wang, C. Zhao, and H. Huang, “Effects of calcium carbonate

nano-particles on the properties of PVDF/nonwoven fabric flat-sheet composite membranes for direct contact membrane distillation," *Desalination*, vol. 347, pp. 25–33, 2014.

[74] A. Razmjou, E. Arifin, G. Dong, J. Mansouri, and V. Chen, "Superhydrophobic modification of TiO 2 nanocomposite PVDF membranes for applications in membrane distillation," *J. Memb. Sci.*, vol. 415–416, pp. 850–863, 2012.

[75] K. Gethard, O. Sae-Khow, and S. Mitra, "Water desalination using carbon-nanotube-enhanced membrane distillation," *ACS Appl. Mater. Interfaces*, vol. 3, no. 2, pp. 110–114, 2011.

[76] M. Bhadra, S. Roy, and S. Mitra, "Enhanced desalination using carboxylated carbon nanotube immobilized membranes," *Sep. Purif. Technol.*, vol. 120, pp. 373–377, 2013.

3. Effect of Nanoparticles and film thickness on Vacuum Membrane Distillation

3.1 Introduction

“All the water that will ever be is, right now”. This quote[1] describes the significance of water in this decade. Though the earth is made up of 71% water, 96.5% of this water is in the ocean which cannot be used directly [2]. The water in the ocean must be treated in some way to make it usable. Thanks to nature, we have water cycles which result from the sun’s evaporation of sea water, making it pure and usable as rain water. Studying this example, scientists earlier adopted this same principle, designing thermal desalination techniques. Although these techniques have results in some higher efficiencies in producing usable water, these techniques also come with some disadvantages including excessive cost. Thus, many other conventional desalination methods have since been adopted. These conventional methods include ultrafiltration (UF), microfiltration (MF), reverse osmosis (RO) and multistage vacuum evaporation. Up until now, RO has been the dominant method used in these industries [3]–[6]. Even though RO has been used extensively, it also has some disadvantages such as high electrical consumption at high operating pressure as well as a tendency towards scaling and fouling. Scientists have been looking for ways to overcome this disadvantage without eliminating efficiency. Another process for recovering usable water is membrane distillation (MD). This has demonstrated to have potential application by providing a high performance durable membrane, which is available with high flux at relatively low operating temperatures to increase membrane life time and enable the utilization of low-quality thermal energy [7]–[10].

Since MD has been discovered, many different configurations like Direct Contact Membrane Distillation (DCMD), Air Gap Membrane Distillation (AGMD), Sweep Gas Membrane Distillation (SGMD), and Vacuum Membrane Distillation (VMD) have been developed and analysed. Each configuration has been studied thoroughly and experiments have

been conducted. Regardless of the configuration, all research has been addressing the question of which type of membrane will perform best with various MD process. Membranes which can withstand pressure higher than the Liquid Entry Pressure of water (LEPw) could be used in all configurations. Carbon nanotube immobilized membrane (CNIM) in polypropylene (PP) were used in a SGMD configuration and reported a higher flux than the neat PP membrane prepared by Gethard et al. [7]. Improvement in the PP membrane permeability through the addition of carboxylated carbon nanotubes have been observed by Bhadra et al. [11] however, the single wall functionalized carbon nanotubes are very expensive to be used in commercial membrane production. Also, in other research work attempted by Hou et al. [12], [13], the addition of hydrophobic modified $CaCO_3$ nanoparticles was effective in increasing the permeability of polyvinylidene fluoride (PVDF) membranes in DCMD Recent work has been done in our research group to increase the efficiency of the membrane used in VMD configuration. Instead of using single molecular weight polymer, a blend of high and low molecular weight polymers proved to increase the membrane's performance in a VMD configuration by Chen et al [14]. Also, work done by Baghbanzadeh et al. [15]–[17] and Efome et al. [15]–[18] proves that the addition of nanoparticles in the membrane certainly increases the performance of the membrane. In addition to this, utilization of backing material has also proven to increase the pore size, porosity and permeate flux. The addition of hydrophilic nanoparticles in hydrophobic polymer with backing material especially yields higher potential membranes with higher flux and higher salt rejection.

In this study, we are using the VMD configuration since it's the least explored configuration among all the MD configurations and VMD also consumes less energy for a given driving force. Though research has been done using nanoparticles, all the nanoparticles that have

been used in the group so far were in the range of 10 – 20 nm and all the membranes were casted with a thickness of 10 mil. This research studied the effect of nanoparticle sizes ranging between 7 and 200 nm. Characterisation has been performed to verify the actual size of the nanoparticles. Experiments were also performed to study the effect of thickness on the performance and stability of the membrane. These membranes were prepared through a phase inversion method using deionised water as the non-solvent additive and N-N-dimethyl acetamide (DMAc) as the solvent. These membranes were casted using a machine to ensure uniform distribution. Membranes were characterised by scanning electron microscope (SEM), porosity, viscosity, VMD, LEPw and water contact angle. Membrane performance was assessed using distilled water and salt rejection of the membranes was tested for desalination using artificial salt water.

3.2 Experimental Methods

3.2.1 Materials

Poly(vinylidene fluoride) (PVDF) of two different molecular weights (Kynar® 740(M = 410 kDa) and Kynar® HSV 900(M = 24.92% 92,840 kDa and 75.08% 1,367 kDa)) both in α-phase, were supplied by Arkema Inc., Philadelphia, PA. Anhydrous N-N-dimethyl acetamide (DMAc) with 99.9% purity was purchased from Sigma Aldrich Inc., St. Louis, MO. Deionized water was used as the casting solution additive and in coagulation bath. Hollytex® 3396 non-woven fabric of air permeability 0.009 cubic feet per minute per square meter (CFM), purchased from Kavon. Two batches of polymer were used in our studies (Old: 16C6108, New: 12C6183). Although the results from both batches did not show any significant differences, few parameters like viscosity have been changed.

Filter Products Co., Farmingdale, NJ was used as the backing material. Two grades of photocatalytic Titanium dioxide nanoparticles (ST-01 (Surface area – 300 m^2/g, Particle size – 7

nm), ST-41 (Surface area – 10 m^2/g, Particle size – 200 nm)) were purchased from Ishihara Sangyo Kaisha ltd, Japan. Hydrophilic amino modified SiO_2 (purity – 99.8% (before treatment), Surface area – 90 to 130 m^2/g, Particle Size – 10-20 nm) and Super-hydrophobic SiO_2 (purity – 99.8% (before treatment), Surface area – 90 to 130 m^2/g, Particle Size – 10-20 nm) surface modified with single layer chain were provided by SkySpring Nanoparticles Inc., Houston, TX. 1-Butanol (Purity - 99.4%) was provided by Caledon Laboratories Ltd., Georgetown, ON.

3.2.2 Preparation of dope solution

The casting solution was prepared by mixing 15 wt.% PVDF [14][19], 83.75 wt.% DMAc and 1.25 wt.% water. The casting solution was then placed in a shaker of 180 rpm and 50^{o}C for 72 h to make sure complete polymers dissolution and homogenous mixing. Then the solution was de-gasified for 24 h at room temperature. The required amount of nanoparticles was then added to the required quantity of casting solution and the suspension was stirred at 100 rpm for 2 h to yield the dope solution. Hereafter "nanoparticle concentration" implies the concentration of nanoparticle in the casting solution.

The viscosity was measured using a rotational rheometer (Brookfield, Synchro-Lectric viscometer model: LVF) at 25^{o}C. The dope solution was loaded in the glass tubes and a spindle connected to the motor at specific speed was allowed to run for 6 to 8 min to make sure that the needle in the dial attained the constant value. The viscosity of the solution was then calculated by the rotation factor, spindle factor and rotation speed. An average was taken from the three trials and reported as the viscosity of the solution.

3.2.3 Membrane fabrication

The dope solution was cast using a casting machine (Shanghai Modern Environmental Engineering Co.Ltd., AFA II) to ensure the membrane uniformity. The casting machine has a bar

with varying clearances (4,6,8 and 10 mil, 1 mil = 0.001 inch), a speed controller (0-10 cm/s), and a glass plate with two different casting lengths. The dope solution was poured on top of the glass plate with and without a backing material to fabricate supported and unsupported membrane, respectively. Then, the cast film was immersed in a coagulation bath together with the glass plate with or without backing material after an interval of three minutes [20]. The membrane was kept in the coagulation media, deionized water of 25^{o}C for 24 h during which the coagulation media was replaced several times with fresh deionized water to ensure complete removal of solvent from the cast film. Then, the membrane was taken out from the coagulation bath and dried at room temperature for 24 h before being subjected to characterisation. Each membrane was tested in the VMD setup at steady state which was noted by the absolute vacuum on the system.

Hereafter, the membranes are coded as MaBc-d, where M means membrane, a indicates the nanoparticle (a=1, TiO_2 7 nm; a=2, TiO_2 200 nm, a = 3, hydrophilic SiO_2, a = 4, super hydrophobic SiO_2), B indicates membrane is unsupported (B = N) or supported (B = S), subscript c indicates the cast film thickness (4 and 10 mil), and –d indicates the nanoparticle concentration in the casting dope (2, 5, and 7 wt%). All fabricated membranes are listed with their codes in **Table 3. 1**.

Table 3. 1 Membrane codes and details

S. No	Membrane Code	Nanoparticles	Nanoparticle Size (nm)	Nanoparticle Concentration in dope (wt%)	Membrane thickness (mil)	Substrate
1	$M1S_{10}$-2	TiO_2	7	2	10	Yes
2	$M1S_{10}$-3	TiO_2	7	3	10	Yes
3	$M1S_{10}$-5	TiO_2	7	5	10	Yes
4	$M1S_{10}$-7	TiO_2	7	7	10	Yes
5	$M1N_4$-2	TiO_2	7	2	4	No
6	$M1N_{10}$-2	TiO_2	7	2	10	No
7	$M1N_4$-5	TiO_2	7	5	4	No
8	$M1N_{10}$-5	TiO_2	7	5	10	No
9	$M2S_{10}$-2	TiO_2	200	2	10	Yes
10	$M2S_{10}$-3	TiO_2	200	3	10	Yes
11	$M2S_{10}$-5	TiO_2	200	5	10	Yes
12	$M2S_{10}$-7	TiO_2	200	7	10	Yes
13	$M2N_4$-2	TiO_2	200	2	4	No
14	$M2N_{10}$-2	TiO_2	200	2	10	No
15	$M3S_4$-7	Philic SiO_2	15-20	7	4	Yes
16	$M3S_{10}$-7	Philic SiO_2	15-20	7	10	Yes
17	$M4N_4$-7	Phobic SiO_2	15-20	7	4	No
18	$M4N_{10}$-7	Phobic SiO_2	15-20	7	10	No

3.3 Characterisation

3.3.1 Nanoparticles characterisation (TEM analysis)

Transmission electron microscopy (TEM) (FEI Tecnai G2 F20 equipped with Oxford Aztec TEM with 80 mm SDD detector) was used to observe the structure of the nanoparticles. Samples were prepared by dispersing nanoparticle powder into propanol. A drop of propanol was used for the dispersion of the nanoparticles on carbon-coated copper grids operated at 300 kV.

3.3.2 Morphology (SEM analysis)

Top and cross-sectional images of the membranes were obtained using Scanning Electron Microscope system (SEM, Vega-II XMU VPSEM and Anatech Hummer VII). The membrane samples were immersed in liquid nitrogen for 10-20s before they were broken or cut by sharp scissors and fixed in a metal holder using conductive tapes. The samples were gold prior to SEM imaging. The SEM images were analysed by using ImageJ software developed by Gribble et al. [21], Zhao et al. [22], and other researchers [23]–[26]. From the images, at least 80 to 100 pores were selected randomly and their average size is reported.

3.3.3 Contact angle measurement

Water contact angle was measured by using VCA optima surface analysis system (AST Products Inc., Billerica, MA). A droplet of water (1 µl) is placed on the membrane surface by a micro-syringe (Hamilton Company, Reno, NV) to measure the contact angle after a wait time of 10 seconds. Ten random measurements were made on the membrane surface and the average is reported.

3.3.4 Liquid Entry Pressure of water (LEPw)

The maximum pressure that can be applied to water without allowing the water to enter into the membrane pore is known as Liquid Entry Pressure of water (LEPw). The measurements

were made using a set up similar to the batch filtration cell, in which water was filled in the feed chamber. Pressure applied from a nitrogen cylinder was increased progressively with an increment of 2 psi. The pressure at which a continuous flow of water was observed on the permeate side of the filtration cell within a wait period of 10 min was recorded as the LEPw. An average of three measurements is reported.

3.3.5 Surface roughness

The surface roughness of the membrane was investigated using a plugin in the ImageJ software called SurfCharJ as developed by Banerjee et al. [29] and other researchers [25], [27], [28]. In this process, the top surface SEM image of the membrane is converted to 32 bit image and the software computes the root mean square roughness (R_q) and the average roughness (R_a). The software will further assign pixel values for each part of the image. The intensity of the darkness indicates the depth of each void. Surface roughness will be calculated by the difference in the pixel values on the membrane surface.

3.3.6 Porosity and pore size

The porosity of the membranes were measured by the method described by Khayet and Matsuura [30]. A piece of membrane was immersed in butanol for 24 h. The blotted membrane was weighed and then dried in an oven at 50^{o}C for 24 h. The dried membrane was weighed and the porosity, %ε, was obtained by

$$\%\varepsilon = \frac{m1-m2}{\rho.A.l} * 100 \qquad (3.1)$$

Where m1(g) and m2(g) are the mass of the wet and dry membranes respectively, ρ(g/m^3) is the density of butanol, A(m^2) is the area of the membrane and l(m) is the thickness of the

membrane. The measurements were made with three random spots of a membrane and the average reported.

3.3.7 Energy Dispersive X-ray Spectroscopy (EDX)

To investigate how the nanoparticles are dispersed within the flat-sheet membranes, EDX analysis of the membrane cross-section was conducted using an Oxford Inca Energy 250X EDX apparatus.

3.4 Vacuum Membrane Distillation (VMD)

The performance of the membranes was evaluated by VMD experiment [14]-[18]. The VMD experimental setup **Figure 3. 1** consists of a membrane module which has 300 mL feed chamber wrapped with a heating coil to maintain uniform temperature profile (27.5^{o}C) throughout the permeation cell. The turbulence of the feed solution was enhanced by a magnetic stirrer to minimize the concentration and temperature polarisation. Vacuum of 1.2 kPa was maintained on the permeate side by a vacuum pump and the permeate vapour was collected in a cold trap cooled with liquid nitrogen. The permeate was collected in the cold trap 2 during the first one hour of operation and then the condenser was switched to 3, assuming that the steady state of the system was reached within the first hour. The condensate collected in cold trap 2 was discarded. The cold trap 1 was used to avoid the contamination of oil in the vacuum pump. The permeate flux was calculated using the following equation.

$$J = \frac{W}{A \cdot t} \qquad \textbf{(3.2)}$$

Where J is the flux (g/m^{2}h), W is the weight of the permeate collected (g) in cold trap 3, through membrane area (A, m^2) during time t (t, h) respectively.

Salt rejection, $\%\boldsymbol{R}$, of VMD was calculated by equation (3.3), where C_f and C_P are the feed NaCl concentration, 35 g/L as that of artificial seawater, and the permeate NaCl concentration measured by a conductivity meter (OAKTON, CON 2700) respectively.

$$\%\boldsymbol{R} = \frac{\boldsymbol{Cf-Cp}}{\boldsymbol{Cf}} * \mathbf{100} \qquad \textbf{(3.3)}$$

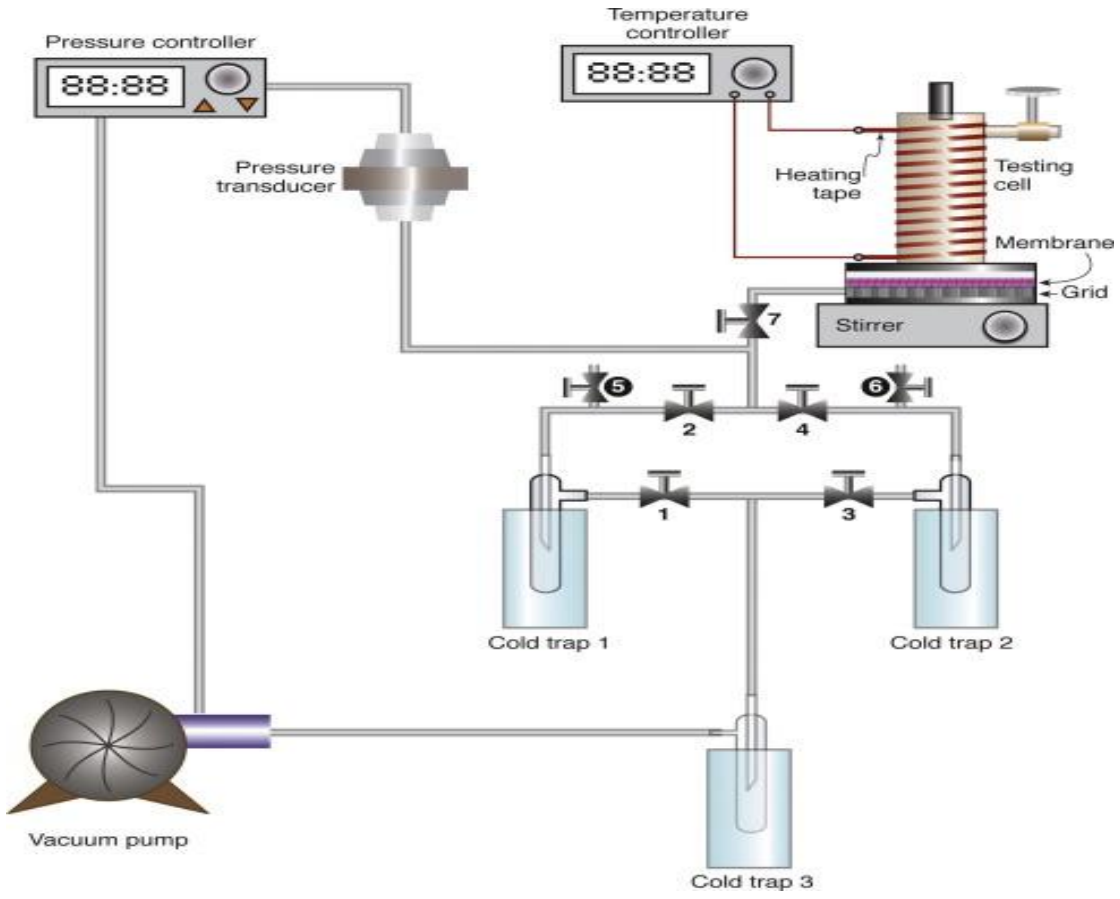

Figure 3. 1 Schematic diagram of Vacuum Membrane Distillation setup[18]

3.5 Results and Discussions

3.4.1 TEM Analysis

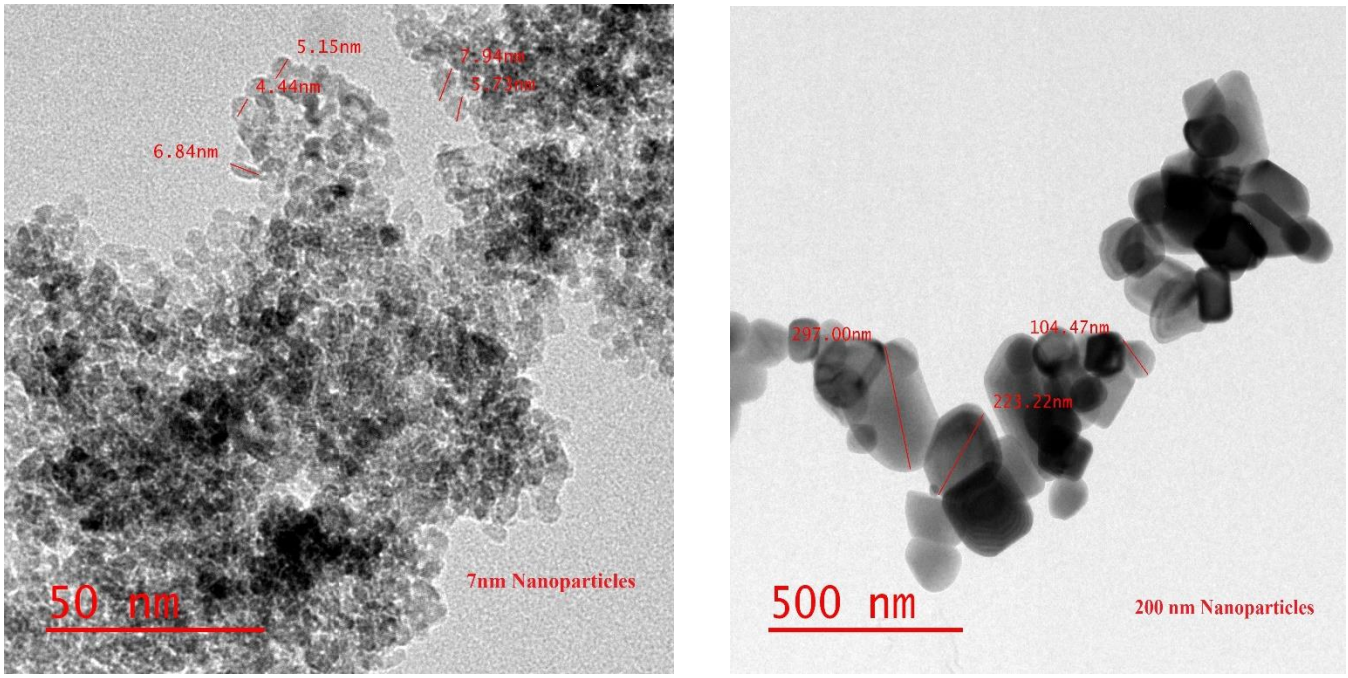

Figure 3. 2 TEM image of (a) 7 nm TiO2 nanoparticles and (b) 200 nm TiO2 nanoparticles

Figure 3. 2 shows the TEM images of ST01 and ST41 TiO_2 nanoparticles which have diameters of 7 nm and 200 nm, respectively. It is clear that the particles are near spherical shape. The diameters of the particles measured using ImageJ proved to be 7 nm and 200 nm, which verifies the supplier's specifics.

3.5.1 Viscosity of dope solution

Figure 3. 3 shows the viscosity of the dope solution vs nanoparticle concentration for with two different nanoparticles measured at room temperature. The viscosity did not change significantly either by the change in nanoparticle size or by the change in particle concentration.

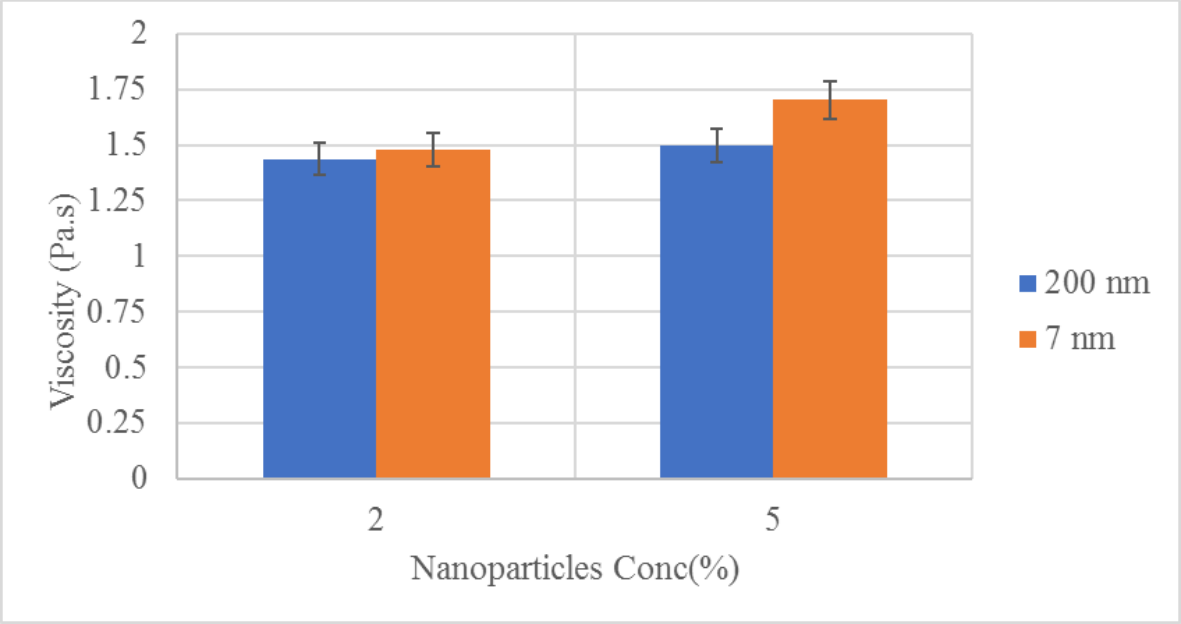

Figure 3. 3 Viscosity of TiO2 dope solutions

Table 3. 2 Composition of dope solutions for viscosity

Dope composition				
Polymer (H:L) 15%	Solvent (83.75 %)	Non-solvent (1.25%)	Nanoparticle and size	Nanoparticle concentration (wt%)
2:8 PVDF	DMAc	Water	TiO_2 - 7nm	2
2:8 PVDF	DMAc	Water	TiO_2 - 7nm	5
2:8 PVDF	DMAc	Water	TiO_2 - 200nm	2
2:8 PVDF	DMAc	Water	TiO_2 - 200nm	5

3.5.2 Membrane morphology study by SEM

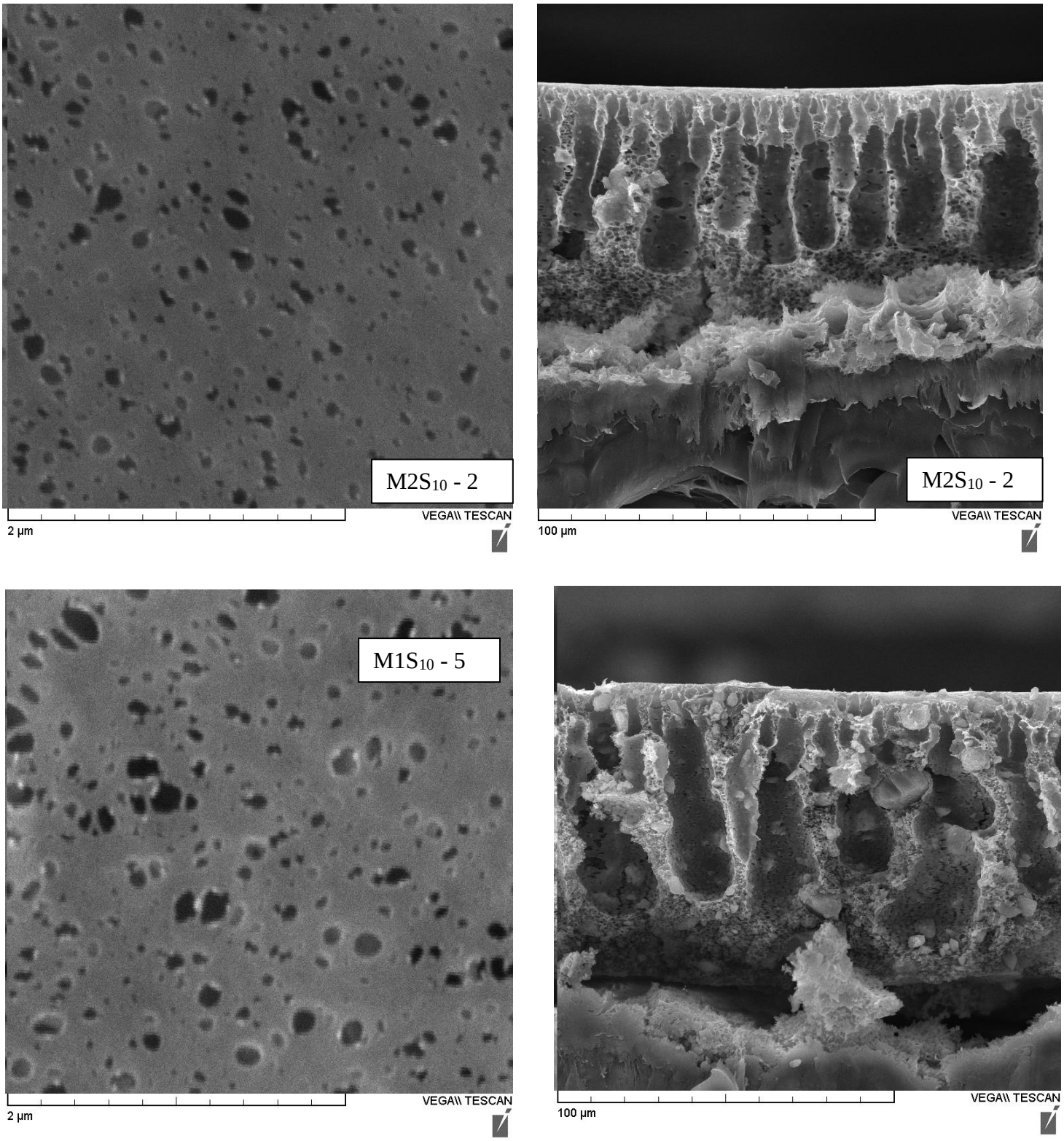

Figure 3. 4 SEM images of PVDF Nanocomposite membranes, T represents top view and C represents cross sectional view

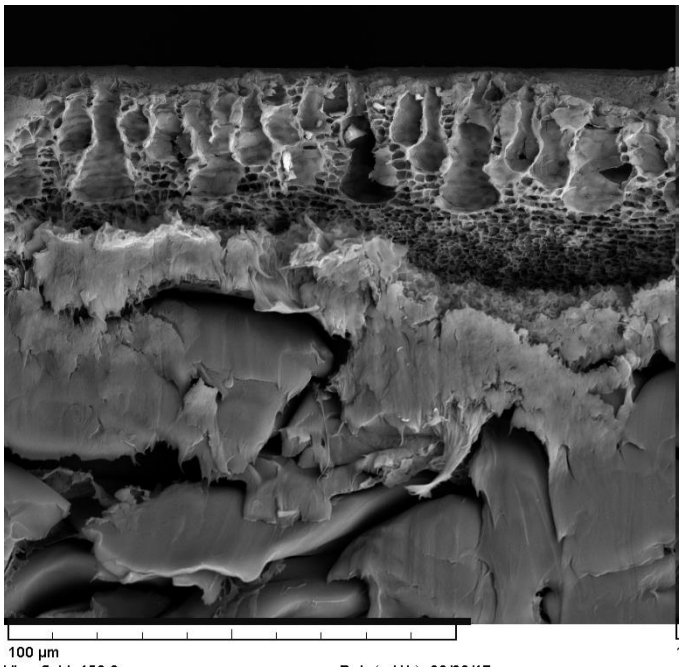

Figure 3.4. 1 Cross Sectional view of Pure PVDF with backing material

Figure 3.4. 1 represents the cross-sectional SEM image of Pure PVDF membrane with backing material. **Figure 3. 4** represents the top and cross-sectional SEM images of $M2S_{10}$ – 2 and $M1S_{10}$ -5 membrane. By increasing the concentration of nanoparticles, the asymmetric structure will keep on decreasing until it forms a symmetric structure. From these images, its evident that the membrane has almost reached their minimum asymmetric structure which ensures that the membranes are at their maximum efficiency [15]-[18], .

The pore size is affected by the size of the nanoparticles since they are vital in demixing process. Water is the non-solvent coagulation medium and titanium dioxide used in here are superhydrophilic due to the photocatalytic process [18] and dispersed well in the dope solution. Since the nanoparticles are superhydrophilic they attract water in to the solution during solvent/non-solvent exchange forming larger and deeper pores. The size of the finger like structure of M1 is larger which can be explained by their distribution. The agglomeration of small nanoparticle (7 nm) is higher compared to large nanoparticle (200 nm) which is evident in the EDX mapping. Thus, it's evident that the large finger like structure is due to the

agglomeration of the nanoparticles. Higher viscosity of the solution provide higher resistance to the solvent/non-solvent exchange which in turn decreases the macro-voids but increase the depth of the finger like layer [31]–[34], this is evident from **Figure 3. 4**.

This shows that the size of the nanoparticles plays a vital role in the formation of finger like structure in the membranes. Also, due to the fine and thorough dispersion of larger size nanoparticle (200 nm) there are formation of substantial number of micro-voids inside the macro voids which can be seen in M2S than in M1S.

Figure 3. 5 and **Figure 3. 6** shows the SEM images of unsupported M1 and M2 membrane, with different thicknesses. But, first comparing $M2S_{10}$-2 (Fig. 3.4) and $M2N_{10}$-2 (Fig. 3.6), the number of pore at the surface decreases and the number of long finger-like pore decreases for the unsupported $M2N_{10}$-2 membrane. This result is in accordance with those reported by Baghbanzadeh et al. [15]. Comparing the different thicknesses of the unsupported membranes ($M1N_{10}$-5 vs $M1N_4$-5 in Fig. 5 and $M2N_{10}$-2 vs $M2N_4$-2 in **Figure 3. 6**), the images of the top surface are almost the same. But in the cross-sectional images, the finger-like pore reaches the bottom of the thin $M1N_4$-5 and $M2N_4$-2 membranes, which seems natural considering that the non- solvent–solvent exchange occurs from the top of the cross-section.

The effect of the cast film thickness on the membrane morphology was further studied when hydrophilic and hydrophobic particles were incorporated. The SEM images of thinner cast films (4 mil) are shown in **Figure 3. 7** while those of the thicker cast films (10 mil) are given in **Figure 3. 8** for comparison. It should be noted that the code M3 is for hydrophilic and M4 is for hydrophobic nanoparticles. Comparing $M3S_4$-7 in **Figure 3. 7** and $M3S_{10}$-7 **Figure 3. 8**, the top surface image has not changed significantly by the change in cast film thickness. Comparing

M4N_4-7 (**Figure 3. 7**) and M4N_{10}-7 (**Figure 3. 8**), the finger-like pore reached again the bottom of the membrane M4N_4-7, confirming the results obtained in Figs. 3.5 and 3.6.

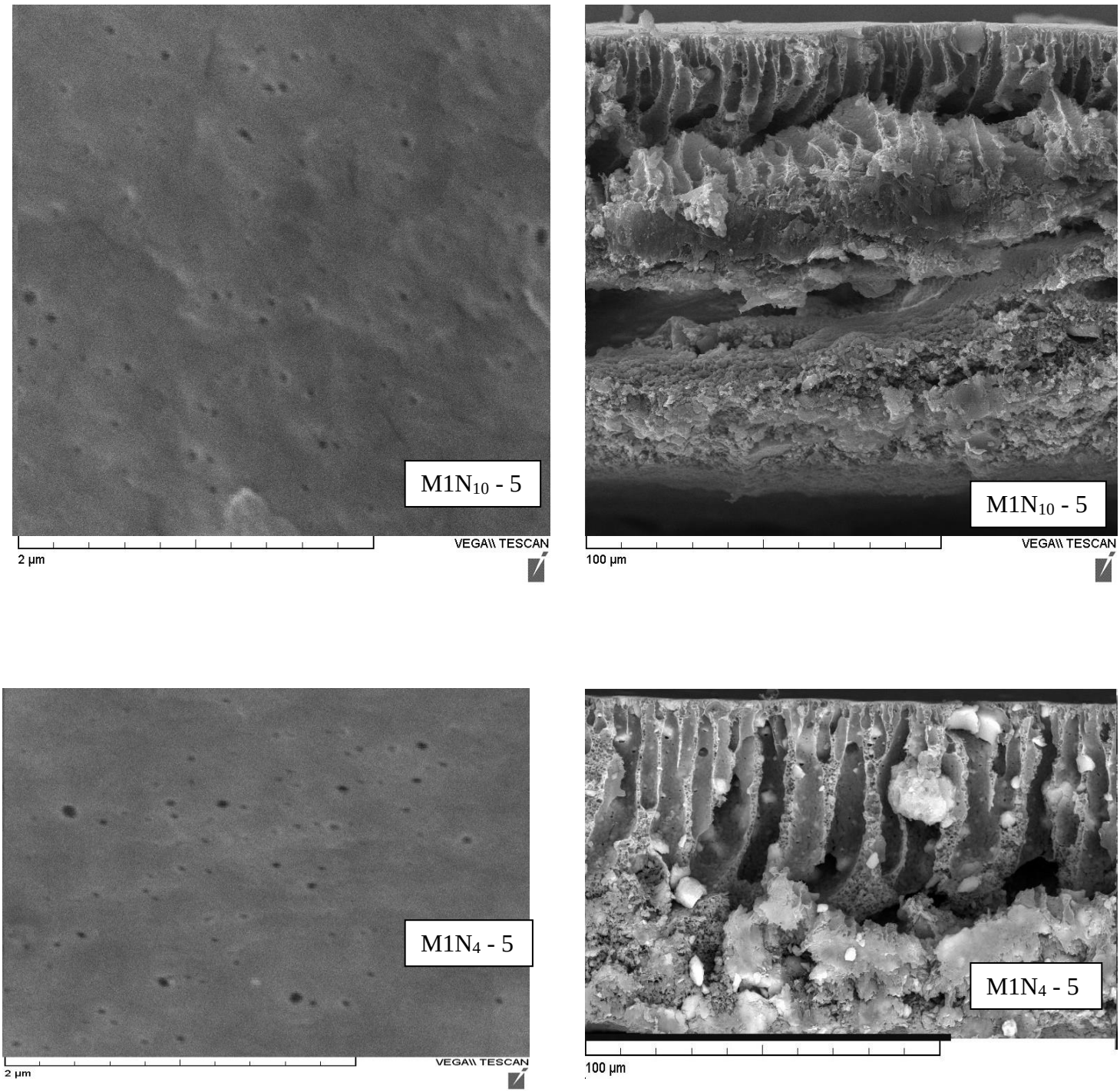

Figure 3. 5 SEM images of unsupported M1 with different thickness 10 mil and 4 mil

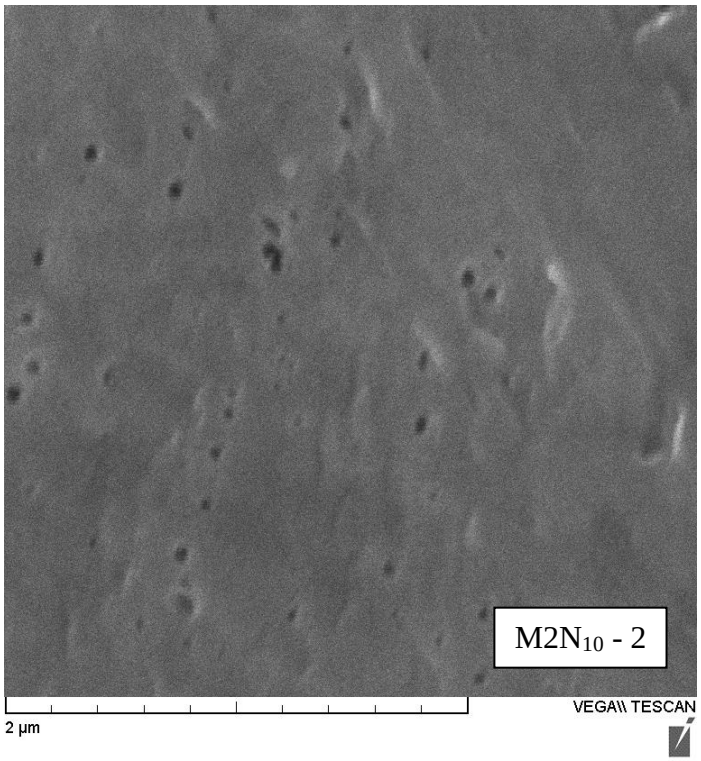

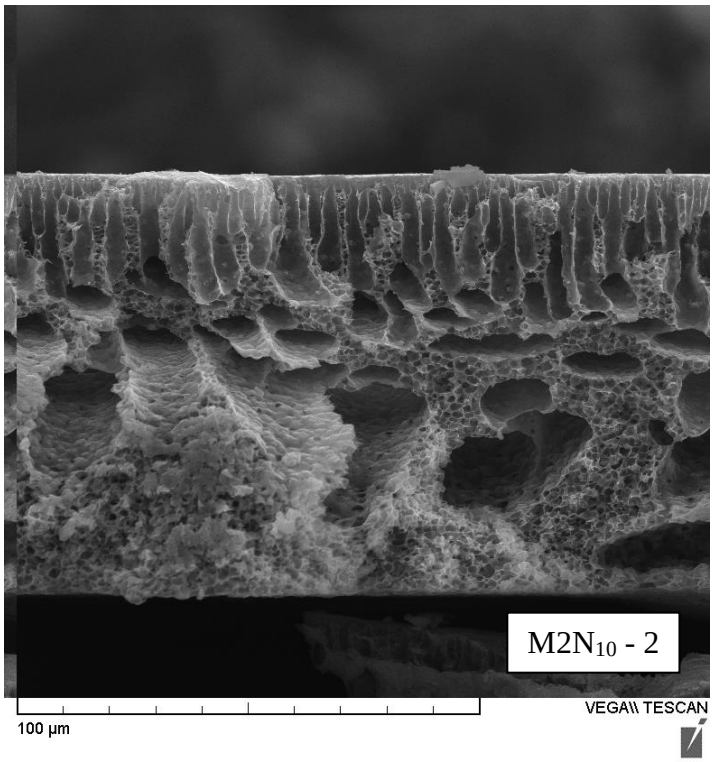

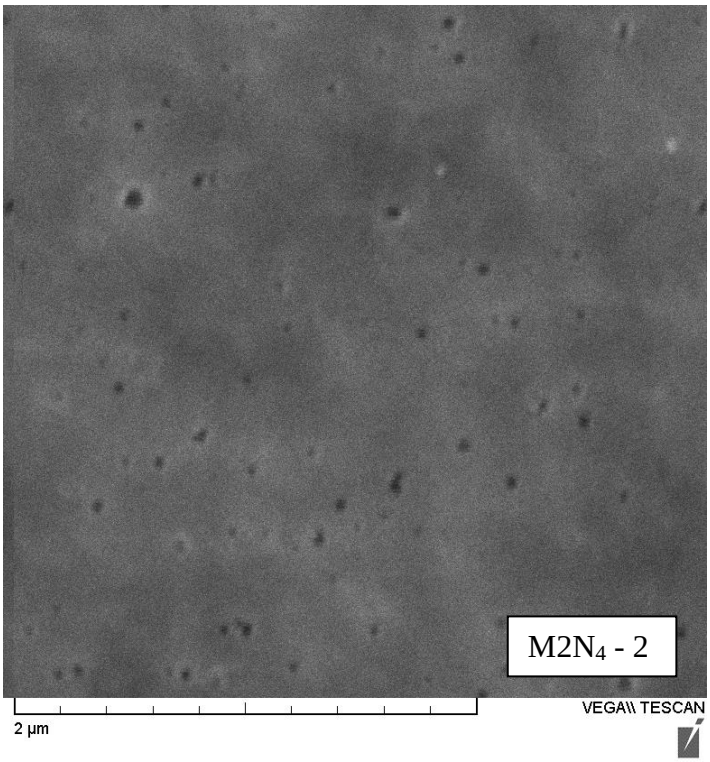

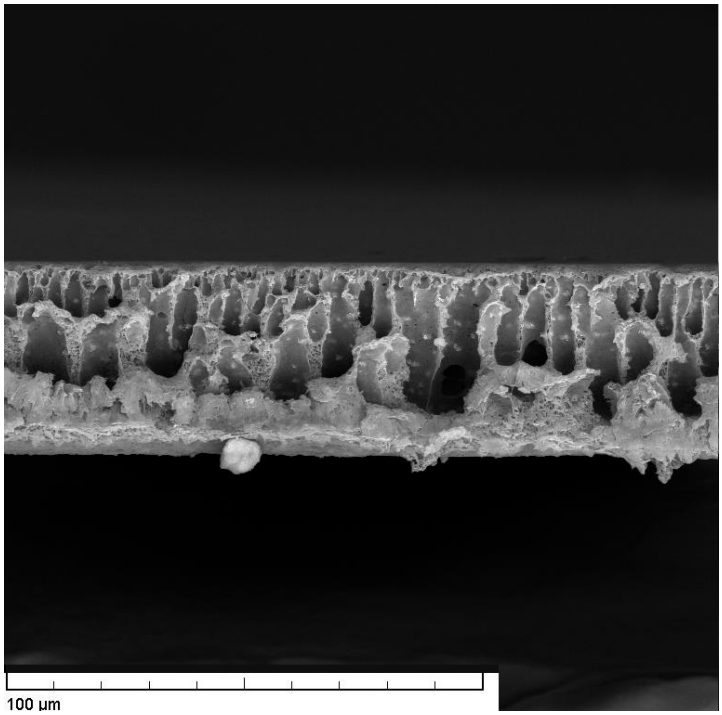

Figure 3. 6 SEM image of unsupported M2 with different thickness 10 mil and 4 mil

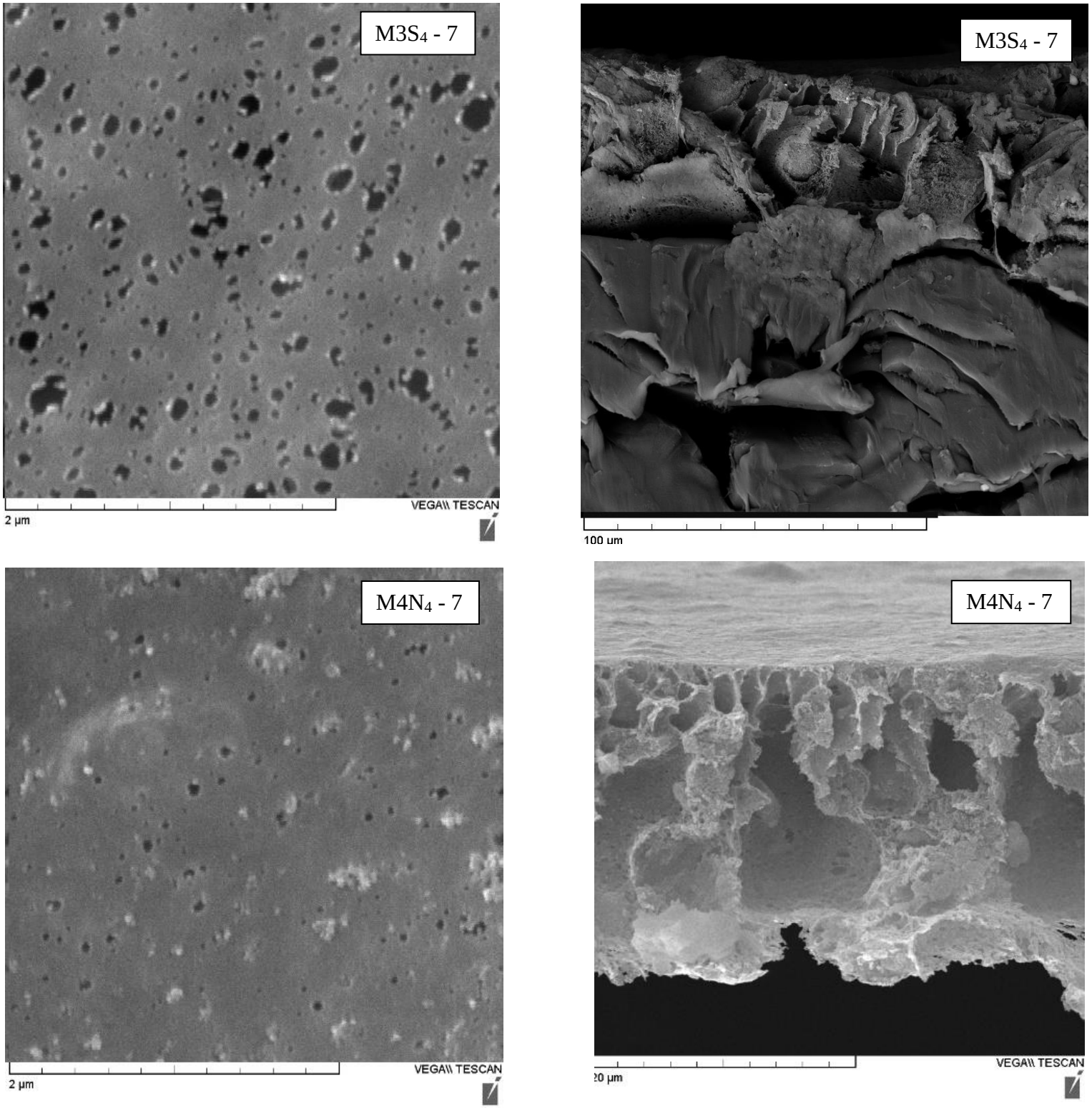

Figure 3. 7 SEM images of M3 and M4 4 mil thickness

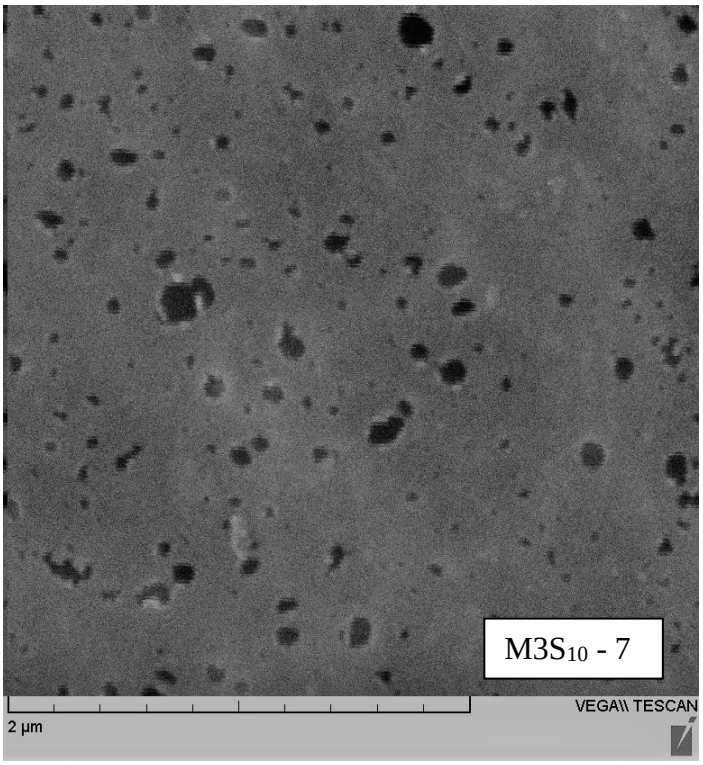

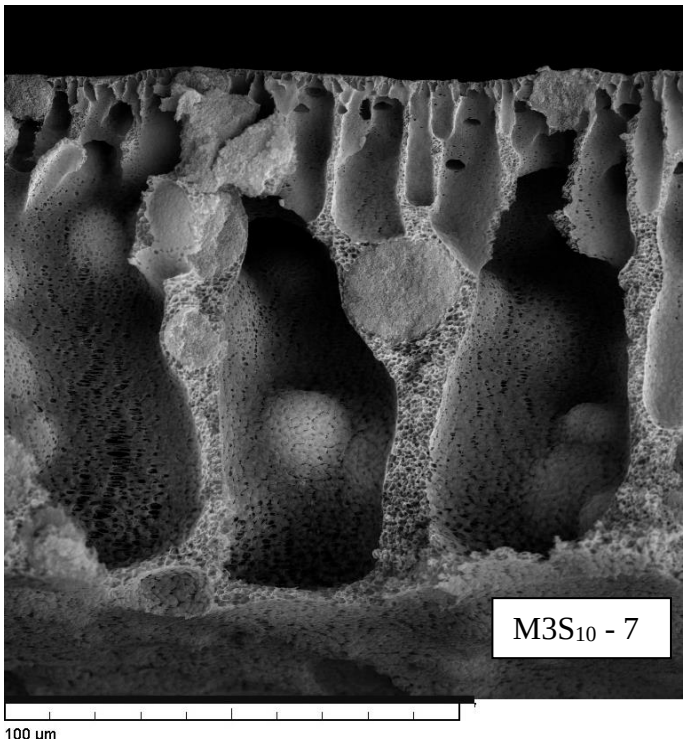

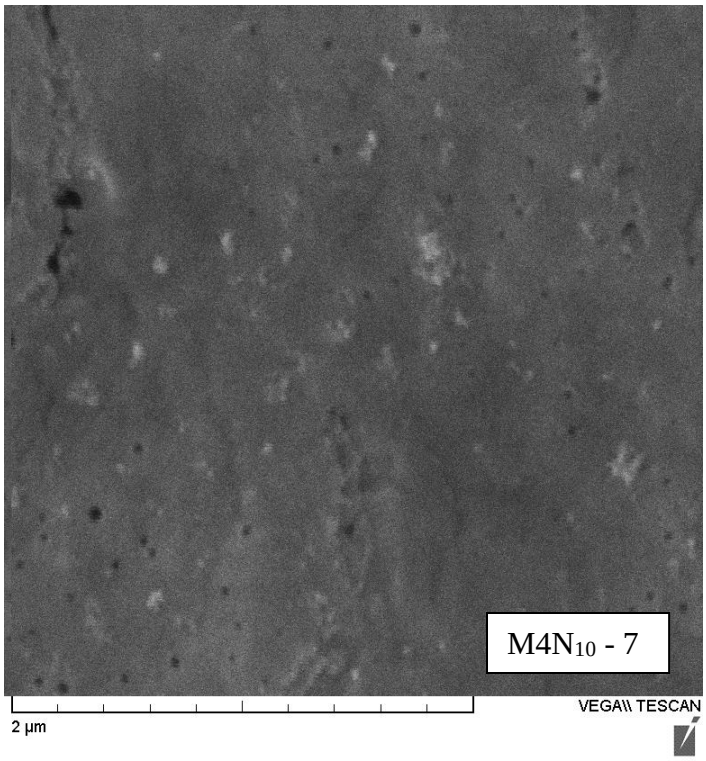

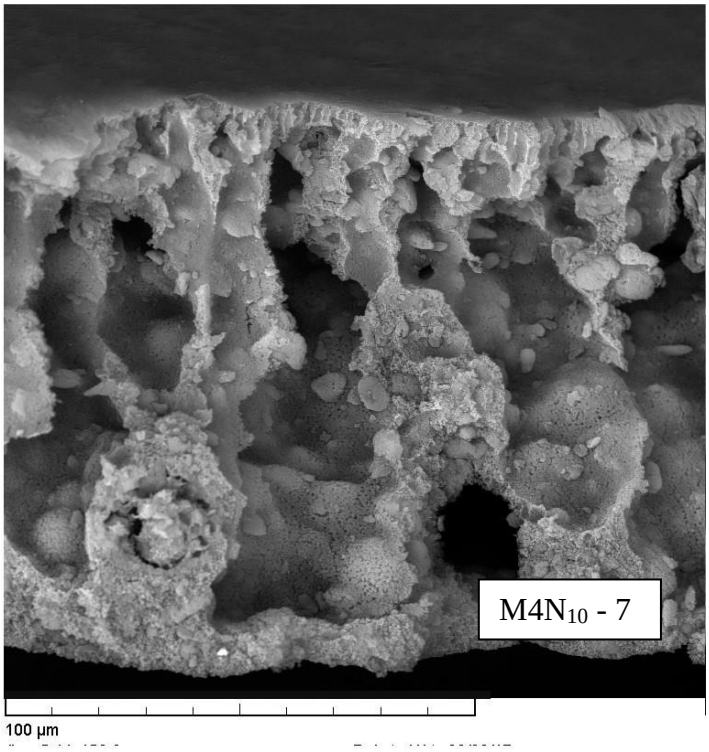

Figure 3. 8 SEM image of M3 and M4 with 10 mil thickness

3.5.3 Wettability of the membrane

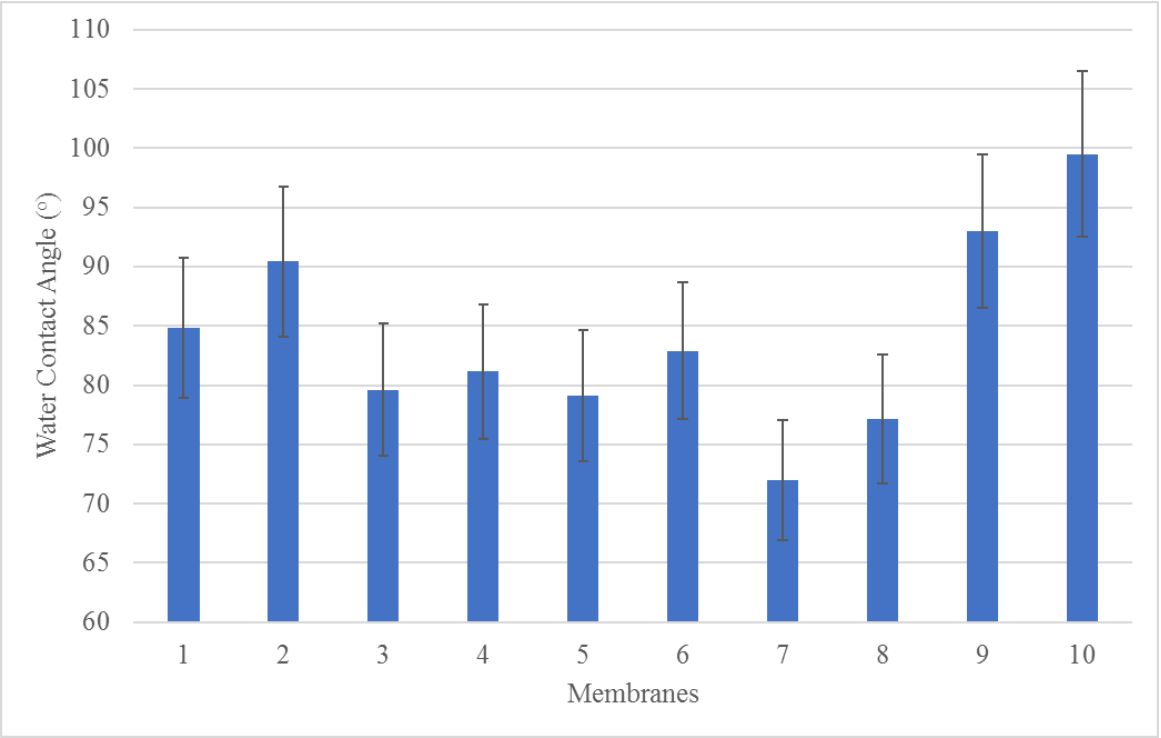

Figure 3. 9 Hydrophobicity of various membranes

Figure 3. 9 shows the water contact angle of various membranes. Comparing 1 vs 2, 7 vs 8 and 9 vs 10, the contact angle increased as the cast film thickness decreased, while, comparing 5 and 6, the increase in nanoparticle loading showed only slight increase in the contact angle. Each data has been obtained by repeating the experiment for atleast 100 different membranes and the average is reported. The contact angle is determined by the interplay of many factors, such as membrane surface morphology, migration of filler nanoparticles to the top surface etc. and, from the results shown in Fig. 3.9, it is difficult to conclude which factor is the most dominant. Nevertheless, a remarkably large contact angle of nearly equal to 100^{o} was achieved by loading hydrophobic nanoparticles and by decreasing the cast film thickness (see 10). It should also be

noted that, with the contact angles less than 90°, except for 2, 9 and 10, the LEPw of all the above membranes were high enough to allow VMD experiments. The discrepancy in contact angle measurements could be explained by the fact that the dense membrane surface roughness is greater than the porous membrane [35]–[37] as a result of nanoparticles being exposed close to the surface.

3.5.4 Liquid Entry Pressure of water (LEPw)

Figure 3. 10 shows the LEPw for supported M1S$_{10}$-n and M2S$_{10}$-n membranes when the nanoparticle concentration was changed from 2-7%.

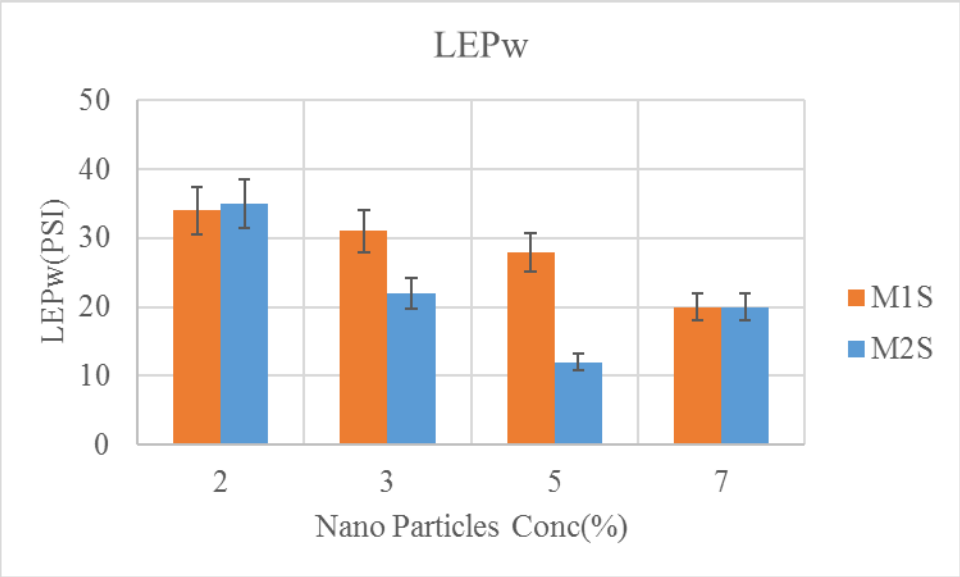

Figure 3. 10 LEPw of the supported membranes with different nanoparticle concentration

The LEPw decreases with an increase in nanoparticle loading except for the change of M2S$_{10}$-d when d was increased from d = 5 to d =7. The above results are natural since the higher loading of hydrophilic TiO_2 nanoparticles renders the membrane more hydrophilic. It should also be noted than M1S$_{10}$-d shows higher LEPw than M2S$_{10}$-d. Despite the change in LEPw, measured LEPws were always above 14 psi, except for M2S$_{10}$-5, allowing the use of the membranes for

VMD experiments. It was also found from a different series of experiments (not reported) that the effect of cast film thickness on LEPw was not very significant. It should only be recorded that a LEPw as high as 80 psi was achieved by $M1N_{10}$-5.

3.5.5 Porosity and pore size measurement

Figure 3. 11 shows the pore size of various membranes. From the figure, only one thing can be concluded, i.e. comparing 5 ($M1N_{10}$-5) vs 6($M1S_{10}$-5), the supported membrane's porosity is larger than unsupported membrane at high NP concentration. The effect is much stronger when small nanoparticles are loaded. These results are in accordance with those of Baghbanzadeh et al. [15].

Figure 3. 12 shows the porosity of the various membranes. In case of M3S, when thickness is decreased there is huge expansion of porosity when compared with the previous work done by Baghbanzadeh et al. $M3S_{10}$-7 that had the porosity of 27%. But in case of M4, decreasing the thickness gave the negative effect on the membrane by decreasing the porosity comparing the previous work done by Efome et al. in which $M4N_4$-7 had the porosity of 55%. This change was assumed to be because of the change in the polymer batches.

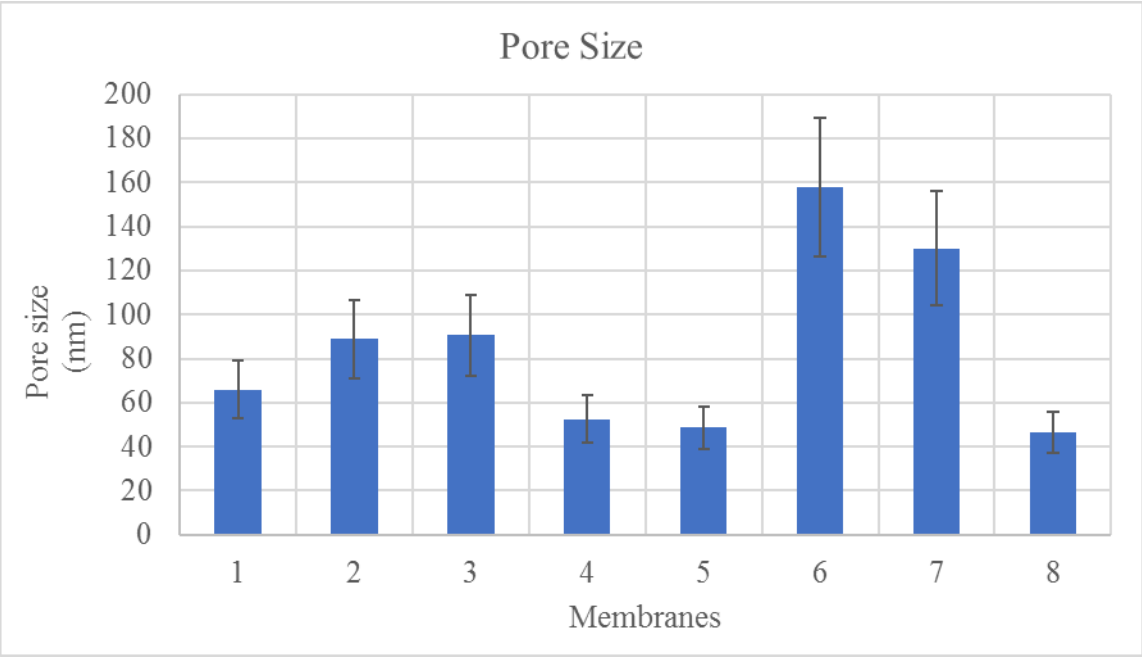

Legends	Membranes
1	$M2N_4$ - 2
2	$M2N_{10}$ - 2
3	$M2S_{10}$ - 2
4	$M1N_4$ - 5
5	$M1N_{10}$ - 5
6	$M1S_{10}$ - 5
7	$M3S_4$ - 7
8	$M4N_4$ - 7

Figure 3. 11 Pore Size Vs Types of membranes

Figure 3. 12 Porosity of various kinds of membranes

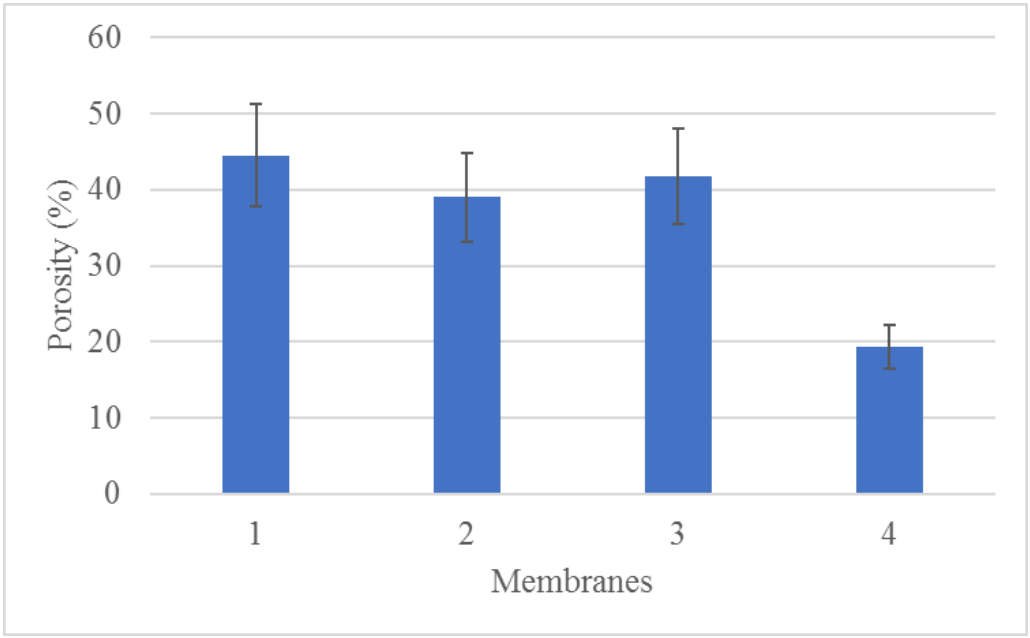

Legend	Membrane Type
1	$M2S_{10}$ - 2
2	$M1S_{10}$ - 5
3	$M3S_4$ - 7
4	$M4N_4$ - 7

3.5.6 Surface roughness

Three roughness parameters, i.e. the average roughness (Ra) defined as the arithmetic average of the absolute values of the measured peak heights from a one-dimensional plane, the root mean square (Rq) defined as the standard deviation and Rp defined as the maximum profile peak height, of various membranes are summarized in Table 3.3. Three-dimensional topographic image was drawn to show the surface roughness of the membrane using ImageJ software and are presented in **Figure 3. 13**

Table 3. 3 Roughness Parameter of various membranes

Membrane Code	**R_A µM**	**R_Q µM**	**R_P**
$M2N_4$ - 2	25.80	45.47	255
$M2N_{10}$ - 2	25.43	44.24	255
$M2S_{10}$ - 2	28.03	46.44	255
$M1N_4$ - 5	24.94	43.60	255
$M1N_{10}$ - 5	27.05	46.50	255
$M1S_{10}$ - 5	27.33	49.14	255
$M3S_4$ - 7	27.47	45.43	255
$M4N_4$ -7	26.48	43.50	255

In **Figure 3. 13**, comparing $M2N_{10}$-2 and $M2S_{10}$-2 it seems that the supported membrane is rougher than the unsupported membrane, but roughness change reported in Table 3.3 is only marginal. The same can be said when $M1N_{10}$-5 and $M1S_{10}$-5 are compared. In general, the change in roughness was insignificant and seems in an experimental error range. Nevertheless, R_a for the neat PVDF membrane found in the literature is 15.53 nm. Therefore, it can be

concluded that nanoparticle loading enhances the surface roughness considerably, which is in accordance with the work done by Baghbanzadeh et al. [15]-[17], [20] and Efome et al.[20], [31], [15], [1718], [16].

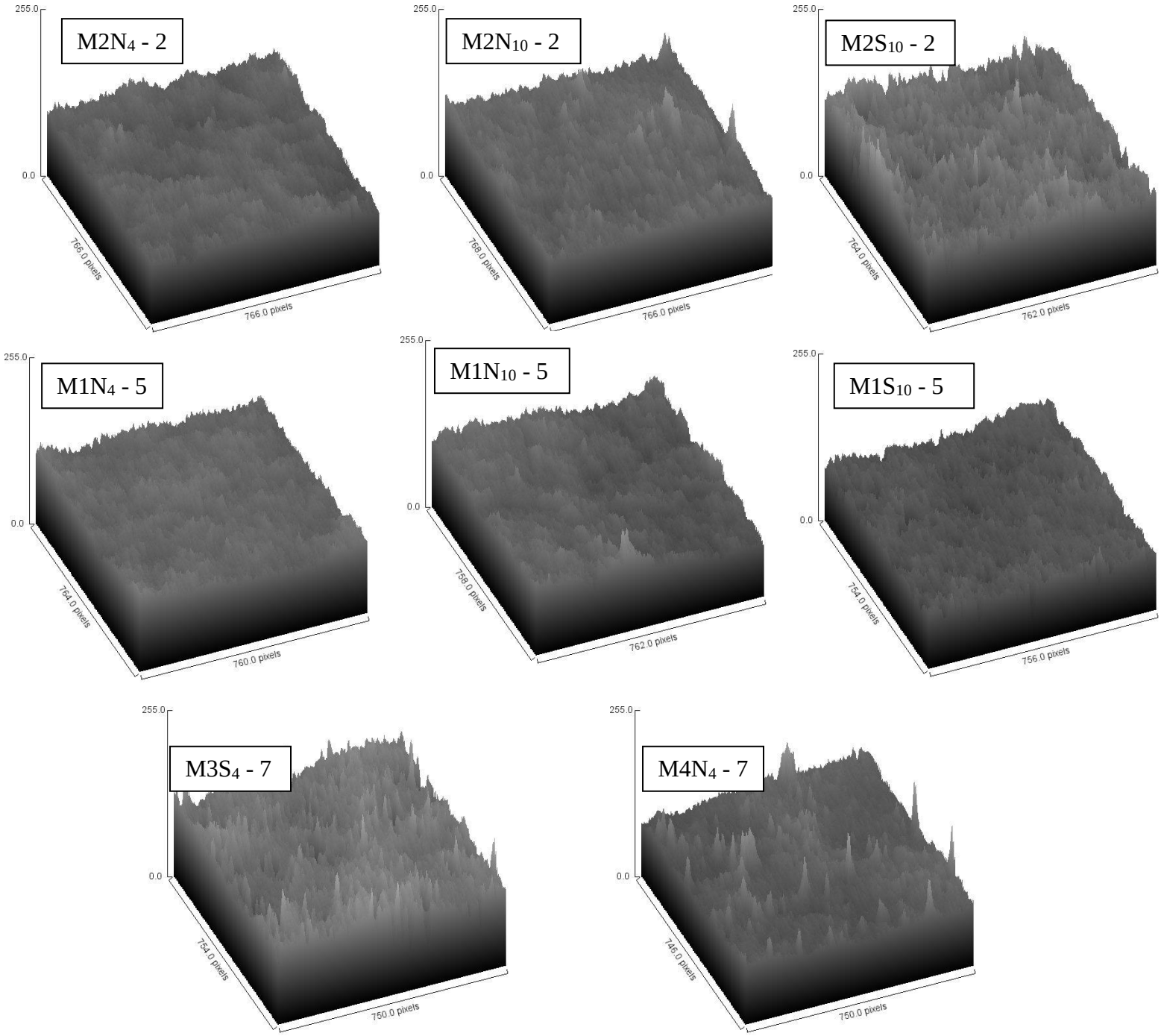

Figure 3. 13 Surface roughness of various membranes in three-dimensional topographic image

3.5.7 Energy Dispersive X-ray Spectroscopy (EDX) Analyses

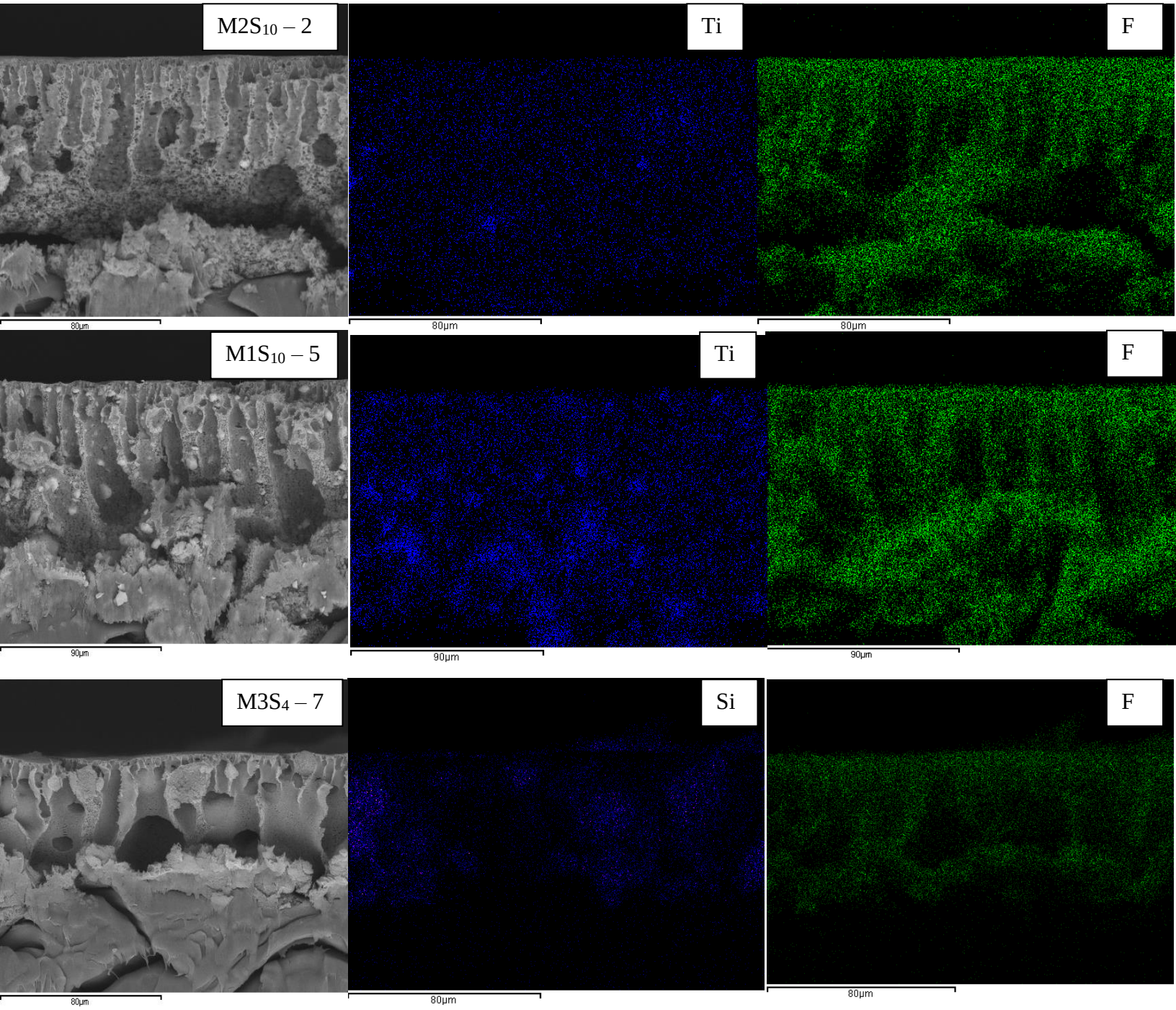

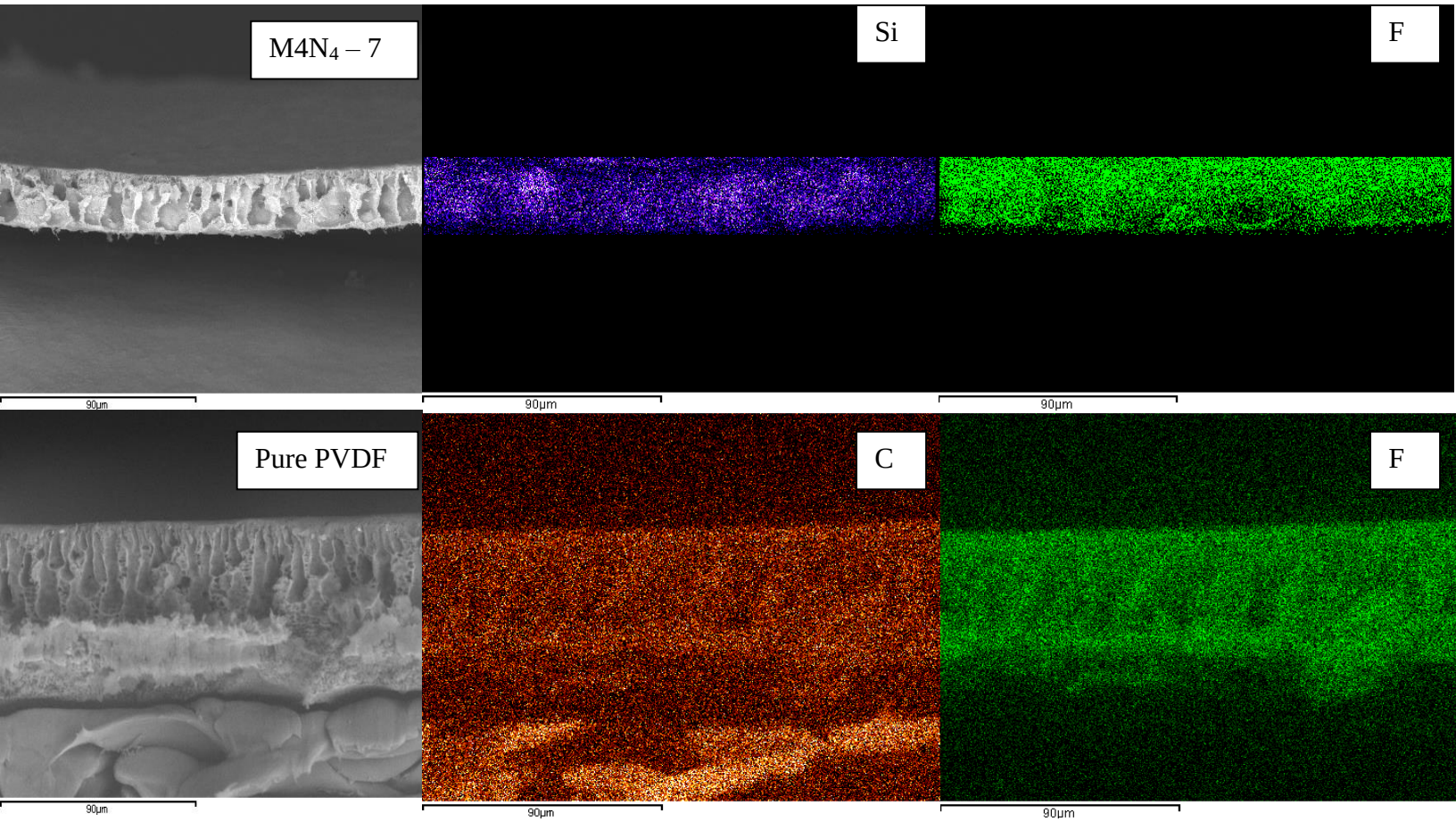

Figure 3. 14 EDS mapping of fluorine and respective nanoparticle of the membrane.

Figure 3. 14 shows the EDS mapping of fluorine (F), titanium (Ti) and silicon (Si). The membranes $M2S_{10}$-2, $M1S_{10}$-5, $M3S_4$-7 and $M4N_4$-7 were chosen to represent each nanoparticle (M1, M2, M3, M4) loaded in the membrane. Each EDX mapping was run for 90 s to obtain clear image of each element. Fluorine mapping is shown for all membranes to represent the host PVDF polymer. Titanium is for M1 and M2 to represent TiO_2 nanoparticle, and silicon is for M3 and M4 to represent SiO_2. It is interesting to note that the presence of finger-like pores is also depicted by F mapping. From these figures, it is clearly noticed that the elemental distribution is uniform across the cross-section.

Figure 3-15 shows the EDX spectrum at three spots of the cross-section, near the top, in the middle and near the bottom. The spectra are nearly identical at three spots, confirming the uniform elemental distribution across the cross-section.

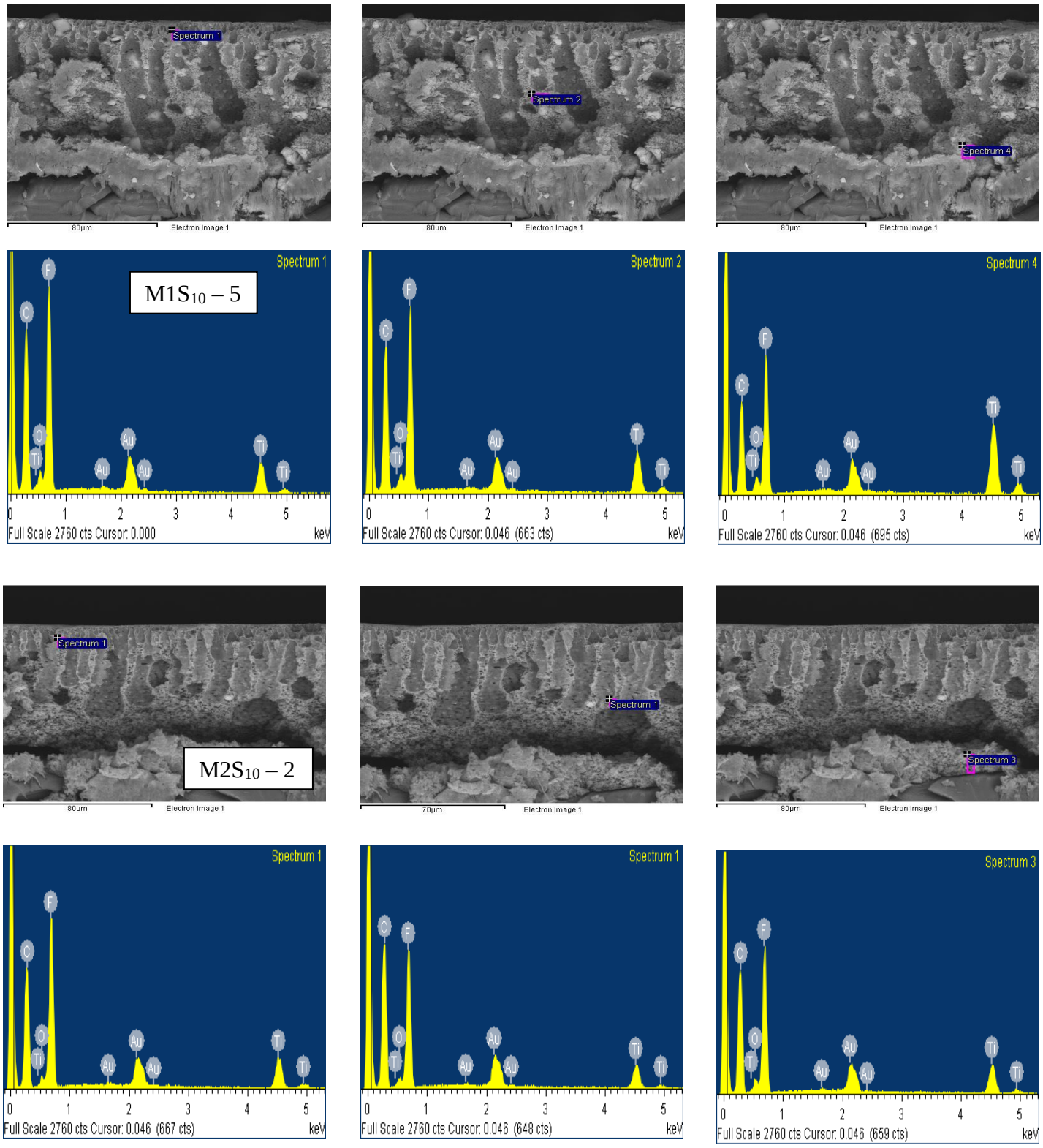

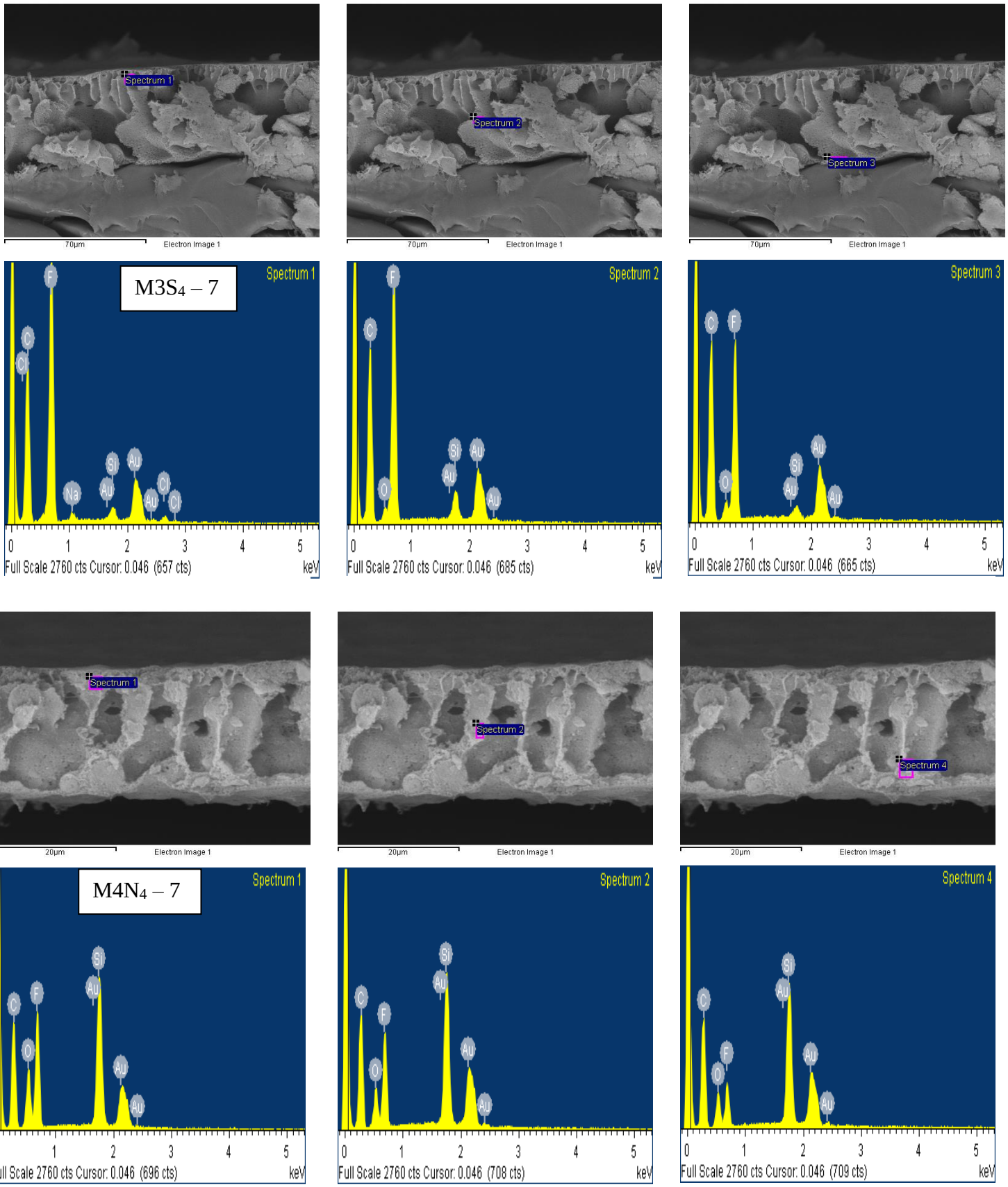

Figure 3. 15 EDX mapping for various kinds of membranes

3.5.8 Membrane performance in VMD experiment

Figure 3. 16-18 summarized the VMD experimental results in terms of water vapour flux. Figures 16 and 17 are the results for the feed pure water, while Fig. 18 compares the water vapour fluxes of pure and salty feed water. Figure 3.16 shows the effect of nanoparticle loading. Comparing the vapour flux of 0.36 kg/m^2 h reported earlier for the neat PVDF membrane, all TiO_2 nanoparticle incorporated membranes exhibited higher vapour fluxes. In particular, M1S$_{10}$-5 membrane achieved the highest flux of 11 kg/m^2 h. The enhancement of vapour flux by nanoparticle incorporation was also reported earlier by Baghbanzadeh et al. [15] -[17], and Efome et al. [15]–[18], [31].

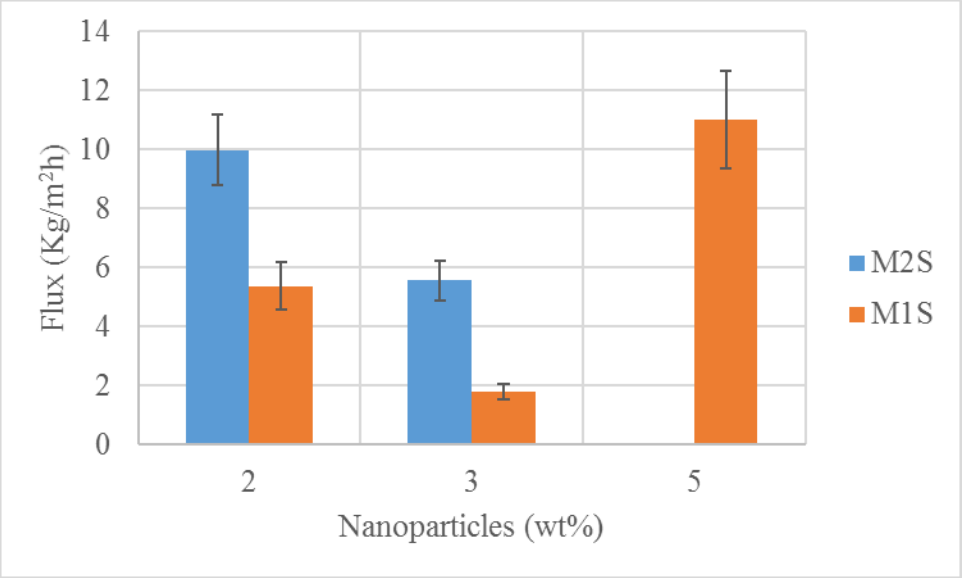

It is clear from **Figure 3. 16**, that the size of nanoparticles play a key role in flux. As it can be seen, by using large nanoparticles we are able to achieve significantly higher flux at lower concentration (i.e. M2S gave us 10 kg at 2 wt% whereas only slight increase was seen with M1S even at 5 wt%). Though the membranes with higher concentration of both nanoparticles had higher LEPw which assures that they could be used in VMD, pore wetting were observed

when they were operated in the VMD. It's hypothesised that this could be due to increase in pore size of the membranes at higher concentrations. Dead end pores formed by higher concentration of nanoparticles could also be another reason for lower flux [36]. As for the effect of nanoparticle loading. The vapour flux decreased as the loading increased for both M2 and M1 nanoparticles but in the M1 series the flux suddenly increased as the loading became as high as 5 wt.%. Figure 3. 17 shows the effect of membrane thickness on the vapour flux.

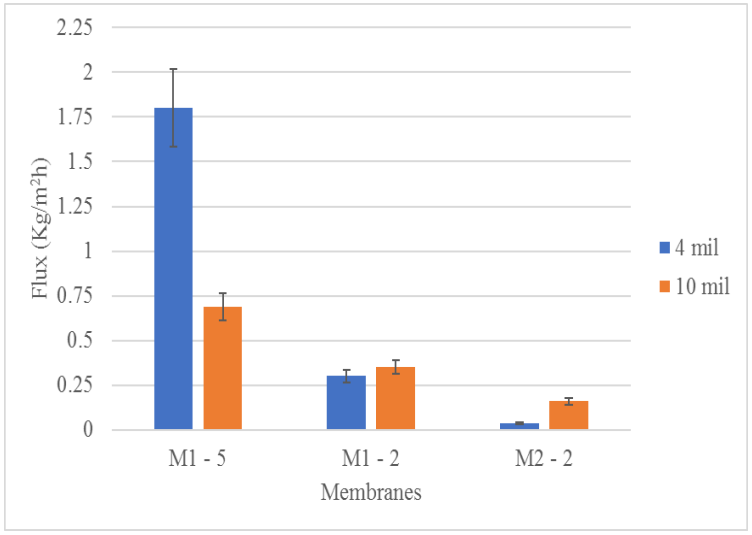

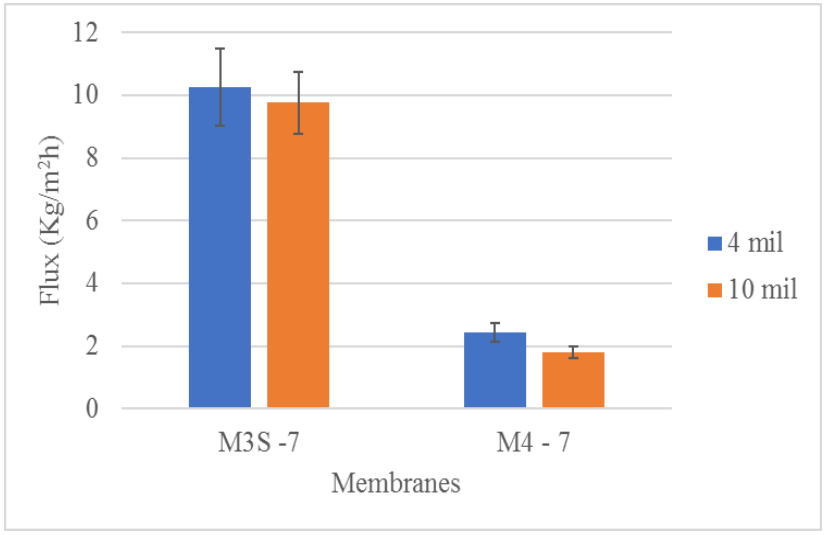

Figure 3. 17 VMD flux as a function of membrane thickness

Figure 3. 17 shows the effect of the cast film thickness (either 4 mil or 10 mil) on the vapour flux. When the nanoparticle loading is as low as 2 wt.% (see data for $M1N_4$-2 vs $M1N_{10}$-2 and $M2N_4$-2 vs $M2N_{10}$-2) the vapour flux increases as the thickness increases. On the other hand, when the nanoparticle loading is equal to or higher than 5 wt.% (see data for $M1N_4$-5 vs $M1N_{10}$-5, $M3S_4$-7 vs $M3S_{10}$-7 and $M4N_4$-7 vs $M4N_{10}$-7) the trend was opposite. This is corresponding to the change in LEPw of the membranes. At lower concentrations, the LEPw slightly decreases when the thickness is increases and at higher concentrations, the LEPw increases along with the increase in thickness.

Figure 3. 18 compares the vapour fluxes of pure and salty water (NaCl 35 g/L) as feed. Two membranes ($M1S_{10}$-5 and $M2S_{10}$-2) were chosen since these membranes showed very high fluxes among the tested membranes for pure water feed (see Fig. 3.17). Membranes with large nanoparticles at low concentration ($M2S_{10}$ – 2) yielded 99.99% salt rejection with higher flux of about 3.2 kg/m^2 h whereas small nanoparticle membrane ($M1S_{10}$-5) gave us 99.98% salt rejection with flux of about 2.1 kg/m^2 h.

The fluxes obtained for the salty water feed are much lower than the pure water feed.

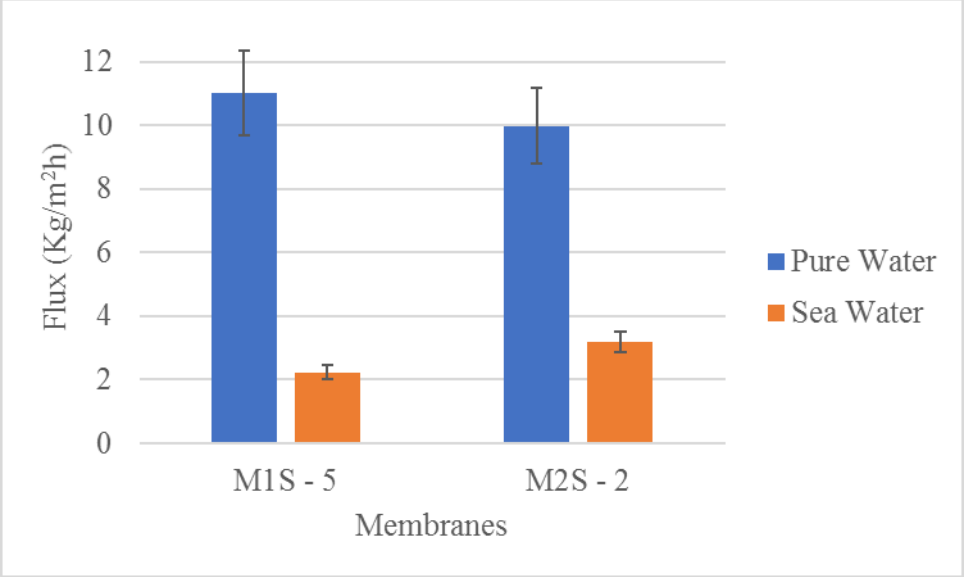

Figure 3. 18 Permeate flux with pure water and artificial seawater

It's clear that, the incorporation of nanoparticle improves the performance of the membranes which satisfies the work done by previous researchers. Also, utilisation of assorted sizes of nanoparticle plays key role in the performance of membranes. It is evident that, by using nanoparticle with larger size we could get membrane with higher flux without significant compromise of LEPw.

3.6 Conclusion

Membranes were prepared by incorporating various nanoparticles (TiO_2 of 7 nm, TiO_2 of 200 nm, hydrophilic SiO_2 and hydrophobic SiO_2) into the host PVDF polymer. The concentration of nanoparticles in the casting dope, the thickness of the cast film and the presence or absence of the backing material were the variables when the membranes were prepared by the phase inversion method. The membranes were subjected to VMD experiments after they were characterized by various methods. The following conclusions were drawn.

1) TEM analysis confirmed the TiO_2 nanoparticle size specified by the nanoparticle supplier.

2) Incorporation of nanoparticles and the presence of backing material enhanced VMD performance in accordance with the earlier reports.

3) A high VMD performance could be achieved when large sized nanoparticles were used at their low concentration.

4) The effect of the cast film thickness is not clear. But, by observing the SEM cross-sectional images, it can be said that the finger-like voids reached the bottom of the membrane when the cast film thickness was as low as 4 mil. This explains the flux increase when the film thickness was lower.

5) By using TiO_2 nanoparticles, salt rejections were higher than 99.9% and the fluxes were higher than 2.1 kg/m^2h. It is thus evident that the incorporation of TiO_2 nanoparticles yielded promising results, especially by the incorporation of TiO_2 nanoparticles of larger particle size (200 nm).

REFERENCE

[1] "National Geographic - Labrador," *National Geographic, First edition*, p. 125, 1993.

[2] H. Perlman, "The USGS Water Science School." .

[3] J. Duan, E. Litwiller, and I. Pinnau, "Preparation and water desalination properties of POSS-polyamide nanocomposite reverse osmosis membranes," *J. Memb. Sci.*, vol. 473, pp. 157–164, 2015.

[4] H. Dong, L. Zhao, L. Zhang, H. Chen, C. Gao, and W. S. Winston Ho, "High-flux reverse osmosis membranes incorporated with NaY zeolite nanoparticles for brackish water desalination," *J. Memb. Sci.*, vol. 476, pp. 373–383, 2015.

[5] F. Guo, A. Servi, A. Liu, K. K. Gleason, and G. C. Rutledge, "Desalination by membrane distillation using electrospun polyamide fiber membranes with surface fluorination by chemical vapor deposition," *ACS Appl. Mater. Interfaces*, vol. 7, no. 15, pp. 8225–8232, 2015.

[6] F. J. García Latorre, S. O. Pérez Báez, and A. Gómez Gotor, "Energy performance of a reverse osmosis desalination plant operating with variable pressure and flow," *Desalination*, vol. 366, pp. 146–153, 2015.

[7] K. Gethard, O. Sae-Khow, and S. Mitra, "Water desalination using carbon-nanotube-enhanced membrane distillation," *ACS Appl. Mater. Interfaces*, vol. 3, no. 2, pp. 110–114, 2011.

[8] I. S. M. Wang-Geun Shim, Ke He, Steve Gray, "Solar energy assisted direct contact membrane distillation (DCMD) process for seawater desalination," *Sep. Purif. Technol.*, no. 143, pp. 97–104, 2015.

[9] G. Guan, X. Yang, R. Wang, and A. G. Fane, "Evaluation of heat utilization in membrane distillation desalination system integrated with heat recovery," *Desalination*, vol. 366, no. April, pp. 80–93, 2015.

[10] J. G. Lee, Y. D. Kim, W. S. Kim, L. Francis, G. Amy, and N. Ghaffour, "Performance modeling of direct contact membrane distillation (DCMD) seawater desalination process using a commercial composite membrane," *J. Memb. Sci.*, vol. 478, no. March 2015, pp. 85–95, 2015.

[11] M. Bhadra, S. Roy, and S. Mitra, "Enhanced desalination using carboxylated carbon

nanotube immobilized membranes," *Sep. Purif. Technol.*, vol. 120, pp. 373–377, 2013.

[12] D. Hou, G. Dai, H. Fan, J. Wang, C. Zhao, and H. Huang, "Effects of calcium carbonate nano-particles on the properties of PVDF/nonwoven fabric flat-sheet composite membranes for direct contact membrane distillation," *Desalination*, vol. 347, pp. 25–33, 2014.

[13] D. Hou, J. Wang, X. Sun, Z. Ji, and Z. Luan, "Preparation and properties of PVDF composite hollow fiber membranes for desalination through direct contact membrane distillation," *J. Memb. Sci.*, vol. 405–406, pp. 185–200, 2012.

[14] Z. Chen, D. Rana, T. Matsuura, D. Meng, and C. Q. Lan, "Study on structure and vacuum membrane distillation performance of pvdf membranes: II. influence of molecular weight," *Chem. Eng. J.*, vol. 276, pp. 174–184, 2015.

[15] M. Baghbanzadeh, D. Rana, C. Q. Lan, and T. Matsuura, "Effects of hydrophilic silica nanoparticles and backing material in improving the structure and performance of VMD PVDF membranes," *Sep. Purif. Technol.*, vol. 157, pp. 60–71, 2015.

[16] M. Baghbanzadeh, D. Rana, C. Q. Lan, and T. Matsuura, "Effects of inorganic nano-additives on properties and performance of polymeric membranes in water treatment," *Sep. Purif. Rev.*, vol. 45, no. 2, pp. 141–167, 2016.

[17] M. Baghbanzadeh, D. Rana, T. Matsuura, and C. Q. Lan, "Effects of hydrophilic CuO nanoparticles on properties and performance of PVDF VMD membranes," *Desalination*, vol. 369, pp. 75–84, 2015.

[18] J. E. Efome, M. Baghbanzadeh, D. Rana, T. Matsuura, and C. Q. Lan, "Effects of superhydrophobic SiO2 nanoparticles on the performance of PVDF flat sheet membranes for vacuum membrane distillation," *Desalination*, vol. 373, pp. 47–57, 2015.

[19] Z. Chen, D. Rana, T. Matsuura, Y. Yang, and C. Q. Lan, "Study on the structure and vacuum membrane distillation performance of PVDF composite membranes: I. Influence of blending," *Sep. Purif. Technol.*, vol. 133, pp. 303–312, 2014.

[20] M. Baghbanzadeh, N. Hirceaga, D. Rana, T. Matsuura, and C. Q. Lan, "Effects of polymer ratio and film-penetration time on the properties and performance of nanocomposite PVDF membranes in membrane distillation," *Ind. Eng. Chem. Res.*, vol. 55, no. 37, pp. 9971–9982, 2016.

[21] C. M. Gribble *et al.*, "Porometry, porosimetry, image analysis and void network modelling in the study of the pore-level properties of filters," *Chem. Eng. Sci.*, vol. 66, no. 16, pp. 3701–3709, 2011.

[22] S. Zhao *et al.*, "Performance improvement of polysulfone ultrafiltration membrane using well-dispersed polyaniline-poly(vinylpyrrolidone) nanocomposite as the additive," *Ind. Eng. Chem. Res.*, vol. 51, no. 12, pp. 4661–4672, 2012.

[23] D. Emadzadeh, W. J. Lau, T. Matsuura, M. Rahbari-Sisakht, and A. F. Ismail, "A novel thin film composite forward osmosis membrane prepared from PSf-TiO2 nanocomposite substrate for water desalination," *Chem. Eng. J.*, vol. 237, pp. 70–80, 2014.

[24] Y. Lu, T. Suzuki, W. Zhang, J. S. Moore, and B. J. Mariñas, "Nanofiltration membranes based on rigid star amphiphiles," *Chem. Mater.*, vol. 19, no. 13, pp. 3194–3204, 2007.

[25] J. Carlos Mierzwa, C. D. Vecitis, J. Carvalho, V. Arieta, and M. Verlage, "Anion dopant effects on the structure and performance of polyethersulfone membranes," *J. Memb. Sci.*, vol. 421–422, pp. 91–102, 2012.

[26] Y. Yang, D. Rana, T. Matsuura, S. Zheng, and C. Q. Lan, "Criteria for the selection of a support material to fabricate coated membranes for a life support device," *RSC Adv.*, vol. 4, no. 73, pp. 38711–38717, 2014.

[27] R. M. H. McMinn, "Scanning electron microscopy," *Proc. R. Soc. Med.*, vol. 69, no. 1, p. 73, 1976.

[28] O. Agboola, J. Maree, and R. Mbaya, "Characterization and performance of nanofiltration membranes," *Environ. Chem. Lett.*, vol. 12, no. 2, pp. 241–255, 2014.

[29] S. Banerjee, R. Yang, C. E. Courchene, and T. E. Conners, "Scanning Electron Microscopy Measurements of the Surface Roughness of Paper," *Ind. Eng. Chem. Res.*, vol. 48, no. 9, pp. 4322–4325, 2009.

[30] M. Khayet and T. Matsuura, "Preparation and characterization of polyvinylidene fluoride membranes for membrane distillation," *Ind. Eng. chem. Res*, vol. 40, no. 24, pp. 5710–5718, 2001.

[31] J. E. Efome, M. Baghbanzadeh, D. Rana, T. Matsuura, and C. Q. Lan, "Effects of superhydrophobic SiO_2 nanoparticles on the performance of PVDF flat sheet membranes for vacuum membrane distillation," *Desalination*, vol. 373, pp. 47–57, 2015.

[32] A. Fujishima, T. N. Rao, and D. A. Tryk, “Titanium dioxide photocatalysis,” *J. Photochem. Photobiol. C Photochem. Rev.*, vol. 1, no. 1, pp. 1–21, 2000.

[33] C. Y. Kuo, H. N. Lin, H. A. Tsai, D. M. Wang, and J. Y. Lai, “Fabrication of a high hydrophobic PVDF membrane via nonsolvent induced phase separation,” *Desalination*, vol. 233, no. 1–3, pp. 40–47, 2008.

[34] J. Koo, J. Han, J. Sohn, S. Lee, and T.-M. Hwang, “Experimental comparison of direct contact membrane distillation (DCMD) with vacuum membrane distillation (VMD),” *Desalin. Water Treat.*, vol. 51, no. 31–33, pp. 6299–6309, Sep. 2013.

[35] M. Khayet and T. Matsuura, *Membrane Distillation - Principles and Applications*. Amsterdam, Netherlands: Elsevier, 2011.

[36] J. M. Ortiz de Zárate, L. Pen˜a, and J. I. Mengual, “Characterization of membrane distillation membranes prepared by phase inversion,” *Desalination*, vol. 100, no. 1–3, pp. 139–148, 1995.

[37] “Analysis Method_ FTIR studies of β-phase crystal formation in stretched PVDF films.pdf.” .

[38] S. Devi, P. Ray, K. Singh, and P. S. Singh, “Preparation and characterization of highly micro-porous PVDF membranes for desalination of saline water through vacuum membrane distillation,” *Desalination*, vol. 346, pp. 9–18, 2014.

[39] A. Razmjou, E. Arifin, G. Dong, J. Mansouri, and V. Chen, “Superhydrophobic modification of TiO 2 nanocomposite PVDF membranes for applications in membrane distillation,” *J. Memb. Sci.*, vol. 415–416, pp. 850–863, 2012.

4. Experimental study on the continuous flow cell Vacuum Membrane Distillation

4.1 Introduction

The demand for fresh water is rapidly increasing every year forcing people to search for new water sources other than fresh water bodies like ponds, lakes and underwater wells. This directs the focus to oceans and seas which have vast resources of water on the earth. However, the crucial issue here has been the inability to use this water directly, which demands at least a small level of treatment to make it usable. Since water is potable only when it contains less than 500 ppm of salt, much of the research has advised the subject of finding efficient methods for removing salt from seawater and brackish water. These are called desalination processes. Desalination of seawater is a promising alternative to compensate for the shortage of drinking water. Generally, desalination can be accomplished using a number of techniques. These techniques include thermal desalination, electrodialysis, filtration methods (UF, MF, NF, RO, etc.), and membrane distillation (MD).

It is worth mentioning that both, thermal and RO processes are the leading desalination processes in the water market [1]. However, these processes suffer from drawbacks and some technical difficulties. They are considered energy intensive either by the heat demand (i.e. thermal processes) or by high-pressure demand as in the RO process and this high-energy consumption generates more pollutants and undesired emissions. The scaling and fouling problem is one of the major challenges that adds to the complexity and cost of these processes. The membrane cost and durability in these membrane processes are still subjects that require more research and development. These drawbacks have affected the economic feasibility of these processes, necessitating the search for alternative, environmentally friendly and sustainable desalination processes.

MD is a promising new method in desalination processes. Unlike RO, MD relies primarily on differences in temperature across the membrane, rather than pressure, to create the necessary gradient in chemical potential that drives separation [2][3]. In MD, the driving force for diffusive transport is the difference in vapor pressure, which varies exponentially with the temperatures of the feed and permeate streams, respectively, according to Antoine's equation [2]–[4]. Separation in MD is made possible by differences in vapour pressures among components of a liquid that does not wet the membrane, resulting in selective enrichment of one component over the others in the vapour phase. MD has been known as an effective desalination technique for more than 50 years. It was introduced in the late 1960s [5], [6] and patented by Bodell in 1963 [7], [8]. MD-related research became very active in the 1980s because of the availability of new membranes[9]–[13]. MD applications are not limited only to desalination, since lower operating temperatures have also made membrane distillation attractive in the food industry where concentrated fruit juices and sugar solutions can be prepared with better flavor and color [14], in the medical field where high temperatures can sterilize biological fluids [15], and in environmental applications such as removal of benzene and heavy metals from water [16]–[19].

Though MD shows better efficiency than RO, when it comes to practical industrialisation, MD is lagging behind RO. Research on continuous flow membrane distillation has been very limited, especially VMD. Thus, this paper focuses mainly on the study of flow rate and temperature on continuous VMD configuration.

4.2 Experimental Methods

4.2.1 Materials

Poly (vinylidene fluoride) (PVDF) of two different molecular weights (Kynar® 740 and Kynar® HSV 900) both in α-phase, were supplied by Arkema Inc., Philadelphia, PA. Anhydrous N-N-dimethyl acetamide (DMAc) with 99.9% purity was purchased from Sigma Aldrich. Deionized water was used as the casting solution additive and in coagulation bath. Hollytex® 3396 non-woven fabric of air permeability 0.009 cubic feet per minute per square meter (CFM), purchased from Kavon.

4.2.2 Preparation of dope solution

The casting solution was prepared by mixing 15 wt.% PVDF [20][21], 83.75 wt.% DMAc and 1.25 wt.% water. The casting solution was then placed in a shaker of 180 rpm and 50^{o}C for 72 h to make sure complete polymers dissolution and homogenous mixing. Then the solution was de-gasified for 24 h at room temperature. The required amount of nanoparticles was then added to the required quantity of casting solution and the suspension was stirred at 100 rpm for 2 h to yield the dope solution. Hereafter "nanoparticle concentration" implies the concentration of nanoparticle in the casting solution. In this paper, the study was mainly focused on the neat PVDF (without nanoparticles).

The viscosity was measured using a rotational rheometer (Brookfield, Synchro-Lectric viscometer model: LVF) at 25^{o}C. The dope solution was loaded in the glass tubes and a spindle connected to the motor at specific speed was allowed to run for 6 to 8 min to make sure that the needle in the dial attained the constant value. The viscosity of the solution was then calculated by the rotation factor, spindle factor and rotation speed. An average was taken from the three trials and reported as the viscosity of the solution.

4.2.3 Membrane fabrication

The dope solution was cast using a casting machine to ensure the membrane uniformity. The casting machine has a bar with varying clearances (4, 6, 8 and 10 mil), a speed controller (0-10 cm/s), and a glass plate with two different casting lengths. The dope solution was poured on top of the glass plate with and without a backing material to fabricate supported and unsupported membrane, respectively. Then, the cast film was immersed in a coagulation bath together with the glass plate with or without backing material after an interval of three minutes [22]. The membrane was kept in the coagulation media, deionized water of 25^{o}C for 24 h during which the coagulation media was replaced several times with fresh deionized water to ensure complete removal of solvent from the cast film. Then, the membrane was taken out from the coagulation bath and dried at room temperature for 24 h before being subjected to characterisation.

4.3 Characterisation

The characterisation of the neat PVDF has been thoroughly defined by the previous researchers [11], [21]–[34]. Thus, most of the characterisation has been cited from the literatures.

4.3.1 Morphology (SEM analysis)

Top and cross-sectional images of the membranes were obtained using Scanning Electron Microscope system (SEM, Vega-II XMU VPSEM and Anatech Hummer VII). The membrane samples were immersed in liquid nitrogen for 10-20s before they were broken or cut by sharp scissors and fixed in a metal holder using conductive tapes. The samples were gold prior to SEM imaging. The SEM images were analysed by using ImageJ software developed by Gribble et al. [35], Zhao et al. [36], and other researchers [37]–[40]. From the images, at least 80 to 100 pores were selected randomly and their average size is reported.

4.3.2 Contact angle measurement

Water contact angle was measured by using VCA optima surface analysis system (AST Products Inc., Billerica, MA). A droplet of water (1 µl) is placed on the membrane surface by a micro-syringe (Hamilton Company, Reno, NV) to measure the contact angle after a wait time of 10 seconds. Ten random measurements were made on the membrane surface and the average is reported.

4.3.3 Liquid Entry Pressure of Water (LEPw)

The maximum pressure that can be applied to water without allowing the water to enter into the membrane pore is known as Liquid Entry Pressure of Water (LEPw). The measurements were made using a set up similar to the batch filtration cell, in which water was filled in the feed chamber. Pressure applied from a nitrogen cylinder was increased progressively with an increment of 2 psi. The pressure at which a continuous flow of water was observed on the permeate side of the filtration cell within a wait period of 10 min was recorded as the LEPw. An average of three measurements is reported.

4.3.4 Surface roughness

The surface roughness of the membrane was investigated using a plugin in the ImageJ software called SurfCharJ as developed by Banerjee et al.[41] and other researchers [31], [39], [42]. In this process, the top surface SEM image of the membrane is converted to 32-bit image and the software computes the root mean square roughness (R_q) and the average roughness (R_a). The software will further assign pixel values for each part of the image. The intensity of the darkness indicates the depth of each void. Surface roughness will be calculated by the difference in the pixel values on the membrane surface.

4.3.5 Porosity and pore size

The porosity of the membranes were measured by the method described by Khayet and Matsuura [43]. A piece of membrane was immersed in butanol for 24 h. The blotted membrane was weighed and then dried in an oven at 50^{o}C for 24 h. The dried membrane was weighed and the porosity, %ε, was obtained by

$$\%\varepsilon = \frac{m1-m2}{\rho.A.l} * 100 \qquad (4.1)$$

Where m1(g) and m2(g) are the mass of the wet and dry membranes respectively, ρ(g/m^3) is the density of butanol, A(m^2) is the area of the membrane and l(m) is the thickness of the membrane. The measurements were made with three random spots of a membrane and the average reported.

4.4 Vacuum Membrane Distillation (VMD)

The performance of the membranes was evaluated by VMD experimentation [20][24][25]. The VMD experimental setup **Figure 4. 1** consists of a membrane module which has a 300mL feed chamber wrapped with a heating coil to maintain a uniform temperature profile (27.5^{o}C) throughout the permeation cell. The turbulence of the feed solution was enhanced by a magnetic stirrer to minimize the concentration and temperature polarisation. A vacuum of 0.95 bar was maintained on the permeate side by a vacuum pump and the permeate vapour was collected in a cold trap cooled with liquid nitrogen. The permeate was collected in cold trap 2 during the first one hour of operation and then the condenser was switched to cold trap 3, assuming that the steady state of the system was reached within the first hour. The condensate collected in cold trap 2 was discarded. Cold trap 1 was used to avoid the

contamination of oil in the vacuum pump. The permeate flux was calculated using the following equation.

$$J = \frac{W}{A \cdot t} \qquad (4.2)$$

Where J is the flux (g/m^2h), W is the weight of the permeate collected (g) in cold trap 3, through membrane area (A, m^2) during time t (t, h) respectively.

Salt rejection, $\%\boldsymbol{R}$, of VMD was calculated by equation (4.3), where C_f and C_P are the feed NaCl concentration, 35 g/L as that of artificial seawater, and the permeate NaCl concentration measured by a conductivity meter (OAKTON, CON 2700), respectively.

$$\%\boldsymbol{R} = \frac{\boldsymbol{Cf - Cp}}{\boldsymbol{Cf}} * \mathbf{100} \qquad (4.3)$$

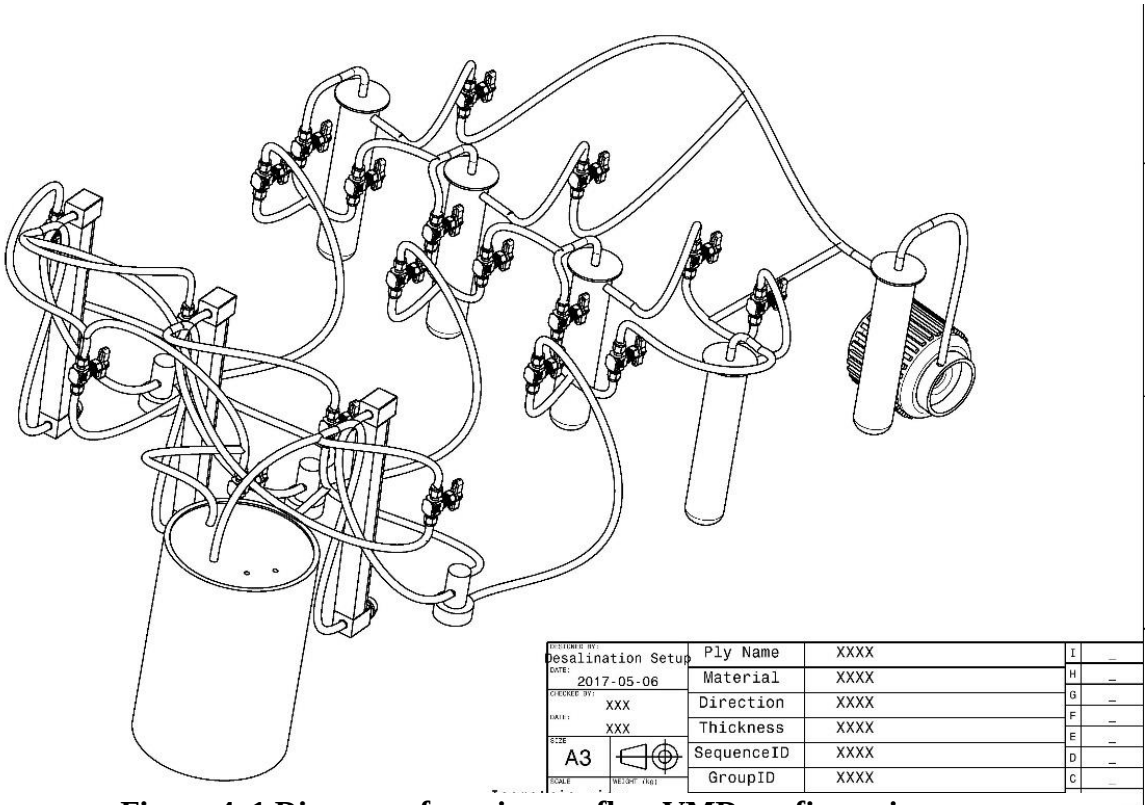

Figure 4. 1 Diagram of continuous flow VMD configuration.

4.5 Results and Discussion

Figure 4. 2 shows the top and cross-sectional view of a neat PVDF membrane. From this cross-sectional image, it was evident that the membrane has two layers which form an asymmetric structure; the top surface with macro voids which resemble finger like structures and a bottom sponge like layer with micro-voids. The sponge like layer is responsible for the membrane strength and durability but it also offers high mass transfer resistance for the vapour to pass through whereas the finger like layer helps the membrane to yield a higher flux with a lower mass transfer resistance. The viscosity of the dope solution was 3.5 Pa.s which is in accordance with the literature values [23][24]. The pore size of the membrane was measured by ImageJ as mentioned in section 4.3.1.

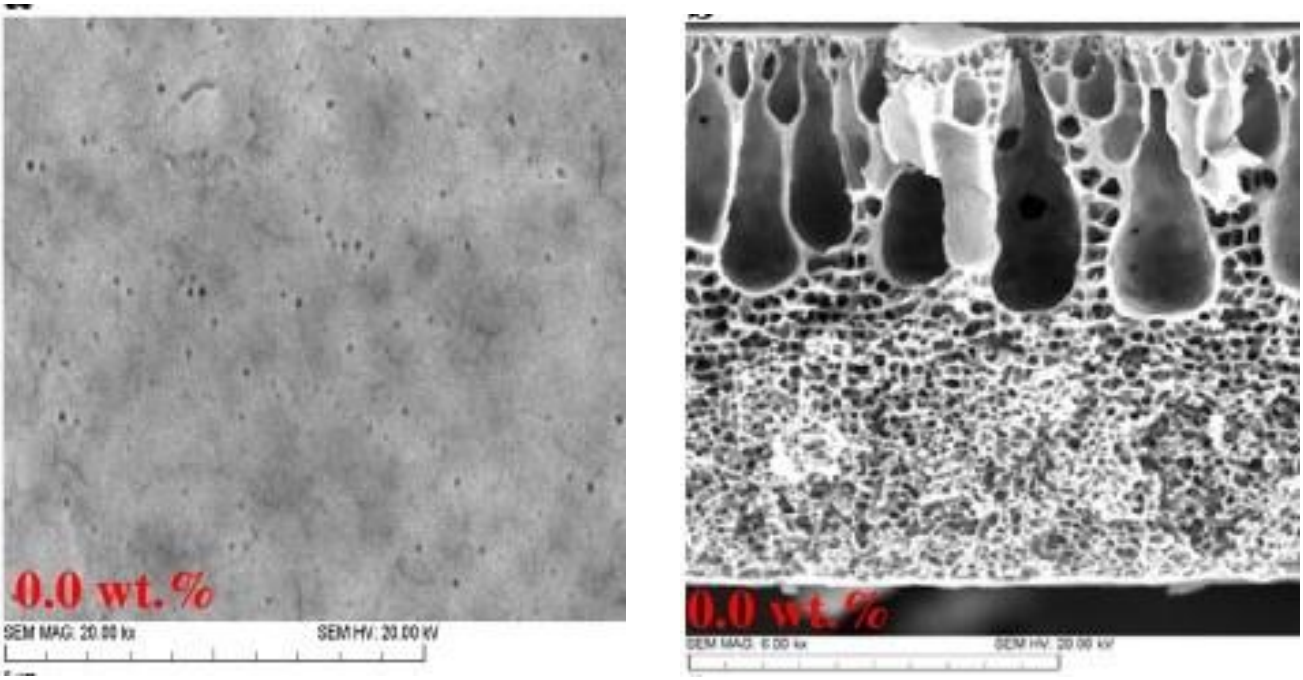

Figure 4. 2 Top and Cross-sectional view of neat PVDF membrane [23].

Figure 4. 3 shows the LEPw, pore size, porosity and contact angle of the neat PVDF membranes. All these values, newly obtained for this study, agree with those obtained earlier for the membrane prepared under the same conditions [23]–[25], within error ranges. Since these values match the literature, it was assumed that all other characterisations would also give relative values within their error ranges. The pore size of the membrane (83 nm) has been taken from the literature as shown in Figure 4.3. According to the Laplace equation, there are two factors that govern LEPw, i.e. pore size and the contact angle [44].

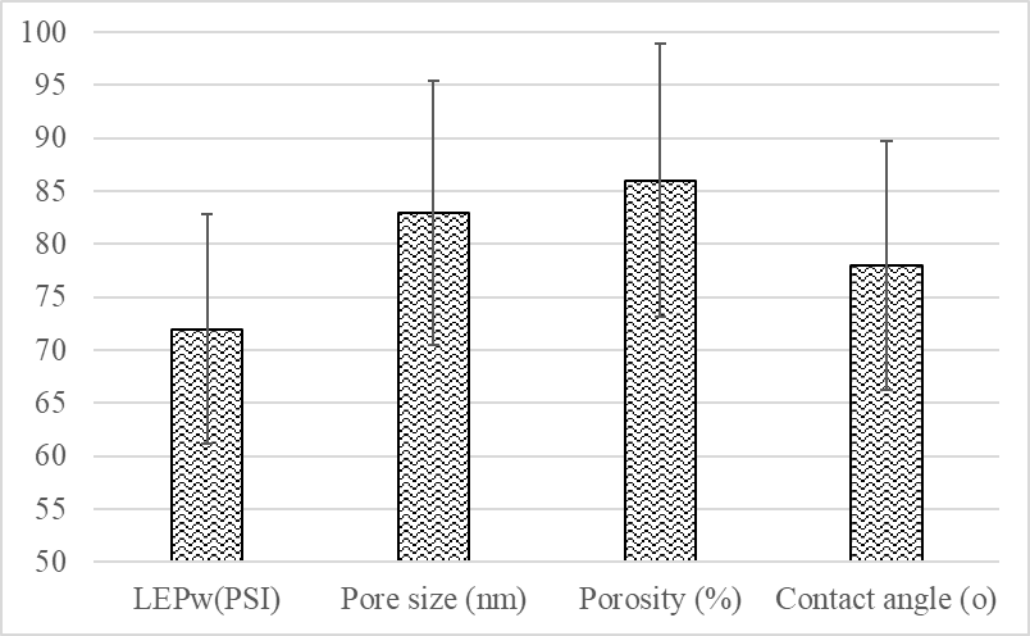

Figure 4. 3 Characterisation of neat PVDF membrane.

Figure *4. 4* shows the effect of the feed flow rate for the experiment in which the continuous flow system was used. The feed was either pure water or a synthetic seawater with NaCl concentration of 35 g/L. For both feeds the flux increases with the flow rate due less temperature polarization, for both pure water and synthetic seawater feed, and less concentration polarization for synthetic seawater [44]. **Figure 4. 4**, also shows that the flux is less for the

synthetic seawater. This is because the vapour pressure of salty water is less than that of pure water and also due to the concentration polarization that does exist only for salty water[45].

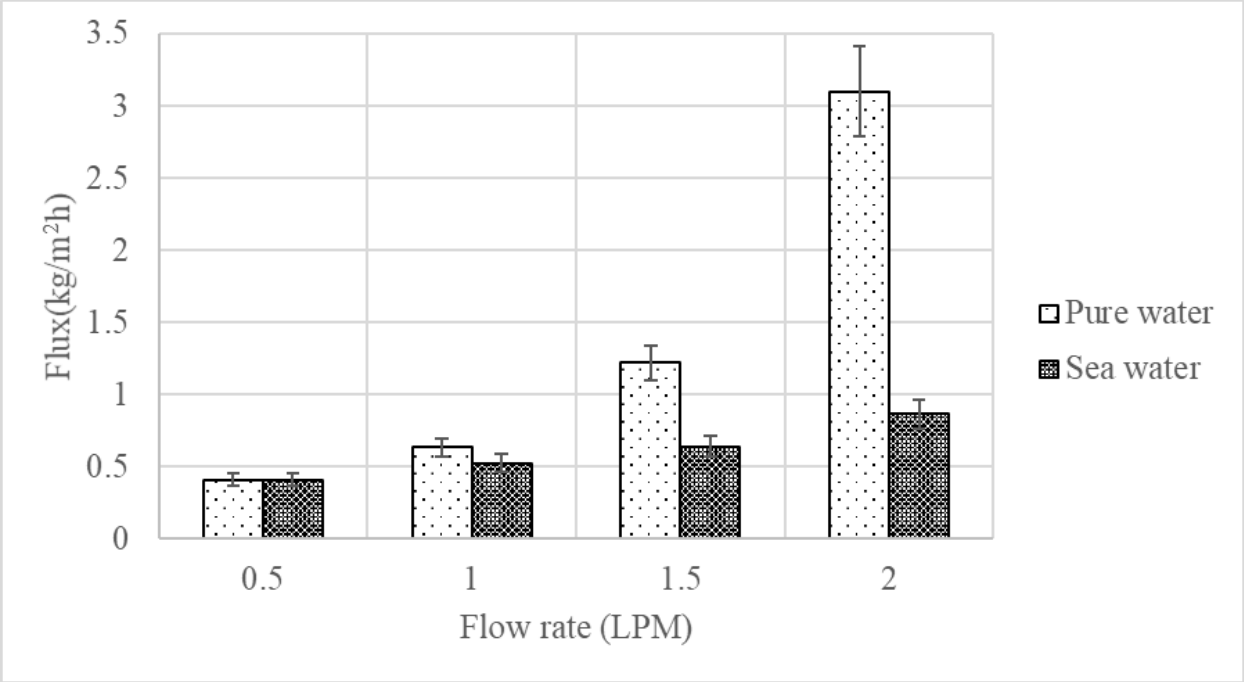

Figure 4. 4 Effect of flow rate on neat PVDF membrane in VMD.

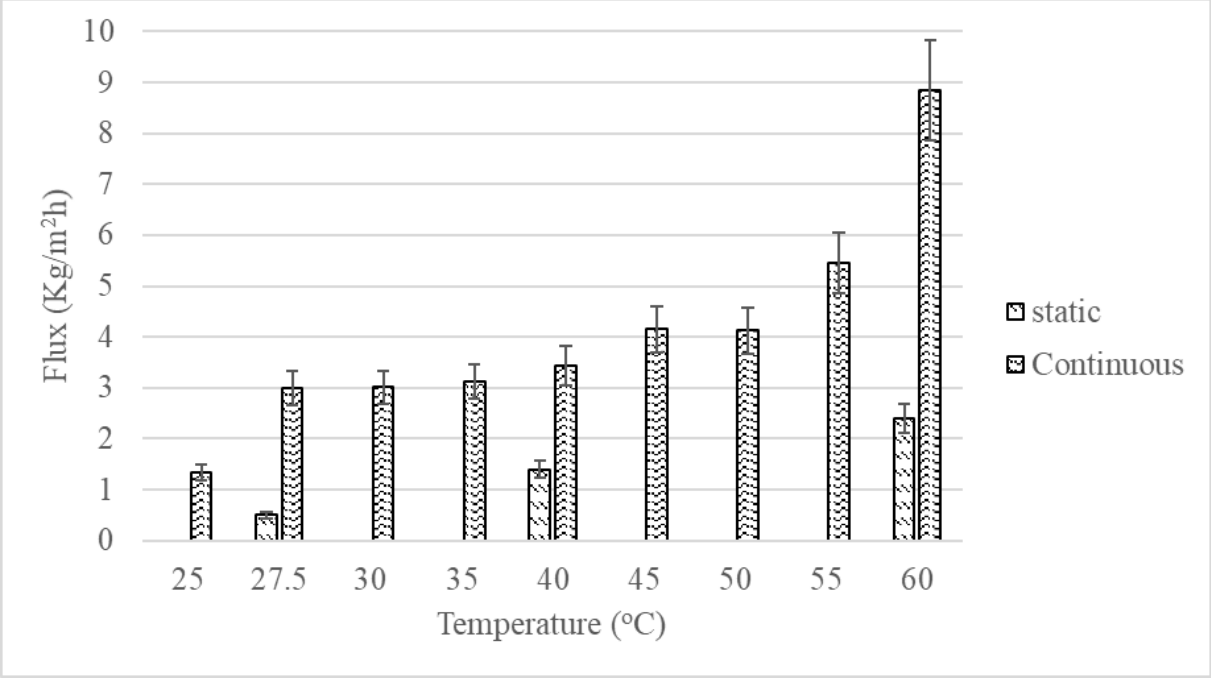

Figure 4. 5 Effect of temperature on the static and continuous flow VMD.

Figure 4. 5 shows the effect of tempearature on both static and continuous flow VMD configuration. In this experiment, the feed flowrate was fixed at 2 L/min for the continuous system and vacuum pressure was 0.95 bar for both systems.

Comparing static and continuous system, the continuous system's flux was about 300 % higher. The vapour flux increased with an increase in temperature for both sustemsas due to the increase in feed vapour pressure. However the effect of temperature was more for the continuous system, i.e. the flux increase was about 600 % and 170 %, for the continuous and static system, respectively, as temperature ineased fom 27.5 to 60 ^{o}C. This can be ascribed to the improved turbulance and decreased temperature polarization in the continuous system.

4.6 Conclusion

A continuous VMD system was constructed and VMD experiments were carried out The study mainly covers the effect of flow rate in the continuous VMD and also comparison of the effect of temperature on the flux between the continuous flow VMD with static VMD configuration. By using continuous system, we were able to achieve 600% higher the flux of 3.1 Kg/m^{2}h by the contimuous system which is 600 % higher than 0.5 Kg/m^{2}h at 27.5^{o}C of the static system when 28 PSI vacuum is applied. The effect of temperature was studied briefly both for the continuous system the static system. By increasing the temperature of feed from 27.5 to 60 ^{o}C, the permeateflux of static system was increased 500% whereas the permeate flux of continuous system was increased more than 800%. When we compare the static and continuous system at their highest and lowest temperature, the increase in flux was almost consistent i.e. continuous system attain flux almost 300% higher than the static system irrespective of the temperature. By looking at this work, it was clear that the conitnuous VMD system yields better flux compared to static VMD at any given condition. Thus more amout of work was planned to

carryon in the system with the best membranes that we have obtained in the static system (i.e. $M1S_{10}$ – 5% , $M2S_{10}$ – 2%) which were mentioned in the previous chapter.

REFERENCE

[1] T. Matsuura, D. Rana, M. R. Qtaishat, and G. Singh, "Recent advances in membrane science and technology in seawater desalination with technology development in the Middle East and Singapore," *Desalin. Water Resour. Membr. Process. V Kotchekov(Ed.), Encycl. Life Support Syst. (EOLSS), Ramsey, Isle Man,* vol. III, pp. 330–381, 2013.

[2] K. W. Lawson and D. R. Lloyd, "Membrane distillation," *J. Membr.Sci.*, vol. 124, no. 1, pp. 1–25, 1997.

[3] K. Schneider and T. J. van Gassel, "Membrandestillation," *Chemie Ing. Tech.*, vol. 56, no. 7, pp. 514–521, 1984.

[4] J. Zhang, N. Dow, M. Duke, E. Ostarcevic, J. De Li, and S. Gray, "Identification of material and physical features of membrane distillation membranes for high performance desalination," *J. Memb. Sci.*, vol. 349, no. 1–2, pp. 295–303, 2010.

[5] M. E. Findley, "Vaporization through porous membranes," *Ind. Eng. Chem. Process Des. Dev.*, vol. 6, no. 2, pp. 226–230, 1967.

[6] P. K. Weyl, "Recovery of demineralized water from saline waters," 3340186A, 1967.

[7] B. R. Bodell, "Silicon rubber vapour diffusion in saline water distillation," 285032, 1963.

[8] B. R. Bodell, "Distillation of saline water using silicone rubber membrane," 3361645A, 1968.

[9] K. S. and A. D. M. Franken, "Terminology for membrane distillation," *Desalination*, vol. 72, no. 1–3, pp. 249–262, 1989.

[10] W. T. Hanbury and T. Hodgkiess, "Membrane distillation - An assessment," *Desalination*, vol. 56, pp. 287–297, 1985.

[11] R. W. Schofield, A. G. Fane, and C. J. D. Fell, "Heat and mass transfer in membrane distillation," *J. Memb. Sci.*, vol. 33, no. 3, pp. 299–313, 1987.

[12] L. Carlsson, “The new generation in sea water desalination SU membrane distillation system,” *Desalination*, vol. 45, no. 2, pp. 221–222, 1983.

[13] S.-I. Andersson, N. Kjellander, and B. Rodesjö, “Design and field tests of a new membrane distillation desalination process,” *Desalination*, vol. 56, pp. 345–354, 1985.

[14] V. Calabrb and E. Drioli, “Theoretical and experimental Study on membrane distillation in the concentration of orange juice,” *Ind. Eng. Chem. Res.*, vol. 33, no. 7, pp. 1803–1808, 1994.

[15] K. Sakai, T. Koyano, T. Muroi, and M. Tamura, “Effects of temperature and concentration polarization on water vapour permeability for blood in membrane distillation,” *Chem. Eng. J.*, vol. 38, no. 3, pp. 33–39, 1988.

[16] A. Alkhudhiri, N. Darwish, and N. Hilal, “Membrane distillation: A comprehensive review,” *Desalination*, vol. 287, pp. 2–18, 2012.

[17] M. S. El-Bourawi, Z. Ding, R. Ma, and M. Khayet, “A framework for better understanding membrane distillation separation process,” *J. Membr.Sci.*, vol. 285, no. 1–2, pp. 4–29, 2006.

[18] M. Khayet, “Membranes and theoretical modeling of membrane distillation: A review,” *Adv. Colloid Interface Sci.*, vol. 164, no. 1–2, pp. 56–88, 2011.

[19] H. Susanto, “Towards practical implementations of membrane distillation,” *Chem. Eng. Process. Process Intensif.*, vol. 50, no. 2, pp. 139–150, 2011.

[20] Z. Chen, D. Rana, T. Matsuura, Y. Yang, and C. Q. Lan, “Study on the structure and vacuum membrane distillation performance of PVDF composite membranes: I. Influence of blending,” *Sep. Purif. Technol.*, vol. 133, pp. 303–312, 2014.

[21] Z. Chen, D. Rana, T. Matsuura, D. Meng, and C. Q. Lan, “Study on structure and vacuum membrane distillation performance of pvdf membranes: II. influence of molecular weight,” *Chem. Eng. J.*, vol. 276, pp. 174–184, 2015.

[22] M. Baghbanzadeh, N. Hirceaga, D. Rana, T. Matsuura, and C. Q. Lan, “Effects of polymer ratio and film-penetration time on the properties and performance of

nanocomposite PVDF membranes in membrane distillation," *Ind. Eng. Chem. Res.*, vol. 55, no. 37, pp. 9971–9982, 2016.

[23] M. Baghbanzadeh, D. Rana, T. Matsuura, and C. Q. Lan, "Effects of hydrophilic CuO nanoparticles on properties and performance of PVDF VMD membranes," *Desalination*, vol. 369, pp. 75–84, 2015.

[24] J. E. Efome, M. Baghbanzadeh, D. Rana, T. Matsuura, and C. Q. Lan, "Effects of superhydrophobic SiO2 nanoparticles on the performance of PVDF flat sheet membranes for vacuum membrane distillation," *Desalination*, vol. 373, pp. 47–57, 2015.

[25] M. Baghbanzadeh, D. Rana, C. Q. Lan, and T. Matsuura, "Effects of hydrophilic silica nanoparticles and backing material in improving the structure and performance of VMD PVDF membranes," *Sep. Purif. Technol.*, vol. 157, pp. 60–71, 2015.

[26] M. Baghbanzadeh, D. Rana, C. Q. Lan, and T. Matsuura, "Effects of inorganic nano-additives on properties and performance of polymeric membranes in water treatment," *Sep. Purif. Rev.*, vol. 45, no. 2, pp. 141–167, 2016.

[27] F. A. AlMarzooqi, M. R. Bilad, and H. A. Arafat, "Improving liquid entry pressure of polyvinylidene fluoride (PVDF) membranes by exploiting the role of fabrication parameters in vapor-induced phase separation VIPS and Non-solvent-induced phase separation (NIPS) processes," *Appl. Sci.*, vol. 7, no. 2, p. 181 (15 pp), 2017.

[28] A. C. Sun, W. Kosar, Y. Zhang, and X. Feng, "Vacuum membrane distillation for desalination of water using hollow fiber membranes," *J. Memb. Sci.*, vol. 455, pp. 131–142, 2014.

[29] M. A. E. R. Abu-Zeid, Y. Zhang, H. Dong, L. Zhang, H. L. Chen, and L. Hou, "A comprehensive review of vacuum membrane distillation technique," *Desalination*, vol. 356, pp. 1–14, 2015.

[30] A. C. M. Franken, J. A. M. Nolten, M. H. V Mulder, D. Bargeman, and C. A. Smolders, "Wetting criteria for the applicability of membrane distillation," *J. Membr.Sci.*, vol. 33, no. 3, pp. 315–328, 1987.

[31] R. M. H. McMinn, "Scanning electron microscopy," *Proc. R. Soc. Med.*, vol. 69, no. 1, p.

73, 1976.

[32] C. Feng *et al.*, “Production of drinking water from saline water by air-gap membrane distillation using polyvinylidene fluoride nanofiber membrane,” *J. Membr.Sci.*, vol. 311, no. 1–2, pp. 1–6, 2008.

[33] Y. Li and K. Tian, “Application of vacuum membrane distillation in water treatment,” *J. Sustain. Dev.*, vol. 2, no. 3, pp. 183–186, 2009.

[34] C. Huayan, W. Chunrui, J. Yue, W. Xuan, and L. Xiaolong, “Comparison of three membrane distillation configurations and seawater desalination by vacuum membrane distillation,” *Desalin. Water Treat.*, vol. 28, pp. 321–327, 2011.

[35] C. M. Gribble *et al.*, “Porometry, porosimetry, image analysis and void network modelling in the study of the pore-level properties of filters,” *Chem. Eng. Sci.*, vol. 66, no. 16, pp. 3701–3709, 2011.

[36] S. Zhao *et al.*, “Performance improvement of polysulfone ultrafiltration membrane using well-dispersed polyaniline-poly(vinylpyrrolidone) nanocomposite as the additive,” *Ind. Eng. Chem. Res.*, vol. 51, no. 12, pp. 4661–4672, 2012.

[37] D. Emadzadeh, W. J. Lau, T. Matsuura, M. Rahbari-Sisakht, and A. F. Ismail, “A novel thin film composite forward osmosis membrane prepared from PSf-TiO2 nanocomposite substrate for water desalination,” *Chem. Eng. J.*, vol. 237, pp. 70–80, 2014.

[38] Y. Lu, T. Suzuki, W. Zhang, J. S. Moore, and B. J. Mariñas, “Nanofiltration membranes based on rigid star amphiphiles,” *Chem. Mater.*, vol. 19, no. 13, pp. 3194–3204, 2007.

[39] J. Carlos Mierzwa, C. D. Vecitis, J. Carvalho, V. Arieta, and M. Verlage, “Anion dopant effects on the structure and performance of polyethersulfone membranes,” *J. Memb. Sci.*, vol. 421–422, pp. 91–102, 2012.

[40] Y. Yang, D. Rana, T. Matsuura, S. Zheng, and C. Q. Lan, “Criteria for the selection of a support material to fabricate coated membranes for a life support device,” *RSC Adv.*, vol. 4, no. 73, pp. 38711–38717, 2014.

[41] S. Banerjee, R. Yang, C. E. Courchene, and T. E. Conners, “Scanning Electron

Microscopy Measurements of the Surface Roughness of Paper," *Ind. Eng. Chem. Res.*, vol. 48, no. 9, pp. 4322–4325, 2009.

[42] O. Agboola, J. Maree, and R. Mbaya, "Characterization and performance of nanofiltration membranes," *Environ. Chem. Lett.*, vol. 12, no. 2, pp. 241–255, 2014.

[43] M. Khayet and T. Matsuura, "Preparation and characterization of polyvinylidene fluoride membranes for membrane distillation," *Ind. Eng. chem. Res,* vol. 40, no. 24, pp. 5710–5718, 2001.

[44] M. Baghbanzadeh, A. Rashidi, A. H. Soleimanisalim, and D. Rashtchian, "Investigating the rheological properties of nanofluids of water/hybrid nanostructure of spherical silica/MWCNT," *Thermochim. Acta*, vol. 578, pp. 53–58, 2014.

[45] M. Khayet and T. Matsuura, *Membrane Distillation - Principles and Applications*. Amsterdam, Netherlands: Elsevier, 2011.

[46] E. Jang, S.-H. Nam, T.-M. Hwang, S. Lee, and Y. Choi, "Effect of operating parameters on temperature and concentration polarization in vacuum membrane distillation process," *Desalin. Water Treat.*, vol. 54, no. 4–5, pp. 871–880, 2015.

5. Conclusion and future works

Membrane Distillation (MD) is one of the emerging non-isothermal membrane separation processes which has been known for about 50 years and still needs further development for adequate industrial implementation. Though it is yielding better results than other conventional membrane processes like RO, it's industrial implementation is still lagging because of two main factors - thermal energy required for vaporization of water and insufficient performance of currently available MD membranes.

In this thesis, the second issue, insufficient performance of nanocomposite membranes, was considered and a few methods have been studied to improve the efficiency of the vacuum MD (VMD) membrane. Also, studies on continuous flow VMD were conducted to gain insight into it's effect upon flow rate and temperature.

In chapter 2, a thorough study on the basics of MD has been presented. It includes a brief introduction to desalination and conventional membrane separation processes, followed by an explanation about individual configurations of MD. Membrane characterisations like LEPw, surface contact angle, roughness, pore size and porosity have been discussed in detail. Then, the types of methods to cast MD membranes have been detailed. Following that, the heat and mass transfer in VMD has been explained as well, the nanocomposite membranes used in MD and the effects of nanoparticles on the membranes were clearly explained to lay a solid fundamental knowledge for this thesis.

In chapter 3, the effects of different sized nanoparticles and the effect of varying casting film thicknesses on VMD were studied. Membranes were prepared through the phase inversion method with or without backing material and nanoparticles. Three different sized nanoparticles

were used in this study (7 nm TiO_2, 200 nm TiO_2, hydrophilic and hydrophobic SiO_2 (15 – 20 nm)). The size of the nanoparticles was authenticated by TEM analysis. The fabricated membranes were characterised extensively with SEM, water contact angle, LEPw, surface roughness, pore size diameter and pore size distribution. The effects of nanoparticle size and membrane thickness were analysed in the static VMD configuration. Incorporating the large size nanoparticle TiO_2 – 200 nm into the supported membrane increases the LEPw to 34 PSI and the permeate flux to 2.1 Kg/m^2h with a salt rejection level of 99% at a lower concentration of 2 wt%. The effect of casting film thickness on the VMD membrane was minimal but this assures that decreasing the thickness will decrease the size of the sponge like layer significantly, leaving a finger like layer throughout the membrane.

In chapter 4, a continuous flow VMD configuration was built to study the effect of flow rate and temperature. Pure PVDF membrane was used to study these effects. The effect of flow rate was studied at a constant operating temperature and vacuum pressure. Also, the effect of temperature was studied and compared with static configuration at a constant flowrate of 2 LPM and a constant vacuum pressure. Using continuous flow VMD, a flux of 3.1 Kg/m^2h was obtained, which was 600% higher than the flux obtained by the static flow VMD at the same temperature and vacuum pressure. While studying the effect of temperature, it was evident that the continuous flow VMD at 2 LPM yields 300% higher flux at any given temperature.

Though this research has provided a good insight about VMD, further research work should be conducted to investigate ways to implement the process at the industry level. In this study, the effect of large nanoparticle was studied only in the VMD configuration, so it would be better to study this same effect on other MD configurations. Also, since it was evident that larger TiO_2 nanoparticles yielded higher permeate flux, this research should focus on some other

nanoparticles of larger particle size. In addition, the effect of flow rate could be studied on the best nanocomposite membranes.